

Unmasking the Supernova Impostors

C. S. Kochanek^{1,2}, D. M. Szczygieł^{1,2}, K. Z. Stanek^{1,2}

ABSTRACT

The canonical picture of a supernova impostor is a $-11 \lesssim M_V \lesssim -14$ optical transient from a massive ($M_* \gtrsim 40M_\odot$) star during which the star ejects a dense shell of material. Dust formed in the ejecta then obscures the star. In this picture, the geometric expansion of the shell leads to clear predictions for the evolution of the optical depths and hence the evolution of the optical through mid-IR emissions. Here we review the theory of this standard model and then examine the impostors SN 1954J, SN 1997bs, SN 1999bw, SN 2000ch, SN 2001ac, SN 2002bu, SN 2002kg and SN 2003gm, as well as the potential archetype η Carinae. SN 1999bw, SN 2000ch, SN 2001ac, SN 2002bu and SN 2003gm all show mid-IR emission indicative of dust, and the luminosities of SN 1999bw, SN 2001ac, SN 2002bu and SN 2003gm are dominated by dust emission. We find only find upper limits on dust emission from SN 1954J, SN 1997bs and SN 2002kg. *We find, however, that the properties of these sources are broadly inconsistent with the predictions of the canonical model.* Ignoring SN 2000ch and SN 2002kg, which are simply variable stars with little or no dust, there appear to be two classes of objects. In one class (η Carinae, SN 1954J, SN 1997bs, and (maybe) SN 2003gm), the optical transient is a signal that the star is entering a phase with very high mass loss rates that must last far longer than the visual transient. The second class (SN 1999bw, SN 2001ac, SN 2002bu and (maybe) SN 2003gm) has the different physics of SN 2008S and the 2008 NGC 300 transient, where they are obscured by dust re-forming in a pre-existing wind after it was destroyed by an explosive transient. There are no cases where the source at late times is significantly fainter than the progenitor star. All these dusty transients are occurring in relatively low mass ($M_* \lesssim 25M_\odot$) stars rather than high mass ($M_* \gtrsim 40M_\odot$) stars radiating near the Eddington limit like η Carinae. The durations and energetics of these transients cannot be properly characterized without near/mid-IR observations, and the fragmentary nature of the available data leads to considerable uncertainties in our understanding of the individual sources. Continued monitoring of the sources at both optical and near/mid-IR wavelengths should resolve these ambiguities.

Subject headings: stars: evolution – supergiants – supernovae:general – supernovae: individual: SN 1954J – supernovae: individual: SN 1961V – supernovae: individual: SN 1997bs – supernovae: individual: SN 1999bw – supernovae: individual: SN 2000ch – supernovae: individual: SN 2001ac – supernovae: individual: SN 2002bu – supernovae: individual: SN 2003gm – supernovae: individual: SN 2000ch – supernovae: individual: SN 2008S – stars: individual: Eta Carinae – outflows – dust, extinction

¹Department of Astronomy, The Ohio State University, 140 West 18th Avenue, Columbus OH 43210

²Center for Cosmology and AstroParticle Physics, The Ohio State University, 191 W. Woodruff Avenue, Columbus OH 43210

1. Introduction

The eruptions of luminous blue variables (LBV) sometimes mimic the spectroscopic properties of Type II_n core collapse supernovae (SNe) and approach their luminosities (see, e.g., Smith et al. 2011). Unfortunately, the Type II_n (narrow $\lesssim 2000$ km/s line widths) spectral type (Schlegel 1990, Filippenko 1997) seems to be a property of almost any stellar eruption, explosion or evolutionary process with a strong interaction between the ejected material and the circumstellar medium, ranging from proto-planetary nebulae to some of the most luminous SNe (see, e.g., Prieto et al. 2009). Van Dyk et al. (2002) introduced the label of “supernova impostors” for LBV transients with Type II_n spectra that approach the luminosity of Type II SN but are believed to be somewhat fainter than the lowest luminosity SNe ($M \lesssim -14$ rather than $-16 \lesssim M \lesssim -18$). The “prototypical” luminous LBV transient is the eruption of η Carinae in the mid-1800s (see the reviews by Humphreys & Davidson 1994, Humphreys et al. 1999, Smith 2009, Vink 2009). We should note, however, that a typical SN impostor like SN 1997bs (see Smith et al. 2011) has completely different velocities, ejected masses and durations from the typical Galactic analogue even if many of these differences can be explained as a selection effect (see Kochanek 2011b).

The need for clearer distinctions between genuine SNe and stellar eruptions is illustrated by the ongoing debate over the nature of SN 2008S and the transient later that year in NGC 300. The dust enshrouded progenitors (Prieto et al. 2008, Prieto 2008) are astonishingly rare, only a few per galaxy, and appear to be extreme AGB stars (Thompson et al. 2009, Khan et al. 2010) with graphitic dust (Prieto et al. 2009, Wesson et al. 2010) rather than the silicate dust typically seen in massive stars. A broad range of physical mechanisms have been proposed for these events: an extension of the LBV phenomenon (Smith et al. 2009, Berger et al. 2009), some other type of massive star transient (Bond et al. 2009, Humphreys et al. 2011), electron capture SN or some other form of low luminosity SN (Thompson et al. 2009, Botticella et al. 2009, Pumo et al. 2009), a binary merger (Kashi et al. 2010), or a mass ejection associated with forming a white dwarf (Thompson et al. 2009). At this point, several years after the optical peaks, both events are still bright mid-IR sources (Ohsawa et al. 2010, Prieto et al. 2010a, Szczygiel et al. 2011) that are well-explained by an explosive transient (Kochanek 2011a). A further consideration is that there appears to be a mismatch between massive star formation rates and supernova rates that could be solved if significant numbers of these fainter transients were SN rather than impostors (see Lien et al. 2010, Horiuchi et al. 2011, Botticella et al. 2011). The alternatives are either that massive star formation rate estimates are significantly in error (by a factor of two) or that the failed SN rate is comparable to the normal SN rate (see the discussion in Kochanek et al. 2008).

The obvious difference between eruptions and supernovae is that stars survive eruptions but not core collapse. Candidate surviving stars have been found for SN 1954J (Smith et al. 2001, Van Dyk et al. 2005), SN 1961V (Filippenko et al. 1995, Van Dyk et al. 2002, Chu et al. 2004), SN 1997bs (Van Dyk et al. 1999, Li et al. 2002), SN 2000ch (Wagner et al. 2004, Pastorello et al. 2010), and SN 2002kg/V37 (Weis & Bomans 2005, Maund et al. 2006). With the exceptions of SN 2000ch and SN 2002kg/V37, which have varied repeatedly, it is probably safe to say that none of these identifications are absolutely certain and that some are likely wrong. Even with near perfect astrometry one can still be fooled by binary companions (see Kochanek 2009) or chance projections. It would be best to have some additional tests.

The standard picture of the impostors is that the visual transient is associated with the radiatively driven ejection of a significant amount of mass (see Humphreys & Davidson 1994), although Dessart et al. (2010) discuss shock driven models in some detail. The high density of the ejected material leads to dust formation, and the expanding shell of material then obscures the surviving star for an extended period. In Kochanek (2011b) we examined the formation of dust in the transients of hot stars, and found that dust formation and (great) eruptions should be essentially synonymous, as the conditions seen in eruptions are also necessary and sufficient conditions for forming dust in the ejecta. The most frequently proposed test of this picture is to search for the mid-IR emission produced by reprocessing the emissions of the surviving star in the dusty ejecta. For the spectacular Galactic example of η Carinae, $\sim 90\%$ of the emission is absorbed and reradiated in the mid-IR, leading to a spectral energy distribution (SED) that peaks near $20\mu\text{m}$ (see Humphreys & Davidson 1994). Indeed, most of the candidate survivors are usually optically fainter than their progenitors, and this is generally explained as being due to absorption in the ejecta. However, there have been attempts to find the predicted mid-IR emission only for SN 1954J (Smith et al. 2001) and SN 1961V (Kochanek et al. 2011, Van Dyk & Matheson 2011), although Van Dyk & Matheson (2011) show some results from a broader survey. Finding the dust emission then allows us to characterize the luminosity of the star and the mass of the ejecta. This test also largely eliminates false detections of non-binary survivors due to chance superpositions because of the small angular extent of the shell and the relative rarity of other luminous dusty stars (see, e.g., Thompson et al. 2009, Khan et al. 2010).

There is a second test, namely that the surviving star should tend to become systematically brighter in the optical. As the shell expands, its optical depth drops, and the survivor should reappear. This steady brightening is observed for η Carinae (see, e.g., Humphreys & Davidson 1994). The rate of brightening further constrains the optical depth of the ejected material. Neither the mid-IR emission nor the optical brightening eliminates the possibility that the “surviving” star is really a binary companion to the progenitor (see Kochanek 2009), but superposed on the steady trend, there should also be the general low level variability of LBVs, which should help to eliminate this possibility. Chu et al. (2004) use the absence of any LBV-like variability of the candidate surviving stars for SN 1961V as one of their arguments in favor of a SN rather than an LBV explanation for this transient.

Here we carry out these tests, as possible, for SN 1954J/V12, SN 1997bs, SN 1999bw, SN 2000ch, SN 2001ac, SN 2002bu, SN 2002kg/V37 and SN 2003gm. We also, for comparison, examine the properties of η Carinae. We do not consider SN 2008S or the 2008 NGC 300-OT because their evolution cannot be described by the “standard” LBV eruption picture – they require explosive transients and dust re-forming in a pre-existing wind (Kochanek 2011a). While we still view SN 1961V as a supernova (Kochanek et al. 2011, Smith et al. 2011), we include a short discussion in response to the rebuttal case by Van Dyk & Matheson (2011). We do not consider many of the candidate impostors in Smith et al. (2011) because they are either too distant (e.g. SN 2006bv) or lack (adequate) mid-IR observations (e.g. SN 2009ip). Table 1 summarizes the distances and Galactic extinctions we use for each source, the transient properties from Smith et al. (2011), and the elapsed time since the transient of the primary data we examine. The radiated energy of the transient is estimated as $E = \nu L_\nu \Delta t_{1.5}$ where νL_ν is the luminosity corresponding to the peak absolute magnitude and $\Delta t_{1.5}$ is the time scale for the transient to fade by 1.5 mag. We have included SN 1961V,

SN 2008S and the NGC 300-OT for comparison even though we will not model their properties in detail because we have done so elsewhere (Kochanek et al. 2011, Kochanek 2011a).

We start in §2 with an overview of the evolution of dusty shells. We first outline the requirements for dust formation and then make several estimates of expected ejecta mass for either radiatively-driven or explosive transients. Then we describe the optical depth and mid-IR evolution of expanding dusty shells. In §3, we summarize the available data and how it will be analyzed. In §4, we discuss each source individually in terms of how well its properties can be explained by an expanding dusty shell. Finally, in §5 we summarize the results and outline the need for future observations.

2. The Physics of Dust in Stellar Transient Ejecta

The scenario we consider consists of a massive luminous star that for a brief period of time (months to decades) undergoes a period of dramatically higher mass loss. Our general focus is not the initial transient but its possible mechanisms, the long term evolution of the ejected material and its observational consequences. In §2.1 we outline the conditions for forming dust, and then in §2.2 we set limits on the mass loss rates. Next, in §2.3 we consider the optical depth of the dust, the resulting optical depths, their evolution and the observational consequences. In §2.4 we describe the DUSTY dust radiation transfer models we use for detailed models of SEDs. Finally, in §2.5 we discuss the effects of more complicated geometries and inhomogeneity.

2.1. Dust Formation

The general assumption about the impostor transients is that they are cool ($T_{peak} \simeq 7000$ K), luminous ($L_{peak} \simeq 10^7 L_{\odot}$) eruptions from otherwise massive ($M_* \gtrsim 40M_{\odot}$), hot ($T_* > 10^4$ K), luminous ($L_* > 10^{5.8} L_{\odot}$) stars (e.g. Humphreys & Davidson 1994, Vink 2009). In Kochanek (2011b) we explored the physics of dust formation around hot stars, finding that a necessary condition for dust formation was that the ejecta wind becomes non-dust optically thick and establishes a cool, external “pseudo-photosphere” with $T_{peak} \simeq 7000$ K. Hotter transients produce so many soft UV (< 13.6 eV) photons that small dust grains photo-evaporate faster than they can grow. Such temperatures are typical of all these eruptions, and indeed of real SNe as well, and are largely a consequence of the rapid rise in non-dust opacities with temperature in this regime (Davidson 1987). As we discuss below, such dense winds must also be optically thick in order to be radiatively accelerated.

We can view the ejecta as a time varying wind surrounding the star characterized by mass loss rate \dot{M} , wind velocity v_w , and the mass fraction of condensible species X_g . Not all the condensible mass need condense onto grains, so the ultimate mass fraction of dust $X_d \leq X_g$. The wind is produced by a star/transient of luminosity L_* , photospheric radius R_* and effective temperature T_* where $L_* = 4\pi R_*^2 \sigma T_*^4$. In Kochanek (2011b) we found that the requirement for dust formation is roughly $\dot{M} \gtrsim 10^{-2.5} M_{\odot}/\text{year}$. This limit is relatively insensitive to other parameters because it is associated with the “exponential” drop in the production

of photons towards short wavelengths.

Once the wind conditions are such that the dust formation region is shielded from the hot stellar photosphere, dust formation can commence once the equilibrium temperature of small grains is low enough (e.g. Draine 2011). This sets the formation radius at

$$\begin{aligned} R_f &= \left(\frac{LQ_P(T, a_{min})}{16\pi\sigma T_d^4 Q_P(T_d, a_{min})} \right)^{1/2} \\ &= 5.2 \times 10^{14} \left(\frac{L}{10^6 L_\odot} \right)^{1/2} \left(\frac{1500 \text{ K}}{T_d} \right)^2 \left(\frac{Q_P(T_*, a_{min})}{Q_P(T_d, a_{min})} \right)^{1/2} \text{ cm} \end{aligned} \quad (1)$$

where T_d is the dust destruction temperature, $Q_P(T, a_{min})$ is the Planck-averaged absorption efficiency for the smallest grains, and L and T are the transient luminosity and temperature. For small grains, R_f is independent of a_{min} because $Q_P \propto a$, and a reasonable approximation for both the graphitic and silicate dust models of Draine & Lee (1984) is that

$$R_f \simeq 1.0 \times 10^{15} \left(\frac{L}{10^6 L_\odot} \right)^{1/2} \left(\frac{1500 \text{ K}}{T_d} \right)^2 \text{ cm} \quad (2)$$

under the assumption that the transient temperature is $T_* \simeq 7000 \text{ K}$ (see Kochanek 2011b). Including the Planck factors makes the formation radius roughly three times larger than if they are ignored. The growth rate of the dust is proportional to the density, so dust growth is essentially complete by the time $R \simeq 2R_f$ because of the rapidly dropping density of the expanding ejecta. Thus, the time scale on which the dust begins to form is

$$t_f = \frac{R_f}{v_w} \simeq 0.6 \left(\frac{L}{10^6 L_\odot} \right)^{1/2} \left(\frac{1500 \text{ K}}{T_d} \right)^2 \left(\frac{500 \text{ km/s}}{v_w} \right) \text{ years} \quad (3)$$

for expansion velocity v_w . In most cases, this is longer than the duration of the optical transient peak (see Table 1), suggesting that dust formation is limited by the fainter post-peak luminosity rather than the luminosity at peak and that the initial decline in the luminosity is usually not due to dust formation. Dust will not form if the transient temperature rises significantly above 7000 K because the increasing numbers of soft UV photons photo-evaporate grains before they can grow (see Kochanek 2011b). While the objects we consider generally lack the detailed light curves needed to probe this phase, the signature of dust formation should be an abrupt dimming in the optical combined with a sudden rise in the near/mid-IR due to the initially high dust temperatures ($T \simeq T_d \simeq 1500 \text{ K}$).

The opacity of the grains depends somewhat on the maximum size to which they grow, a_{max} , (see Draine 2011) and $a_{max} \propto \dot{M}$ depends on the density of the wind (see Kochanek 2011b). Thus, the dust opacity at any wavelength depends on the grain composition and growth history, but not by enormous factors given plausible distributions. Hence, for our present study we all simply adopt the standard opacities used by DUSTY (Ivezic & Elitzur 1997, Ivezic et al. 1999, Elitzur & Ivezic 2001).¹ We provide the detailed

¹These opacities can be derived from the parameters DUSTY supplies for its dusty wind solutions, although it would be helpful if DUSTY simply reported the values.

parameters below in §2.4 and scale our analytic results to an opacity of $\kappa_V = 100 \text{ cm}^2/\text{g}$. Many uncertainties in the opacities can also simply be absorbed into the uncertainties in the dust mass fraction X_d .

2.2. The Amount of Ejecta

The total mass of the ejecta plays a key role for any expectation about the subsequent evolution. The peak mass loss rate inferred for the Great Eruption of η Carinae is roughly $\dot{M} = 1M_\odot/\text{year}$ for a period of order $\Delta t = 10$ years, leading to a total ejecta mass of $M \simeq 10M_\odot$ (Smith et al. 2003). Other shells observed around hot stars in the Galaxy are inferred to have masses from $0.1M_\odot \lesssim M \lesssim 10M_\odot$ (e.g. Clark et al. 2009). Unfortunately, we have little knowledge of their mass loss rates. Typical estimates assume that some estimate of the radial spread in the dusty ejecta can be used to estimate the lifetime of the transient, and the generic estimates are $\sim 10^4$ years and thus $\dot{M} \sim 10^{-4}M_\odot/\text{year}$. As we argue in Kochanek (2011b), this argument for the lifetimes is almost certainly wrong based on both the data (it would mis-predict the statistical properties of the shell geometries and the rate of observable transients) and our theoretical models (no dust would form at such low mass loss rates). Rather, the radial spread must be dominated by the spread in ejecta velocities and the true ages are much shorter and the mass loss rates much higher. The lower bound based on the need to form dust is $\dot{M} \gtrsim 10^{-2.5}M_\odot/\text{year}$ (Kochanek 2011b). Very crudely, this suggests bounds of $0.1M_\odot \lesssim M \lesssim 10M_\odot$ and $10^{-2.5}M_\odot/\text{year} \lesssim \dot{M} \lesssim M_\odot/\text{year}$ for mechanisms having anything in common with the Galactic systems.

If the ejection is radiatively driven, the radiation has to provide the energy and momentum needed to generate the outflow, with negligible contributions from the initial thermal energy of the material. The momentum imparted to the ejecta satisfies $\dot{M}v_\infty = \tau L_{peak}/c$ where v_∞ is the asymptotic velocity and the optical depth τ determines the number of times a photon is scattered before escaping (see the reviews of hot stellar winds by Kudritzki & Puls 2000 or Puls et al. 2008). For the high mass loss rates of interest, the wind has to be optically thick, with

$$\tau \simeq 2 \times 10^3 \left(\frac{\dot{M}}{M_\odot/\text{year}} \right) \left(\frac{10^7 L_\odot}{L_{peak}} \right) \left(\frac{M_*}{40M_\odot} \right)^{1/2} \left(\frac{10^6 L_\odot}{L_*} \right)^{1/4} \left(\frac{T_*}{2 \times 10^4 \text{ K}} \right) \frac{v_\infty}{v_e} \text{ km/s}, \quad (4)$$

where

$$v_e = \left(\frac{2GM_*}{R_*} \right)^{1/2} = 430 \left(\frac{M_*}{40M_\odot} \right)^{1/2} \left(\frac{10^6 L_\odot}{L_*} \right)^{1/4} \left(\frac{T_*}{2 \times 10^4 \text{ K}} \right) \text{ km/s}, \quad (5)$$

is the escape velocity from the stellar surface set by the quiescent luminosity L_* and temperature T_* . For a line-driven wind, $v_\infty = v_e |1 - L_*/L_E|^{1/2}$ where L_E is the (continuum opacity-dependent) Eddington luminosity (again, see Kudritzki & Puls 2000 or Puls et al. 2008). Thus, the optical depth requirement for accelerating the wind (Eqn. 4) generally results in the formation of a “pseudo-photosphere” in the wind (i.e. $\tau > 1$) that will shield the dust formation region from soft ultraviolet radiation and allow the formation of dust (see Davidson 1987, Kochanek 2011b). There is also an upper bound on the mass loss rate set by using all available energy to lift material out of the potential well of the star. This is referred to as the “photon tiring limit” by Owocki et al. (2004). Given an observed transient luminosity L_{peak} and temperature T_{peak} ,

the upper limit on the mass loss is

$$\dot{M}_{max} \lesssim \frac{2L_{peak}R_*}{GM_*} = 1.3 \left(\frac{L_{peak}}{10^7 L_\odot} \right) \left(\frac{L_*}{10^6 L_\odot} \right)^{1/2} \left(\frac{40M_\odot}{M_*} \right) \left(\frac{2 \times 10^4}{T_*} \right)^2 \left(\frac{T_0}{T_{peak}} \right)^4 M_\odot/\text{year}. \quad (6)$$

Here we have modeled the losses due to accelerating the wind as a redshifting of the transient spectrum, as might be appropriate for a continuum opacity. The true transient luminosity is $L_{peak}(T_0/T_{peak})^4$ where $T_0 > T_{peak}$ is the unobserved temperature of the transient at the stellar surface. The radiative efficiency of this process is of order

$$f = \frac{2L_{peak}}{\dot{M}v^2} \simeq \left(\frac{\dot{M}_{max}}{\dot{M}} \right) \left(\frac{T_{peak}}{T_0} \right)^4 \quad (7)$$

and $f \gtrsim 1$ unless the transient is in the extreme limit where most of the underlying luminosity is absorbed into expelling the ejecta ($\dot{M} \simeq \dot{M}_{max}$ with $T_0 > T_{peak}$). The “tiring limit” on the mass loss rate (Eqn. 6) combined with the (somewhat arbitrary) event duration $\Delta t_{1.5}$ from Table 1 leads to a first rough estimate $M_E = \dot{M}_{max} \Delta t_{1.5}$ of the ejected mass. As reported in Table 2, most of the sources can have ejected only 0.1–1.0 M_\odot of material even at the “tiring limit,” albeit with significant uncertainties from the sensitivity of the mass loss rate to the stellar escape velocity ($\propto L_*^{1/2} T_*^{-2}$). Only SN 1961V, due to its high peak luminosity, and η Carinae, due to its long transient duration, can have ejected more than 10 M_\odot as radiatively driven transients.

In an explosion, the ejecta are shock heated and accelerated to temperatures and velocities exceeding the escape velocity and then expand. The observed luminosity is a balance between the diffusion of radiation out of the ejecta and losses due to the expansion. If the expansion time scale is $t_{exp} = R/v_w$ and the diffusion time scale for electron scattering is $t_{diff} \simeq 9M_E \sigma_T / 4\pi R m_p c$, then the transient duration is approximately the geometric mean

$$t_{rad} \equiv (t_{exp} t_{diff})^{1/2} = \left(\frac{9M_E \sigma_T}{4\pi m_p c v_w} \right)^{1/2} = 0.6 \left(\frac{M_E}{M_\odot} \frac{500 \text{ km/s}}{v_w} \right)^{1/2} \text{ years}, \quad (8)$$

if the expansion time is shorter than the diffusion time (e.g. Falk & Arnett 1977). If we identify t_{rad} with the event time scale $\Delta t_{1.5}$, then we obtain an estimate of the ejected mass

$$M_{diff} = \frac{4\pi m_p c v_w t_{rad}^2}{9\sigma_T} = 0.018 \left(\frac{t_{rad}}{30 \text{ days}} \right)^2 \left(\frac{v_w}{500 \text{ km/s}} \right) M_\odot. \quad (9)$$

Table 2 reports M_{diff} for each source. These mass estimates tend to be slightly smaller than the estimated upper limits $\dot{M}_{max} \Delta t_{1.5}$ for radiatively driven transients except when the transient durations are long. SN 1961V and η Carinae again stand out as having the largest mass loss estimates. The radiative efficiency of an explosive transient is roughly determined by

$$\frac{t_{exp}}{t_{diff}} = \frac{c m_p L_{peak}}{9M_E \sigma_T v_w \sigma T_{peak}^4} \simeq 0.02 \left(\frac{L_{peak}}{10^7 L_\odot} \right) \left(\frac{7000 \text{ K}}{T_{peak}} \right)^4 \left(\frac{M_\odot}{M} \right) \left(\frac{500 \text{ km/s}}{v_w} \right), \quad (10)$$

which means that explosive transients are generally radiatively inefficient because they lose energy due to expansion faster than it can be diffusively radiated.

This suggests that uncertainties about the mechanism can be described by the radiative efficiency f , where the ejected mass is

$$M_E = \frac{2E_{rad}}{fv^2} = 0.04f^{-1} \left(\frac{L_{peak}}{10^7 L_\odot} \right) \left(\frac{\Delta t_{1.5}}{30 \text{ days}} \right) \left(\frac{500 \text{ km/s}}{v_w} \right)^2 M_\odot. \quad (11)$$

Radiatively driven transients tend to have $f > 1$ and explosive transients tend to have $f < 1$, while radiatively driven transients close to the tiring limit and weak explosions have $f \simeq 1$. This leads to the final mass estimate in Table 2.

2.3. Optical Depth and Temperature Evolution

Where dust formation and growth depends on density through \dot{M} and v_w , the optical depth also depends on the duration of the transient Δt and the time of observation t . These are related to the mass of the ejecta $M_E = \dot{M}\Delta t$, the radius of the shell $R_{out} = v_w t$ and the thickness of the shell $R_{out} - R_{in} = \Delta R = v_w \Delta t$. These quantities likely vary with azimuth, leading to some smearing of the dust properties, temperatures and opacities with viewing angle. The outermost ejecta is at

$$R_{out} = 1.6 \times 10^{16} \left(\frac{v_w}{500 \text{ km/s}} \right) \left(\frac{t}{\text{decade}} \right) \text{ cm}, \quad (12)$$

and the optical depth of the shell at wavelength λ is

$$\tau_\lambda = \frac{\dot{M}\kappa_\lambda}{4\pi v_w} \left(\frac{1}{R_{in}} - \frac{1}{R_{out}} \right) \quad (13)$$

where κ_λ is the dust opacity. If we are focused on the apparent extinction of a central source, the appropriate optical depth (or opacity) for these analytic approximations is the effective absorption optical depth $\tau_e = (\tau_{abs}(\tau_{abs} + \tau_{scat}))^{1/2}$ rather than the total $\tau_{tot} = \tau_{abs} + \tau_{scat}$, absorption τ_{abs} or scattering τ_{scat} optical depths. These distinctions are important, particularly for silicate dusts with their larger scattering opacities (e.g. Draine & Lee 1984).

It is useful to recast this in terms of the time evolution of the optical depth under the assumption of a constant expansion velocity,

$$\tau(t) = \tau_0 t_f \left[\frac{1}{\max(t_f, t - \Delta t)} - \frac{1}{\max(t_f, t)} \right] \quad \text{where} \quad \tau_0 = \frac{\dot{M}\kappa_\lambda}{4\pi v_w R_f}. \quad (14)$$

Here $t_f = R_f/v_w$ is the time scale on which dust begins to form (Eqn. 1), Δt is the duration of the transient, and τ_0 , the optical depth for a wind extending from R_f to infinity, sets the peak optical depth. As illustrated in Fig. 1, the optical depth begins to rise at $t = t_f$ when material first reaches the dust formation radius. It peaks with optical depth $\tau_0 \Delta t / (t_f + \Delta t)$ at time $t_{peak} = t_f + \Delta t$ when all the material has been ejected and the last material to be ejected lies at the dust formation radius. If the duration of the transient Δt is long compared to the flight time to the dust formation radius, t_f , the optical depth approaches the value for a fully

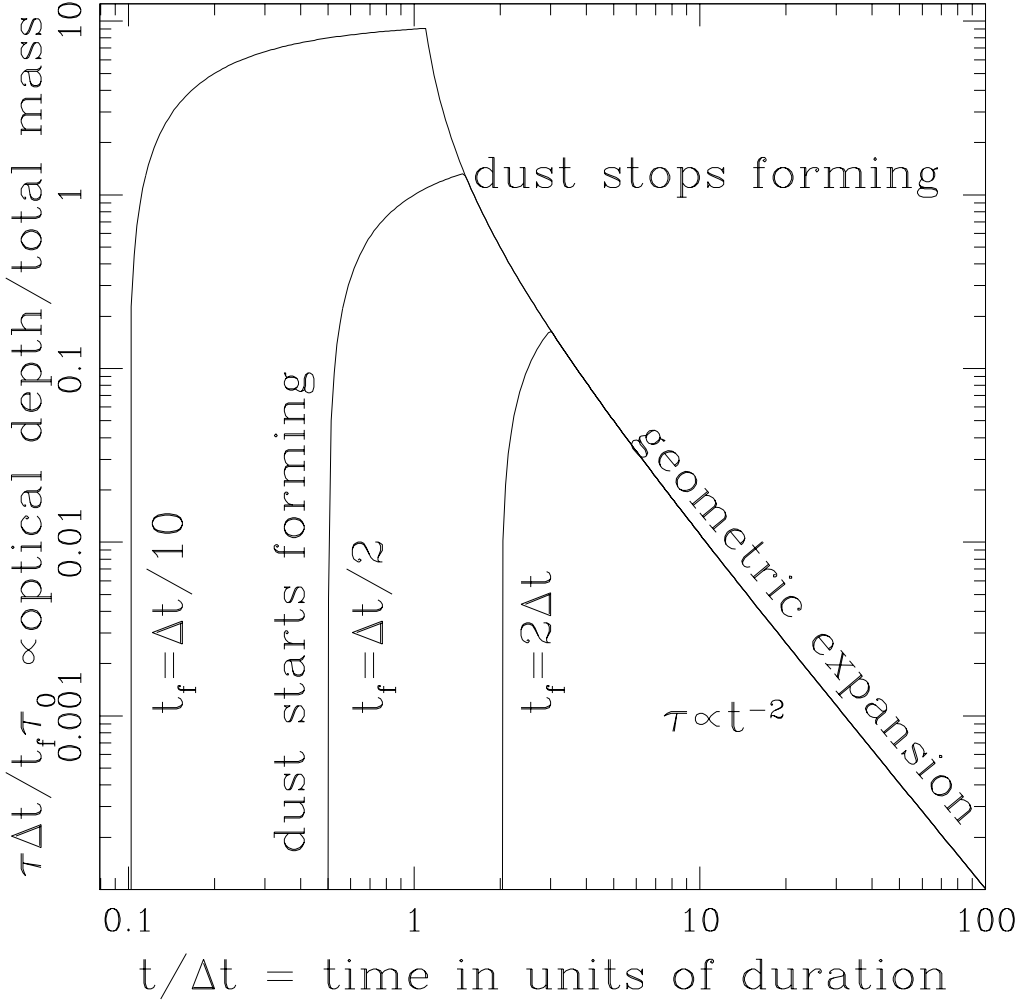


Fig. 1.— The optical depth evolution of a transient (Eqn. 14). The time is in units of the transient duration, $t/\Delta t$. The optical depth is normalized as $\tau \Delta t / (t_f \tau_0)$, which corresponds to the optical depth per unit ejected mass ($\propto \tau / M_E$). The scalings are shown for dust formation time scales that are short ($t_f = \Delta t / 10$), comparable ($t_f = \Delta t / 2$) or long ($t_f = 2\Delta t$) compared to the transient duration. The optical depth rises from t_f until $t_{peak} = \Delta t + t_f$, but it has a higher peak and an increasingly long plateau for a given amount of ejected mass as the formation time scale becomes shorter compared to the transient duration. The maximum possible optical depth corresponds to a fully formed wind with the mass loss rate of the transient. The optical depth then drops on time scale t_f and finally asymptotes to the $\tau \propto t^{-2}$ of an expanding shell.

formed wind, τ_0 , and is then almost constant for the remaining duration of the transient. The optical depth then drops as

$$\tau(t = t_{peak} + \delta) = \frac{\tau_0 t_f \Delta t}{(t_{peak} + \delta)(t_f + \delta)} \quad (15)$$

where δ is the time elapsed since the optical depth peak. The initial drop of $\tau \propto 1/(t_f + \delta)$ on timescales of $t_f = R_f/v_w$ is rapid, and then once $\delta > t_{peak}$ it asymptotes to the quadratic decline of a thin shell, $\tau(t) = \tau_0 t_f \Delta t / t^2$. Taking the limit of a thin shell at late times, the optical depth is

$$\tau_\lambda = \frac{\dot{M} \kappa_\lambda \Delta R}{4\pi v_w R_{out}^2} = \frac{M_E \kappa_\lambda}{4\pi R_{out}^2} = 64 \left(\frac{M_E}{M_\odot} \right) \left(\frac{\kappa_\lambda}{100 \text{ cm}^2/\text{g}} \right) \left(\frac{500 \text{ km/s}}{v_w} \right)^2 \left(\frac{\text{decade}}{t} \right)^2. \quad (16)$$

Table 2 gives the estimated visual optical depth τ_V for the sources we consider at the time of the primary observations assuming an opacity of $\kappa_V = 100 \text{ cm}^2/\text{g}$ and scaled by M_E (Eqn. 11).

A transient can maintain high optical depth only for the duration of the transient, after which the optical depth begins to decline very rapidly and the central source should become steadily brighter. The rate of brightening for $t > t_{peak} = \Delta t + t_f$ is

$$\frac{dm}{dt} = -\frac{2.5}{\ln 10} \frac{\tau}{t} \left(1 + \frac{t}{t - \Delta t} \right) \rightarrow -\frac{5}{\ln 10} \frac{\tau}{t}, \quad (17)$$

where the limit is for very late times when $t \gg t_{peak}$. Close to the end of the transient, the rate of change can be very much faster because the term in parenthesis approaches $2 + \Delta t/t_f$ as $t \rightarrow t_{peak}$ (see Fig. 1). Even at late times, a source detected with a significant optical depth at time t doubles in flux on the fast time scale of $t/(3\tau)$. This evolution could be balanced by changes in the star, and modeling the star as a black body, the luminosity at wavelength λ evolves as

$$\lambda L_\lambda = L(t) G(x) \exp(-\tau_{e,\lambda}(t)) \quad \text{where} \quad G(x) = \frac{15}{\pi^4} \frac{x^4}{\exp(x) - 1} \quad \text{and} \quad x = 1.44 \left(\frac{\mu\text{m}}{\lambda} \frac{10^4 \text{ K}}{T(t)} \right). \quad (18)$$

The spectral term $G(x)$ has a maximum at $x_{max} = 3.92$ corresponding to $T \simeq 6700 \text{ K}$ for the V band, so these transients tend to be most efficient at producing visual light near peak.

A recurring theme of our paper, however, will be that it is very hard to fight the optical depth evolution because it is large and sitting in an exponential (Eqn. 18). Most post-transient detections of surviving stars are interpreted as requiring an obscuring optical depth of $\tau_{e,V} \simeq 3$ (see §4). If this is the optical depth at time t , then at time $2t$ the optical depth will have dropped to $\tau_{e,V} = 3/4$ and the star should be almost ten times brighter. To a limited extent, such changes can be balanced by lowering the stellar luminosity or raising its temperature, but it requires fine tuning (there are no obvious physical correlations between the optical depth and expansion of the shell with the stellar properties) and can only be fine tuned at one wavelength. To hold the apparent flux constant in the face of a $\Delta\tau_e = 2.3$ reduction in optical depth requires either reducing the stellar luminosity by an order of magnitude or the equivalent of raising the stellar temperature from that of the cool, eruptive state ($T_{peak} \simeq 7000 \text{ K}$) to a typical quiescent temperature of a hot star, $T_* \simeq 27000 \text{ K}$. It is essentially impossible for the star to balance significantly larger changes in optical depth.

Once the dust has formed and the grains have grown in size, the Planck absorption efficiencies are significantly different than those for the smallest grains that control dust formation and we need a temperature averaged over a distribution of grain sizes. Individual grain temperatures are still controlled by $L_*\pi a^2 Q_P(T_*, a)/4\pi R^2 = 4\pi a^2 \sigma T^4 Q_P(T, a)$, but for a particle size distribution dn/da we can estimate a mean temperature by averaging this equation over the grain size distribution so that $L_* Q_P(T_*) = 16\pi\sigma T^4 Q_P(T)$. It is convenient to use polynomial approximations for the size averaged Planck factors.² With these assumptions the mean dust temperature is

$$T = \left(\frac{L_*}{16\pi\sigma R^2} \right)^{1/4} \left(\frac{Q_P(T_*)}{Q_P(T)} \right)^{1/4} = 270 \left(\frac{L_*}{10^6 L_\odot} \right)^{1/4} \left(\frac{500 \text{ km/s}}{v_w} \right)^{1/2} \left(\frac{Q_P(T_*)}{Q_P(T)} \right)^{1/4} \left(\frac{\text{decade}}{t} \right)^{1/2} \text{ K.} \quad (19)$$

The corrections due to the Planck factors are significant and typically increase the expected temperatures by almost a factor of two. Assuming a λ^{-1} emissivity, λL_λ then peaks at $\lambda = 2.9(1000 \text{ K}/T)\mu\text{m}$ and we report this nominal peak wavelength in Table 2 assuming a source with $L_* = 10^6 L_\odot$ and $T_* = 10^4 \text{ K}$. The oldest sources should have SEDs peaking at $24\mu\text{m}$ while the youngest sources should peak in the short wavelength IRAC bands.

2.4. DUSTY Models

In addition to these simple scaling laws, we will model the SEDs using DUSTY (Ivezic & Elitzur 1997, Ivezic et al. 1999, Elitzur & Ivezić 2001), which properly solves for radiation transfer through a spherically symmetric dusty medium. We use models based on either pure silicate or pure graphitic dust from Draine & Lee (1984). DUSTY parametrizes its models by the total optical depth from both absorption and scattering $\tau_V \equiv \tau_{tot} = \tau_{abs} + \tau_{scat}$, while the optical depth in our analytic models is the effective absorption optical depth $\tau_e \simeq (\tau_{abs}\tau_{tot})^{1/2}$ representing the net absorption. At V band, the DUSTY models have total opacities of $\kappa_{tot} \simeq 170$ and $84 \text{ cm}^2/\text{g}$ assuming a bulk density for the dust of $\rho_{bulk} = 3 \text{ g/cm}^3$ and a dust to gas ratio of $X_d = 0.005$ ($\kappa \propto (\rho_{bulk} X_d)^{-1}$), scattering opacities of $\kappa_{scat} = \kappa_{tot} w \simeq 80$ and $72 \text{ cm}^2/\text{g}$, absorption opacities of $\kappa_{abs} = \kappa_{tot}(1-w) \simeq 90$ and $12 \text{ cm}^2/\text{g}$, and scattering albedos of $w = 0.47$ and 0.86 for graphitic and silicate dusts, respectively. Thus, the effective absorption opacities we should use in the analytic models are $\kappa_e = (\kappa_{abs}\kappa_{tot})^{1/2} \simeq 120$ and $31 \text{ cm}^2/\text{g}$, respectively. The effective visual absorption optical depths for a DUSTY model defined by $\tau_{e,V}$ are then $\tau_e = (1-w)^{1/2}\tau_V = 0.73\tau_V$ and $0.37\tau_V$ for graphitic and silicate dusts, respectively, so we should generically find that silicate models require DUSTY model optical depths roughly twice that of graphitic models in order to produce the same net V-band absorption. These distinc-

²For $Q_P(T) \equiv \int da (dn/da) a^2 Q_P(T, a) / \int da (dn/da) a^2$ and the Mathis et al. (1977) distribution $dn/da \propto a^{-3.5}$ with $0.005\mu\text{m} < a < 0.25\mu\text{m}$ assumed by DUSTY we can build an adequate approximation for $Q_P(T)$ as follows. Let $Q_1(T)$ apply for $t = \log(T) < t_0$ and $Q_2(T)$ apply for $t > t_0$ with $\log_{10} Q_i = \sum_{j=0}^3 a_{ij}(t-t_0)^j$ where $a_{10} = a_{20}$ forces continuity at $t = t_0$. For Draine & Lee (1984) graphitic dusts over the temperature range $1 < t < 5$, we find $a_{1j} = -1.967, -1.379, -2.605, -0.641$, and $a_{2j} = -1.967, -1.384, 3.054, -0.940$ with $t_0 = 2.867$, an rms error of 0.021 dex and a maximum error of 0.073 dex. For Draine & Lee (1984) silicate dusts we find $a_{1j} = -1.968, -1.388, -2.612, -0.6434$ and $a_{2j} = -1.968, -1.375, 3.050, -0.940$ with $t_0 = 2.869$, an rms error in 0.035 dex and a maximum error of 0.094 dex.

tions become unimportant in the mid-infrared because the opacities are much smaller, with $\kappa_{tot} \simeq 5.9$ and $1.7 \text{ cm}^2/\text{g}$ at $3\mu\text{m}$ for the graphitic and silicate dusts, respectively, and because the opacity is dominated by absorption as the albedos are only $w \simeq 0.13$.

It is important to remember that the effects of circumstellar dust are quantitatively different from the effects of a foreground, intervening dust screen even for dust with identical physical properties because the geometries have different balances between absorption and scattering (e.g. Goobar 2008). As already noted, the relationship between an apparent visual extinction of A_V and the DUSTY optical depth τ_V is not $A_V = 2.5\tau_V/\ln 10$ but $A_V \simeq 2.5\tau_V(1-w)^{1/2}/\ln 10$ to first order. It is also important to remember that dust contributes to the emission, and that for winds these contributions begin to matter in the near-IR. These differences lead Walmswell & Eldridge (2011) to significantly overestimate the effects of dusty winds on the photometric properties of supernova progenitors on three levels. First, a given amount of mass loss produces less net absorption (by a factor of $(1-w)^{1/2} \simeq 0.4$ for silicates). Second, for the same amount of net absorption at V band, a silicate wind absorbs more strongly at bluer wavelengths and less at redder. Third, the shift to increased emission compared to a dust free star already starts at H-band for a 1500 K dust formation temperature. These issues will be important for our discussion of SN 1961V in §4.

We generally modeled the dust geometry as a shell with a ratio between the inner and outer radii $R_{out}/R_{in} = 2$ and we are generally citing R_{in} as the shell radius because the optical depth is dominated by the inner edge. We experimented with shells where the radius ratio is 1.2 and 4, although in most cases changing the thickness had little effect. The shell is heated by a simple blackbody model of the central star with temperature T_* and luminosity L_* . We tabulated models for both dust types as a function of stellar temperature ($T_* = 5000, 7500, 10000, 15000, 20000, 30000$ and 40000 K), dust temperature ($T_d = 50$ to 1500 K in steps of 50 K) and optical depth ($\tau_V = 0$ to 6 in steps of 0.1 and $\tau_V = 6$ to 30 in steps of 0.5 and $\tau_V = 40$ to 100 in steps of 10). The dust temperature is related to the shell radius and stellar luminosity, so we will usually set the dust temperature based on an estimate of the shell radius given the elapsed time and an estimate of the expansion velocity (Eqns. 12 and 19).

2.5. Asymmetry and Inhomogeneity

While DUSTY addresses any shortcomings of the analytic models for spherical systems, the ejecta probably are not spherically symmetric (as illustrated by the structure of η Carinae). For dust emission, the primary consequence of asymmetry is that the spread in radius with azimuth produces a spread in the dust temperature that is likely far greater than the spread introduced by the finite shell thickness. In our quantitative models we use shells with $R_{out}/R_{in} = 2$ in large part to mimic this effect, although in many cases changes in the shell thickness have few consequences for interpreting the available data. Geometry can produce differences between the apparent optical depths in absorption, as measured by the optical/UV flux, and emission, as measured by the mid-IR flux. The observed optical/UV flux is dominated by scattered photons rather than direct emission along the line of sight, so the two measures will be relatively tightly coupled. In silicate DUSTY models with $R_{out}/R_{in} = 2$, the half-light radii of the total V-band luminosity

are roughly 0.3, 1.2 and $1.5R_{in}$ for optical depths of $\tau_V = 1, 10$ and 100. Because scattering is not strongly forward directed, the surviving optical/UV photons “sample” a large fraction of the ejecta rather than a narrow pencil beam along the line of sight to the source (see, for example, the models of η Carinae by Davidson & Ruiz 1975). As a result, we should not see enormous differences between these two means of estimating the optical depth even in complex geometries.

Complex geometric structures also have only limited effects on the expected evolution of the emission. Consider the optical flux escaping a thin, axisymmetric, expanding shell under the assumption that the photon directions are isotropic at the surface. At some initial time t_0 the shell has optical depth $\tau_0(x)$ in direction $x = \cos \theta$, so the observed flux at later times is essentially

$$\propto \int dx \exp(-\tau_0(x)t_0^2/t^2) \simeq (t/t_0) |\tau_0''(x_{min})|^{-1/2} \exp(-\tau_0(x_{min})t_0^2/t^2) \quad (20)$$

where x_{min} is the direction in which the optical depth is lowest (sum over multiple minima if needed). The pre-factor, which is the effective area over which photons escape (and becomes a constant in the limit that there are no significant optical depth variations over the shell), only makes it harder to combat the geometric evolution of the optical depth. Adding an anisotropic scattering function ($dx \rightarrow g(x)dx$) or making the distribution non-axisymmetric ($\tau_0(x, \phi)$) does not qualitatively change anything because neither changes the temporal scaling of the exponential. Thus, geometry complicates the relationship between optical depth and ejected mass, but does not fundamentally alter the temporal scaling of the optical depth.

Another potential problem is the effect of small scale optical depth fluctuations on the observed “effective” optical depth – when the optical depth is high, the observed optical flux becomes exponentially sensitive to leaks through the optically thick medium, similar to the arguments about super-Eddington winds in Owocki et al. (2004). At least in simulations of a turbulent molecular cloud, Ostriker et al. (2001) found log-normal column density fluctuations with a variance on the order of a factor of 2. While a model of dust radiation transfer through an expanding three dimensional medium with large spatial variations in the optical depth is beyond the scope of this paper, it is instructive to consider a simple model. Suppose the dust optical depth has a log normal distribution about τ_0 with logarithmic fluctuations σ , and we estimate the effective optical depth as

$$\tau_e = -\ln \left[\frac{1}{(2\pi)^{1/2}\sigma} \int_{-\infty}^{\infty} d \ln \tau \exp(-\tau) \exp(-(\ln^2(\tau/\tau_0)/2\sigma^2)) \right], \quad (21)$$

corresponding to averaging the fraction of escaping radiation over the probability distribution of optical depths. If we assume $\sigma = \ln 2$ following the simulations of turbulent molecular clouds, then the effective optical depths for $\tau_0 = 1, 3, 10, 30$ and 100 are $\tau_e = 0.99, 2.3, 4.9, 8.7$ and 14.9, respectively. Reducing the amplitude of the fluctuations σ brings the effective optical depth closer to the mean optical depth, but even if we halve the amplitude to $\sigma = (1/2)\ln 2$, we find $\tau_e = 1.00, 2.7, 7.2, 15.4$ and 30.5. The problem, however, with using clumping to mitigate the optical depth evolution is that the clumping itself generally evolves towards larger density inhomogeneities at later times (e.g. Garcia-Segura et al. 1996, Toalá & Arthur 2011 for stellar winds/shells). While constant inhomogeneities can slow the evolution of the effective optical depth, their growth as the shell expands will greatly accelerate it, to say nothing of the additional acceleration of the evolution produced by the geometric pre-factor in Eqn. 20.

3. Data and Analysis

Table 3 presents our estimates of the Spitzer IRAC (3.6, 4.5, 5.8 and 8.0 μ m) and MIPS 24 μ m fluxes for our targets. We downloaded the Post-Basic Calibrated Data (PBCD) for these programs from the Spitzer archive. These IRAC images are two-times oversampled and have a pixel scale of 0''60, while the MIPS 24 μ m images have a pixel scale of 2''45. Where there were multiple epochs, we aligned and combined the data using the ISIS (Alard & Lupton 1998, Alard 2000) image subtraction package. We also used ISIS to difference image between the available epochs, to search for any signs of variability, and to difference image between the IRAC wavelengths. When we scale and subtract the 3.6 μ m image from the longer wavelength IRAC images, all normal stars vanish to leave only the red stars dominated by dust emission and emission by the interstellar medium (see Khan et al. 2010). This wavelength differencing procedure isolates the relatively rare, dusty stars while eliminating the crowding from the normal stars. Extended PAH emission at 8.0 μ m sometimes cause the procedure to fail. The residual fluxes in the longer wavelength bands are then a good indicator of the dust emission. In some cases our astrometric match is imperfect, but dusty stars are relatively rare so we have chosen to adopt obvious mid-IR sources as the counterparts – in general, rejecting this possibility then requires the transient to have been a true SNe with no surviving star.

We estimated the source fluxes using aperture photometry (the IRAF apphot package). In some cases, especially when the local environment was crowded and the background strongly variable, we would find large variations in the source flux for different choices of the source and sky apertures. For this reason, we measured the fluxes of the sources f_i using the nine combinations of three source apertures (1''2, 1''8, and 2''4) and three sky annuli (2''4-7''2, 7''2-14''4, and 14''4-24''0). For the standard 2''4 aperture we used the standard Spitzer aperture corrections, while the non-standard aperture corrections were derived from bright stars in the images. The larger source apertures more securely determine the source flux while being more sensitive to uncertainties in the sky estimate, while the smaller source apertures require larger aperture corrections but are less sensitive to uncertainties in the sky estimate. We then calculated the mean flux

$$\langle f \rangle = \frac{\sum_i f_i \sigma_i^{-2}}{\sum_i \sigma_i^{-2}} \quad (22)$$

combining all nine flux estimates f_i weighted by their estimated statistical uncertainties σ_i . We estimated the uncertainties as a statistical error σ_0 , defined by the statistical error estimate for the 1''8 radius source aperture and the 2''4-7''2 background annulus, combined with the systematic scatter between the nine flux estimates,

$$\sigma^2 = \sigma_0^2 + \frac{\sum_i (f_i - \langle f \rangle)^2 \sigma_i^{-2}}{\sum_i \sigma_i^{-2}}, \quad (23)$$

to include an estimate of the systematic uncertainties.

In general we could use HST photometry of the sources from the literature. There were two exceptions, the near-IR limits for SN 1999bw and the optical limits for SN 2002bu. Here we estimated the detection limits presented in Table 4 using simple aperture photometry and standard aperture corrections. For the ACS/HRC data the apertures, aperture corrections and zero points were taken from Sirianni et al. (2005),

while those for the NICMOS/NIC2 observations were taken from the NICMOS data handbook.³

Finally, we have been monitoring NGC 2403 (SN 1954J and SN 2002kg/V37) and NGC 3627 (SN 1997bs) in the UBVR bands with the Large Binocular Telescope (LBT) as part of our project to set limits on the existence of failed supernovae (Kochanek et al. 2008). After carrying out standard data reductions, these data were also analyzed with ISIS. The ISIS reference images were analyzed with DAOPHOT (Stetson 1987). Table 5 presents the DAOPHOT magnitudes at the positions of SN 1954J and SN 1997bs in the ISIS reference images and the light curve of SN 2002kg. There is no clearly detected source at the position of SN 1997bs and the source at the position of SN 1954J is known to be composite of several unresolved stars (see below), so these should be regarded as upper limits.

We provide the differential ISIS light curves of SN 1954J and SN 1997bs in Table 6. These are the changes in flux at each epoch relative to the reference image. We present the differential light curves because the absolute fluxes of these sources in the reference image are not known due to crowding. Fortunately, the images are not crowded with variable stars, so any observed variability is almost certainly dominated by a single source. In addition to the ISIS light curves, we can use the subtracted images to visually and quantitatively characterize the variability. In what follows, it is important to realize that all the subtracted images are on the common flux scale of the reference image. First, we try to convolve the images to a standard FWHM corresponding to a Gaussian of dispersion $\sigma_0 = 3$ pixels ($0''.672$) by convolving each image with a Gaussian of width $\sigma^2 = \max(0, \sigma_0^2 - FWHM^2/8\ln 2)$. We then produce images representing the best fit linear model of the time variability of the pixels in each image I_i and the rms residual from this model. If $\Delta t_i = t_i - \langle t_i \rangle$ is the time relative to the average epoch $\langle t_i \rangle$, we have the mean image $\bar{\Delta I} = \langle \Delta I_i \rangle$, the slope image $S = \langle \Delta t_i \Delta I_i \rangle / \langle \Delta t_i^2 \rangle$ and the rms residual image $\langle \sum_i (\Delta I_i - \bar{\Delta I} - S \Delta t_i)^2 (N-2)^{-1} \rangle^{1/2}$. The slope image emphasizes steady trends while the rms image emphasizes more erratic or periodic behavior.

4. Results

We now discuss each object in turn, beginning with a short summary of the properties of the system followed by our new results. Table 1 summarizes the general properties of each transient, and Table 2 summarizes our crude estimates of the ejected mass, the expected optical depths and the peak wavelength of any mid-IR emission. Some of these estimates are very sensitive to the expansion velocity we adopted from Smith et al. (2011) since $\tau \propto v^{-2}$ even for a velocity-independent estimate of the ejected mass. We start with an examination of η Carinae because of the frequency with which it is used as an analogy to the SN impostors. We note, however, that while the physics of its expanding shell should be similar, it had radically different energetics, time scales and (probably) mass budgets from most of the other systems. For example, if the impostors have radiative efficiencies $f \simeq 1$ like η Carinae, they are almost two orders of magnitude less energetic ($\Delta t_{1.5} \nu L_\nu$) and have ejected far less mass (see Table 2). As a result, the optical depths expected for the typical impostor are relatively low and it is difficult to obscure a surviving star for

³http://www.stsci.edu/hst/nicmos/documents/handbooks/DataHandbookv8/nic_ch5.9.3.html

extended periods of time.

4.1. η Carinae

We had to use relatively old data to assemble a global SED for η Carinae similar to what can be obtained for extragalactic systems. We combined the mid-IR observations from 1.65 to $20\mu\text{m}$ of Robinson et al. (1973) from JD 2441517.9 (18 July 1972), with the optical measurements by van Genderen & The (1984) on JD 2442125 (18 March 1974) and the near-IR measurements by Whitelock et al. (1994) on JD 2442491 (19 March 1975). Where they overlap in wavelength, the Robinson et al. (1973) and Whitelock et al. (1994) flux estimates agree and we adopted the average value. We define the measurement epoch by the optical data since the near/mid-IR will evolve much more slowly than the optical, and we use 1 January 1845 as the start of the transient. The resulting SED is in reasonable agreement with that shown in Humphreys & Davidson (1994) for an unspecified epoch. We set the quiescent V band magnitude of the star to be approximately $V = 3$ mag (see the light curve compilation of Fernández-Lajús et al. 2009). This corresponds to a luminosity of $L_* = 10^{6.1}$ ($T_* = 7500$ K) to $10^{6.7}L_\odot$ ($T_* = 20000$ K). We matched the SED in 1974 to the library of DUSTY models, initially ignoring the wavelength range from 2.2 to $5\mu\text{m}$. These wavelengths are energetically less important, and the emission probably comes from a sub-dominant, hotter dust component (e.g. Robinson et al. 1987). We also discuss only the silicate dust models for simplicity because the strong silicate features in the SED cannot be fit by the graphitic models. Each SED is associated with a shell radius which we can turn into an expansion velocity $v_r = r/t$ where t is the elapsed time given in Table 1.

The velocity for η Carinae in Table 1 corresponds to the long axis of the Homunculus, so we use a prior of $v_{out} = 650 \pm 50$ km/s over 124 years (1850 to 1974) for the outer radius. The best fit models prefer a somewhat slower expansion rate of $v_{out} = 460 \pm 30$ km/s for R_{out} even with the prior. The star is hot ($T_* = 20000$ K) and luminous ($L_* = 10^{6.49 \pm 0.02}L_\odot$). The DUSTY optical depth is $\tau_V = 4.5 \pm 0.3$, which corresponds to an estimated shell mass of order $\log(M\kappa_{100}/M_\odot) \simeq 0.67 \pm 0.06$ that is consistent with standard estimates (Smith et al. 2003). As we see in Fig. 2, the fit to the SED is reasonable in both the optical and far-IR, but fails badly in the near-IR. Unlike most cases we consider, the SED of η Carinae is clearly inconsistent with our standard assumption of a shell with $R_{out}/R_{in} \equiv 2$.

As an experiment, we embedded DUSTY inside a Markov Chain Monte Carlo (MCMC) driver and used this to fit a model and then estimate uncertainties for the full SED of η Carinae including the near-IR data points. We varied T_* , τ_V , the dust temperature T_{in} at the inner edge, and the shell thickness R_{out}/R_{in} , where the location of R_{out} was constrained by a prior on the velocity of $v_{out} = R_{out}/(124 \text{ years}) = 600 \pm 50$ km/s for a time line from 1850 to 1974. The solution has $T_* = 22000 \pm 1000$ K, $\tau_V = 4.8 \pm 0.2$, $T_{in} = 687 \pm 16$ K and $R_{out}/R_{in} = 5.7 \pm 0.5$, where it is the greater thickness that lets the model better fit the near-IR data compared to our standard models (see Fig. 2). Derived parameters are the stellar luminosity $L_* = 10^{6.53 \pm 0.02}L_\odot$, $R_{in} = 10^{16.61 \pm 0.03}$ cm and $R_{out} = 10^{17.37 \pm 0.03}$ cm. The inner and outer radii correspond to expansion velocities of 100 and 600 km/s, respectively, for material ejected circa 1850. The mass estimate is now $\log(M\kappa_{100}/M_\odot) \simeq 0.47 \pm 0.04$. Compared to the more restricted models, there is little change in the stellar properties or the

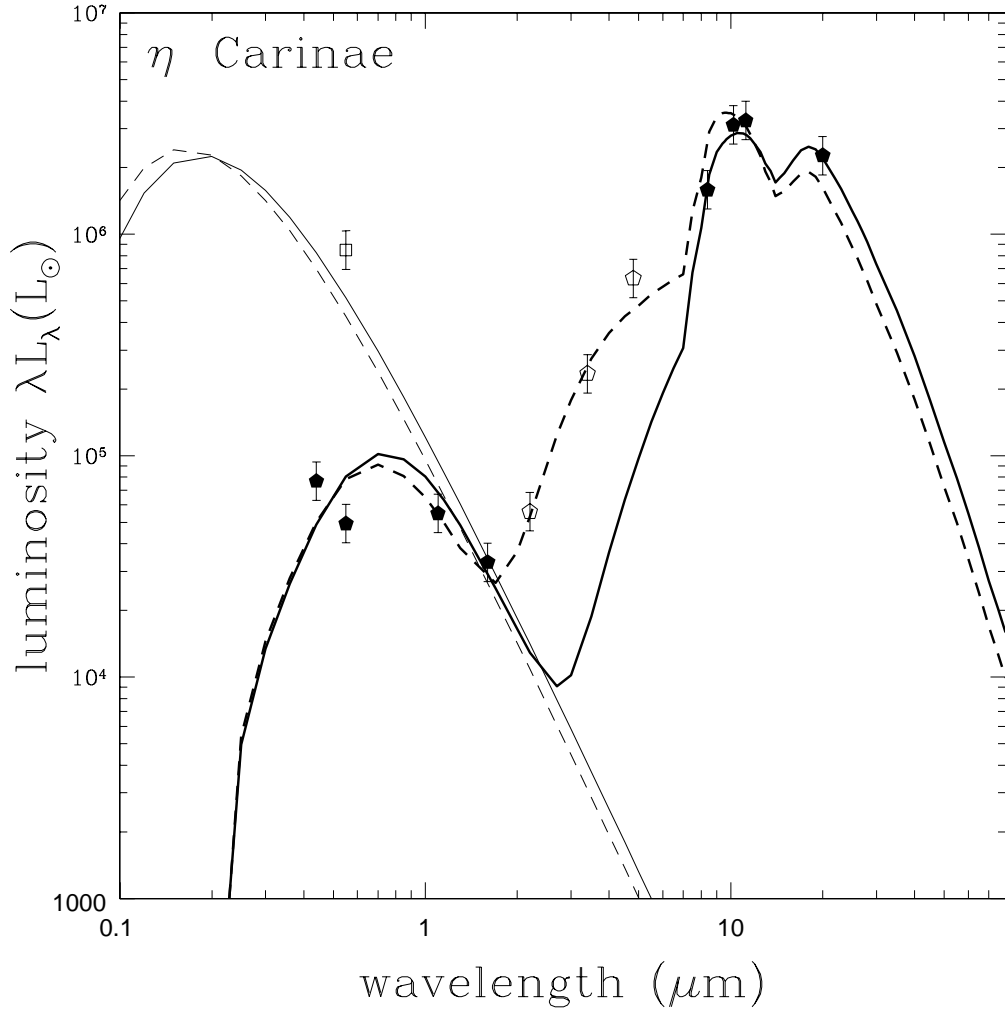


Fig. 2.— The spectral energy distribution of η Carina circa 1974. The pentagons show the optical, near-IR and mid-IR luminosities from van Genderen & The (1984), Whitelock et al. (1994) and Robinson et al. (1973). The solid curves show the standard model fits where the shell thickness $R_{out}/R_{in} \equiv 2$. These models are only fit to the filled pentagons and excluded the near-IR data (the open pentagons). The dashed curves show the better fits obtained by allowing a thicker shell with $R_{out}/R_{in} = 5.7$ in 1974. These models were fit to the full SED. The thick curves show the model SEDs, while the thin curves show the black body models of the intrinsic stellar SED fit to the estimated quiescent V-band magnitude (open square).

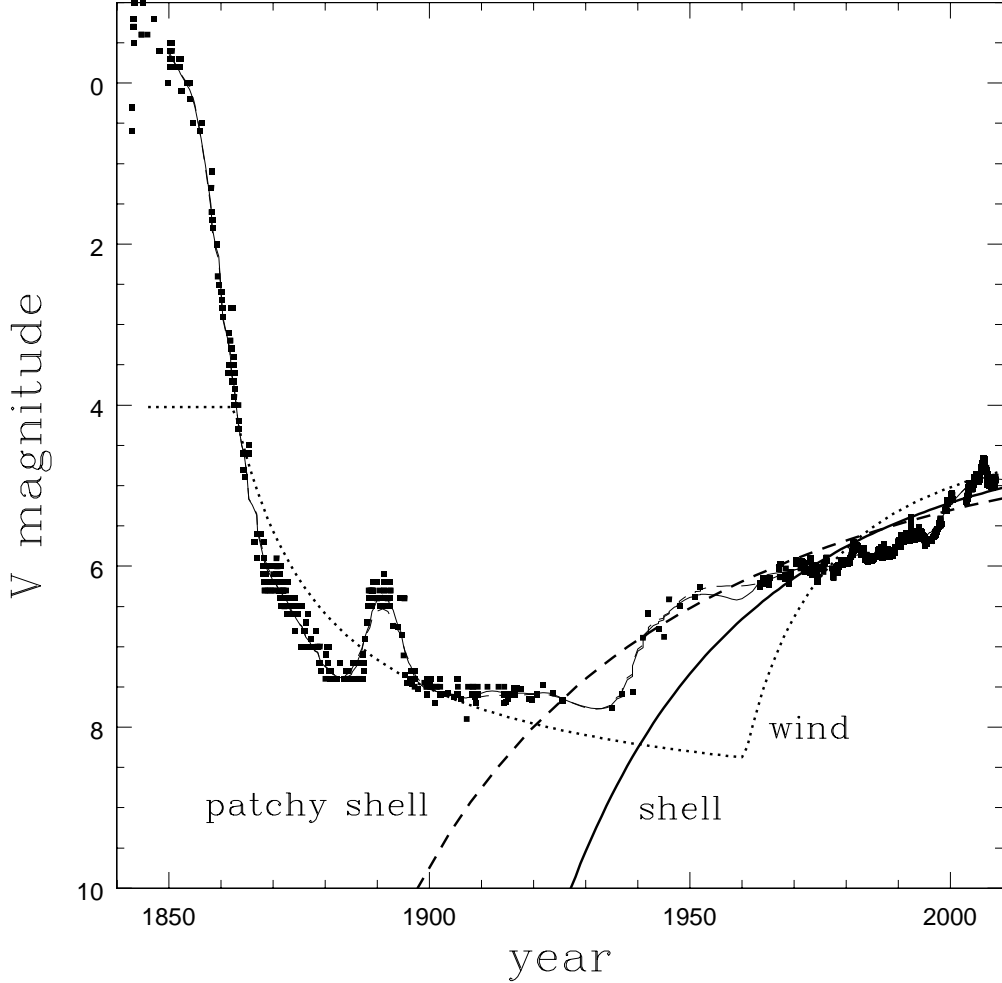


Fig. 3.— V band light curve (points) of η Carinae from the tabulation by Fernández-Lajús et al. (2009). The curves show 5 models for the light curves. The thick solid (dashed) curves show the evolution expected if we simply evolve the optical depth of the $T_* = 20000$ K SED model (the $R_{out}/R_{in} = 2$ model in Fig. 2) using the geometric $\tau \propto t^{-2}$ scaling of the optical depth for a thin expanding shell assuming it is homogeneous (inhomogeneous following Eqn. 21). While these models assume a fixed stellar luminosity and temperature, no physically plausible changes in these variables can overcome the optical depth evolution of these models and reproduce the observed light curve. The thick dotted line shows a wind model (Eqn. 14) with fixed luminosity and temperature where dust formation (somewhat arbitrarily) begins in 1862 and ends in 1943. The differences are now small enough that they can be explained by variations in luminosity and temperature. The thin solid and dashed lines, which largely overlap and are hidden by the data points, are the non-parametric models of the light curve from Fig. 4 for the homogeneous and inhomogeneous absorption models.

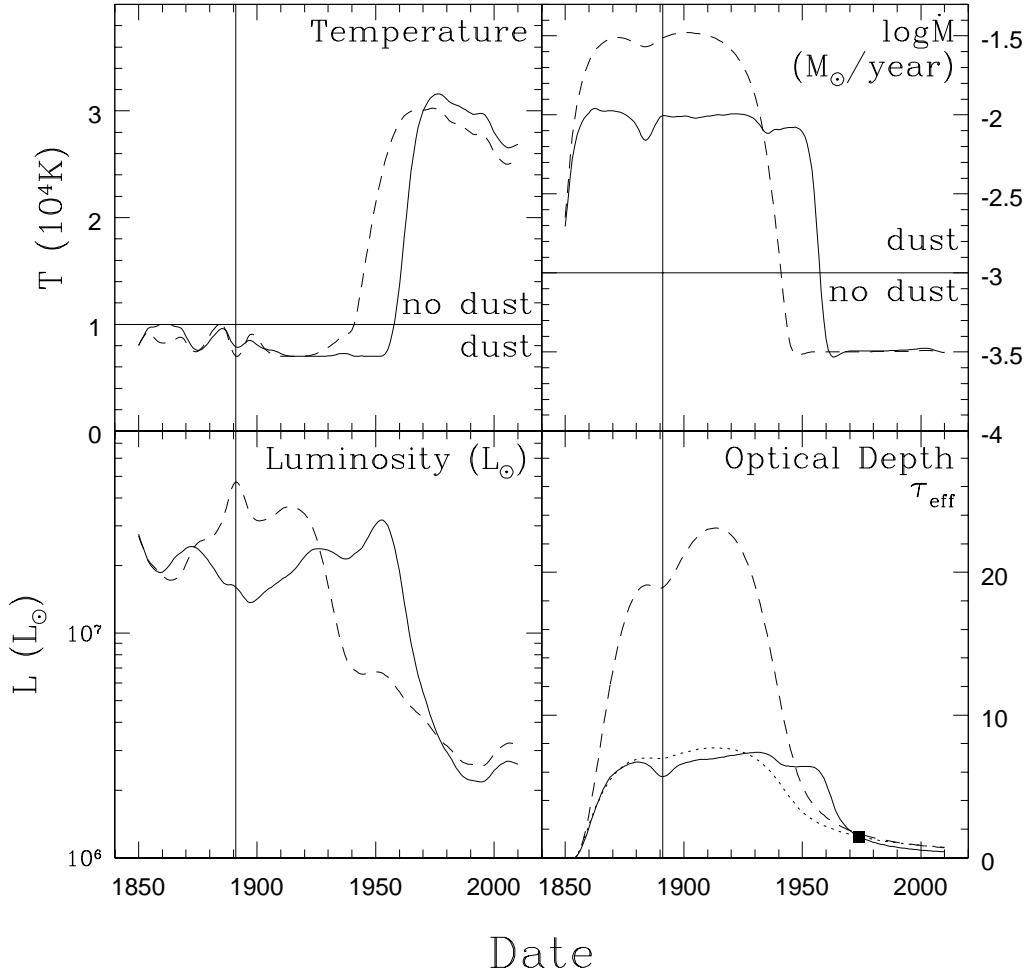


Fig. 4.— Physical properties of the non-parametric models for the V-band light curve of η Carinae. The panels on the left show the stellar luminosity (bottom) and temperature (top), while the panels on the right show the mass loss rate (top) and the resulting effective absorption optical depth (bottom). The solid (dashed) lines are for the homogeneous (inhomogeneous, Eqn. 21) dust models. In the optical depth panel, the dotted line shows the net optical depth of the inhomogeneous model after correcting for the inhomogeneities. The horizontal lines in the temperature and \dot{M} panels show the maximum temperature and minimum mass loss rates for dust formation. The vertical line at 1890 marks the secondary peak in the light curve. The solid point in the optical depth panel indicates the value inferred from the SED models in 1974 to which the models are normalized.

optical depth, but results for velocities, radii and thicknesses are clearly closely related and can produce factor of ~ 2 uncertainties in the absence of a well-sampled SED.

Fig. 3 shows the V band light curve compilation for η Carinae from Fernández-Lajús et al. (2009). There is a bright peak circa 1850 followed by a steep decline to a plateau from 1850 to 1940 punctuated by the shorter eruption from 1890-1900, followed by a steady rise to the present day (e.g. van Genderen & The 1984). We now know from Rest et al. (2011) that the star was surprisingly cool ($T_* \simeq 5000$ K) during the Great Eruption, which is quite different from the other sources we discuss. This light curve represents the total optical emission of the source rather than the direct unabsorbed emission from the star (see, e.g., Martin et al. 2006). Superposed is the expected light curve assuming the $\tau \propto t^{-2}$ scaling of an expanding shell, and it is a reasonable model of the trend since roughly 1960. At earlier times it fails catastrophically. The “leaky” dust model of Eqn. 21, where the optical flux is dominated by light leaking out through lower opacity channels in an inhomogeneous medium, can extend the agreement to roughly 1920 but then fails.

As shown in Eqn. 18, the only variables available are the luminosity $L(t)$, temperature $T(t)$ and optical depth $\tau_{e,V}(t)$. The light curve $L_V(t)$ implies a strict upper bound on the effective absorption optical depth for a given total luminosity

$$\tau_{e,V} < -\ln\left(\frac{L_V}{G_{max}L}\right) < 6 + \ln\left(\frac{L}{5 \times 10^6 L_\odot}\right) \quad (24)$$

because the V-band luminosity is maximized at the temperature $T_{max} = 6700$ K where $G_{max} = G(x_{max}) = 0.74$. Raising (or lowering) the temperature from T_{max} lowers the limit on the optical depth and even an order of magnitude increase in the luminosity only raises the limit by $\Delta\tau_{e,V} = \ln 10 = 2.3$. This limited ability to use luminosity and temperature to balance changes in optical depth means that the V-band light curve very tightly constrains the history of η Carinae. In particular, it makes it impossible to explain the light curve with dust formed in a thin shell created during a short-lived (\sim decade) eruption in the mid-nineteenth century – no plausible variation in luminosity and temperature is large enough to compensate for the changing optical depth (see Fig. 3). The light curve does, however, have the qualitative properties of a long lived wind, as illustrated in Fig. 3 by a model based on Eqn. 15 for a wind where dust formation commenced around 1862 and ended in 1943. It is not a perfect fit, but it is now close enough to the light curve that the differences can be explained by changes in luminosity and temperature.

Fig. 3 also shows two models that fit the light curve almost exactly. As detailed in the Appendix, the model uses a non-parametric luminosity, temperature and mass loss history to fit the light curve and the optical depth estimate from the SED fits while trying to maximize the overall mass loss. We used an expansion velocity of 500 km/s and a dust formation time of $t_f = 5$ years corresponding to a dust formation radius of roughly $R_f = 7 \times 10^{15}$ cm. Fig. 4 shows the evolution of the physical parameters in this model – it is a long-lived wind with $\dot{M} \simeq 10^{-2} M_\odot/\text{year}$ ejecting roughly $1 M_\odot$ of material in the dust creating phases. If we use our “leaky” dust model (Eqn. 21), we can triple the mass lost, but the general structure of the solution is unchanged. As discussed in §2.5, inhomogeneities in the ejecta primarily affect this balance between optical depth and associated mass rather than the temporal scaling of the optical depth and the observed flux.

The star in outburst is luminous but relatively cool, with conditions that favor the formation of dust

in the wind (Kochanek 2011b). While not imposed on the models, dust formation ceases just as the star reverts to its lower luminosity, quiescent hot state, and this transition in luminosity and temperature removes the mismatch between the light curve and the simple wind optical depth model seen in Fig. 3 – the initial rapid drop in optical depth is balanced by the rapid drop in the V-band flux as the star returns to a higher temperature. Available evidence is that the spectrum of the star was consistent with this relatively cool (F star) state over the dust formation period, and while the implied B–V colors of our model are somewhat redder than interpretations of the historical data, they come far closer to these estimates of the observed color than any model with the mass ejection occurring over a short period circa 1850 (see the discussion in van Genderen & The 1984). The brightening circa 1890 can be reproduced using either a fluctuation in the luminosity or in the rate of mass loss. While geometry is clearly an important factor, we note that a constant velocity wind starting in 1850 and ending in 1950 has $R_{out}/R_{in} = 5.2$ in 1974, matching the best fitting SED models (but only $R_{out}/R_{in} = 2.7$ in 2010).

No attempt to drive the solution to a significantly shorter duration was successful because no physically plausible luminosity and temperature variations can balance the optical depth evolution. As we discussed in §2.5, this conclusion should hold for radially expanding shells of arbitrary angular structure short of a long lived hole through the dust directly to the star (which is known not to have been present from the 1950’s to the present day, see Martin et al. 2006). The only remaining possibility is to identify a process which causes the (effective) opacity to increase with time in order to balance the expansion. It cannot be continued dust formation because particle growth shuts off very quickly (within $2R_f$) and dust in η Carinae appears to have grown to sizes where further growth reduces rather than increases the opacity (Smith et al. 2003). Forming very large grains ($a \simeq 10\mu\text{m}$) initially and then steadily breaking them up into smaller dust grains, would provide a mechanism, because the opacity scales as $\kappa \propto 1/a$ provided $a \gtrsim 0.3\mu\text{m}$ (e.g. Draine 2011). The dynamic range in opacity from steadily shrinking a from $10\mu\text{m}$ to $0.3\mu\text{m}$ is large enough to balance the expansion, but there is no obvious mechanism to drive this evolution. Alternatively, if the ejecta evolved from being inhomogeneous to homogeneous, the effective optical depth for a given mean optical depth would rise and could balance the expansion. This makes little sense because ejected material generally evolves from (locally) homogeneous to inhomogeneous (e.g. Garcia-Segura et al. 1996, Toalá & Arthur 2011), and thus exacerbates rather than ameliorates the optical depth evolution problem.

In summary, our models can fit the properties of η Carinae to the accuracies we need for the extragalactic sources. The SED models are roughly consistent with both the physical scale and ejected masses derived in more detailed studies. As was already known, the visual light curve is consistent with the declining optical depth of an expanding shell at late times but not at early times. We are able to successfully model the complete light curve, but are driven to models with a relatively steady mass loss rate from 1850-1950 that are at variance with most interpretations of η Carinae’s history. Since the only real assumptions of the model are steady, smooth expansion and dust mass conservation, it is not easy to escape this conclusion. It is not obvious to us that this conflicts with any other observations of η Carinae, but even if it did, we would really simply face a stalemate of contradictions since the standard model provides no plausible, quantitative explanation of the light curve. Further investigation of these issues is beyond the scope of our present goals, but they inform analysis of our subsequent results.

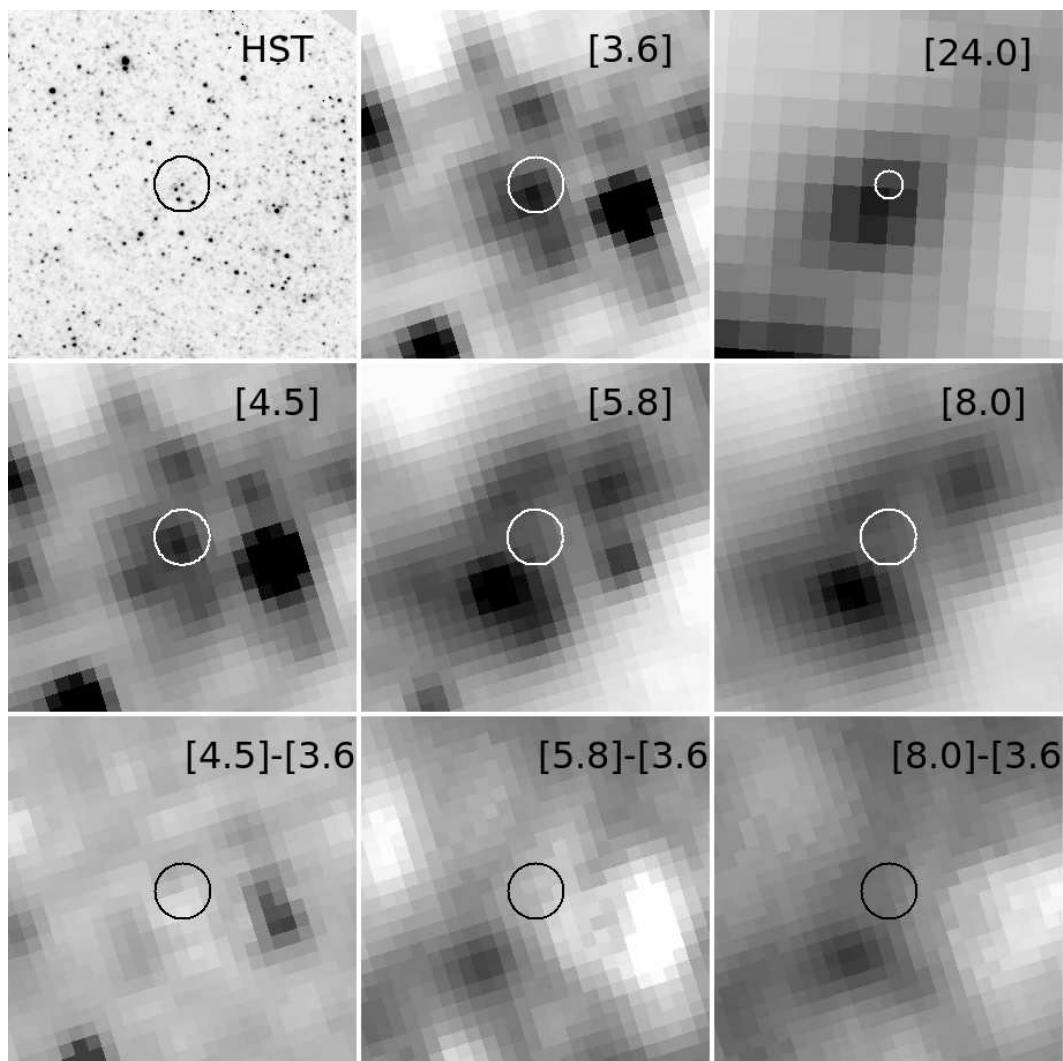


Fig. 5.— The environment of SN 1954J. The top left, middle and right panels show the HST, 3.6 and $24\mu\text{m}$ images of the region. The center left, middle and right panels show the 4.5, 5.8 and $8.0\mu\text{m}$ images. The bottom left, middle and right panels show the $[4.5]-[3.6]$, $[5.8]-[3.6]$ and $[8.0]-[3.6]$ wavelength-differenced images. The circles in all panels have a radius of $1''.2$ in this and all subsequent figures. Similarly, the $24\mu\text{m}$ panel shows a region two times larger than the other panels. Star #4, which Van Dyk et al. (2005) identify with SN 1954J, is the upper right star of the trapezoid of four bright stars seen inside the circle on the HST image.

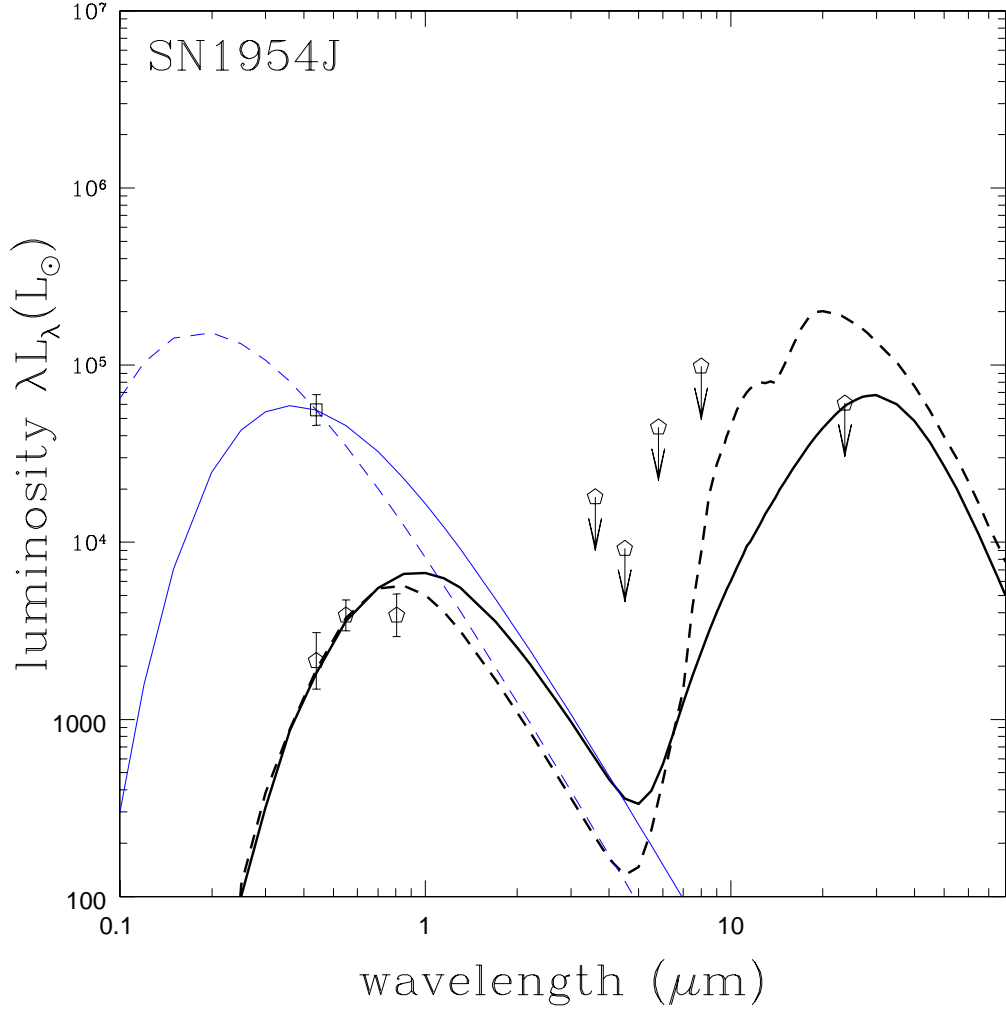


Fig. 6.— The spectral energy distribution of SN 1954J. The open pentagons are the optical magnitudes of star #4 from Van Dyk et al. (2005) and our mid-IR limits. The open square is the estimated magnitude in quiescence prior to 1949. The thin solid (dashed) curve shows the the SED of a $T_* = 15000$ K, $L_* = 10^{4.9}L_\odot$ ($T_* = 20000$ K, $L_* = 10^{5.3}L_\odot$) progenitor normalized to match the pre-transient B band magnitude. The thick solid (dashed) curves show graphitic (silicate) DUSTY models where the optical depths of $\tau_V = 3.0$ ($\tau_V = 5.3$) were selected to fit the optical magnitudes of star #4 while remaining under the mid-IR limits for an expansion velocity of roughly 820 km/s.

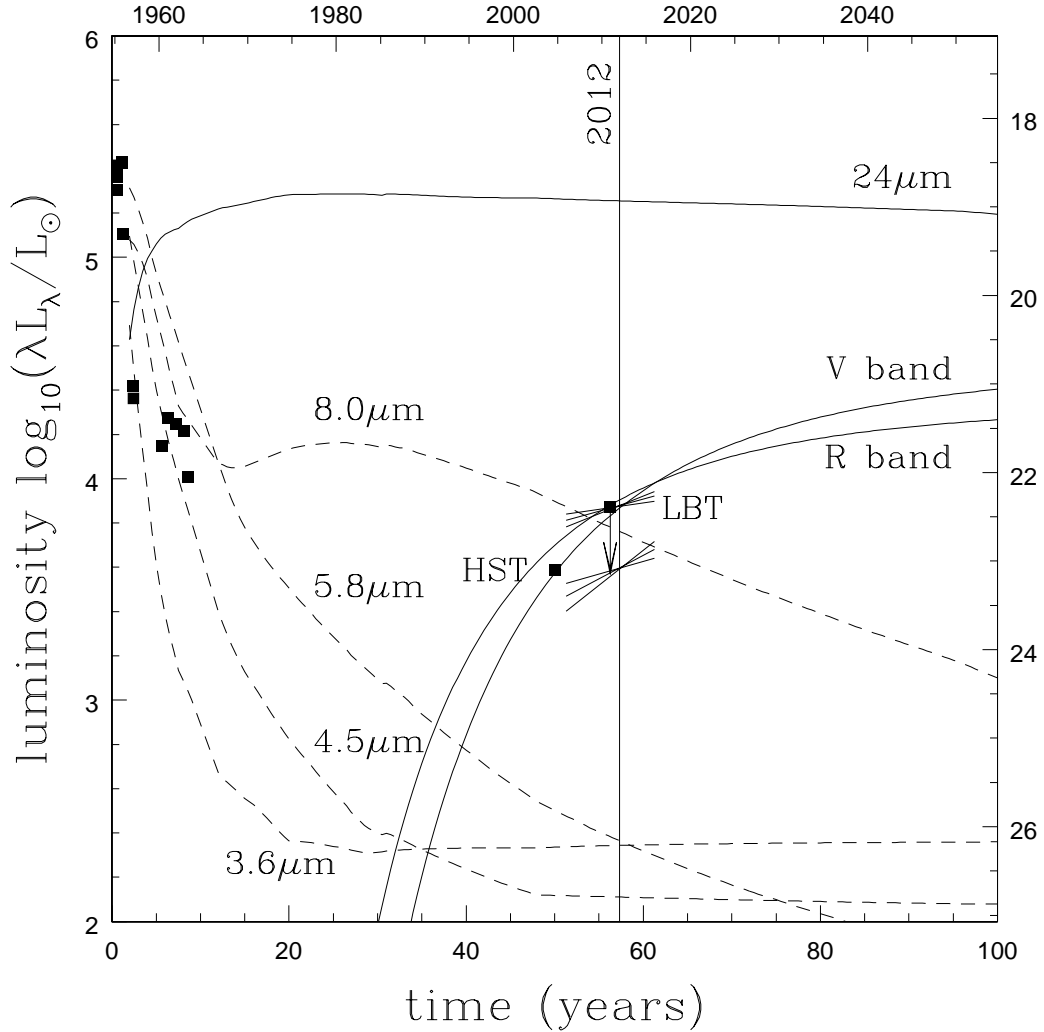


Fig. 7.— Expected light curves for SN 1954J. The curves show the expected V and R band (solid), IRAC bands (dashed) and $24\mu\text{m}$ (solid) light curves normalized by the best fit silicate SED model. The early time points are the B band data from Tammann & Sandage (1968), the point labeled HST is the V-band flux from late 2004 from Van Dyk et al. (2005), and the arrow labeled LBT is the R-band upper limit from our LBT observations. The “wedges” at the LBT epoch show the formal slope of the light curve and its uncertainties when normalized either at the LBT or HST magnitude – the lower the reference flux, the larger the implied fractional change.

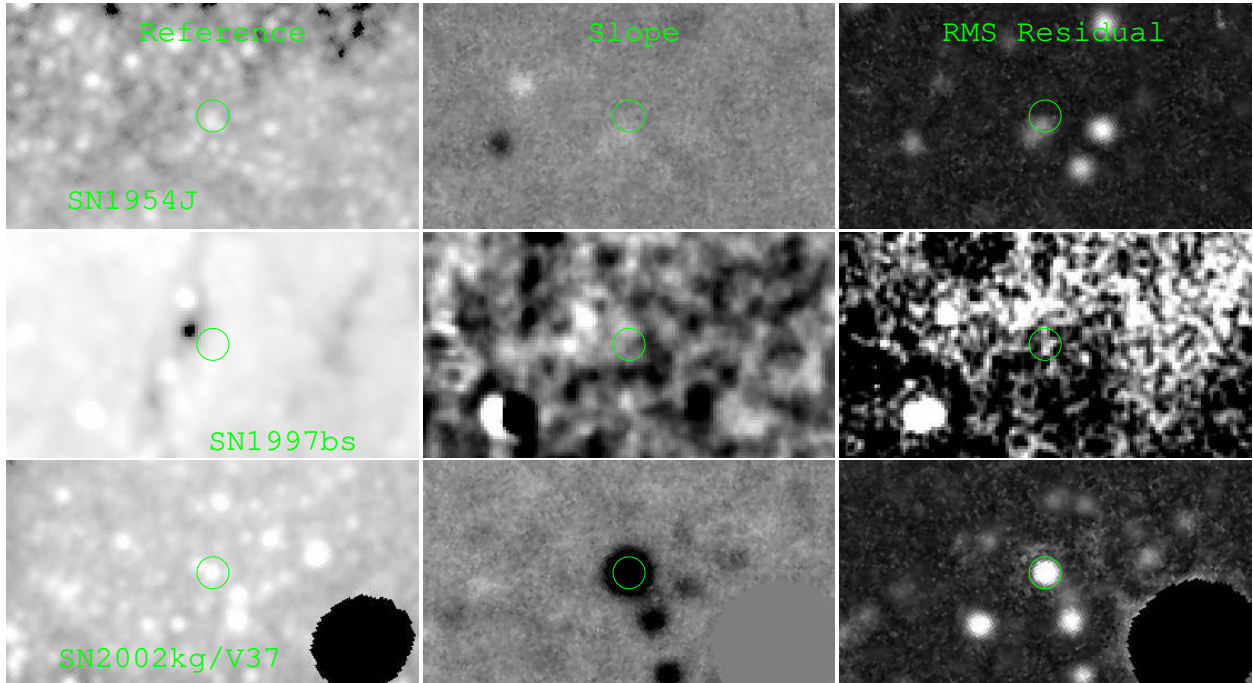


Fig. 8.— LBT R band data for SN 1954J (top), SN 1997bs (middle) and SN 2002kg/V37 (bottom). The left panel shows the R band reference image for each source, the middle panel is the Slope image, and the right panel is the RMS image as defined in §3. The $2''.24$ (10 pixel) diameter circle in each panel marks the source position. Each type of image is on the same gray scale. The reference image is on a logarithmic scale. The Slope image is on linear scale covering $\pm 10^3 L_{\odot}/\text{year}$ (about 10% the slope observed for SN 2002kg/V37). Similarly, the RMS residual image is on a linear scale from 0 to $10^3 L_{\odot}$ in (the rms residuals for SN 2002kg/V37 are about twice this).

4.2. SN 1954J/V12 in NGC 2403

SN 1954J (Tammann & Sandage 1968; Humphreys et al. 1999) is considered a classic example of an extragalactic η Carinae-like eruption. Originally identified as the luminous blue variable star V12, it was relatively quiescent prior to 1949 with a blue photographic magnitude of $m_{pg} \sim 21$. It became increasingly variable from 1949 to 1954 with a largely unobserved eruption in late 1954, mainly noted as a steep decline from an observed peak magnitude of ~ 16.5 to be about a magnitude fainter than its pre-eruption flux by 1960. We adopt 1 September 1954 (JD 2434987) as the nominal date of the peak. Smith et al. (2001) searched for a surviving star using ground-based optical and near-IR images, and identified a candidate source roughly 10 times fainter than the pre-outburst star with signs of a near-IR (K-band) excess (U, B, V, R, I, J, H and K of 22.5 ± 0.3 , 22.7 ± 0.2 , 21.9 ± 0.3 , 21.1 ± 0.2 , 20.9 ± 0.2 , 20.3 ± 0.2 , 19.9 ± 0.2 , and 19.0 ± 0.2 mag). The optical observations were taken in February 1999 and the near-IR in April 2000. They modeled the spectral energy distribution (SED) as a roughly 10^4 K black body with ~ 1.5 mag of visual extinction. Van Dyk et al. (2005) found that this candidate source broke up into 4 stars at the resolution of HST, and they identified star #4 as the surviving star based on its $H\alpha$ emission and an SED consistent with a hot ($T_* = 30,000$ K), luminous ($L_* \simeq 10^6 L_\odot$) supergiant obscured by $A_V \simeq 4$ mag of dust. The optical magnitudes of star #4 are $B = 24.3 \pm 0.4$, $V = 23.1 \pm 0.2$ and $I = 22.2 \pm 0.3$, respectively. The HST observations were taken 17 August 2004, and Van Dyk et al. (2005) also had optical observations from 20 October 1996 and 13 October 1997. Both Smith et al. (2001) and Van Dyk et al. (2005) attribute the extinction to material ejected during the eruption. A spectrum of the $H\alpha$ emission from the region shows broad $H\alpha$ emission, with a line width of order 700 km/s (Smith et al. 2001). For comparison, if we correct the progenitor magnitude following Smith et al. (2001) and then subtract the fluxes from the contaminating stars found by Van Dyk et al. (2005), the progenitor luminosity is $L_* = 10^{4.9}$ ($T_* = 7500$ K) to $10^{5.4} L_\odot$ ($T_* = 20000$ K).

The mid-IR observations of SN 1954J/V12 were made over a 5 year period from 2004 to 2009. We found no evidence for time variability associated with the source, so we analyzed the combined data. As we can see in Fig. 5, the mid-IR emission in the vicinity of SN 1954J comes from multiple sources and there is a ridge of PAH emission extending over the region at the longer wavelengths. There appears to be a (probably composite) source at the position of SN 1954J in the shorter wavelength 3.6 and $4.5\mu\text{m}$ bands and no identifiable source at the longer bands. The ratio of the 3.6 and $4.5\mu\text{m}$ fluxes is very close to that for a Rayleigh-Jeans spectrum, $F_{4.5}/F_{3.6} = 0.64 \pm 0.26$ compared to $(3.6/4.5)^2 = 0.64$. If we scale and subtract the $3.6\mu\text{m}$ flux from the $4.5\mu\text{m}$ flux, the estimated dust emission at $4.5\mu\text{m}$ is only 0.00 ± 0.02 mJy, consistent with the absence of any sources in the wavelength-differenced images in Fig. 5. Thus, the observed emission is probably dominated by the composite emission of the normal stars seen in the HST images and we simply treat the mid-IR fluxes as upper bounds on the emission from SN 1954J.

Fig. 6 shows the SED of this system along with two representative SEDs for graphitic and silicate dusts. Since there was no evidence of time variability in the mid-IR data, this should be viewed as the SED at the time of the HST observations in late 2004, 50 years after the peak. We constrained the unobscured SED to match the pre-1949 B-band (m_{pg}) luminosity, and the obscured SED to fit the HST photometry of star #4 and the mid-IR limits. We used a velocity prior of $v_{in} = 700 \pm 70$ km/s for the expansion of the inner

edge of the shell, although the results change little if we apply it to the outer edge instead. Fig. 6 shows the two best fits including the velocity prior. The graphitic models fit somewhat better because the silicate peak tends to exceed the limit on the $24\mu\text{m}$ luminosity. The graphitic models prefer $T_* = 10000$ or 15000 K with $L_* = 10^{5.0\pm 0.1} L_\odot$, a DUSTY optical depth of $\tau_V = 3.1 \pm 0.2$ and an inner dust radius of $R_{in} = 10^{16.99\pm 0.04}$ cm, corresponding to a velocity of 620 ± 60 km/s. The silicate models prefer a somewhat hotter $T_* = 15000$ or 20000 K star with $L_* = 10^{5.3\pm 0.1} L_\odot$, $\tau_V = 5.2 \pm 0.3$ and an inner dust radius of $R_{in} = 10^{17.05\pm 0.06}$ cm corresponding to a velocity of 720 ± 100 km/s. The effective absorption optical depths of the two models are the same, with $\tau_{e,V} \simeq 2$ (see the discussion in §2.4). If we use the limits on the mid-IR emission from the wavelength-subtracted images, the graphitic models are in conflict with the $4.5\mu\text{m}$ limit. The star cannot be as hot or luminous as proposed by Van Dyk et al. (2005) without being in gross conflict with the mid-IR limits – the present day luminosity of the star has to be well below the minimum luminosity of $L_* \gtrsim 10^{5.8} L_\odot$ sometimes used for LBVs (e.g. Smith et al. 2004). The ejecta masses needed to have these optical depths 50 years after the transient are high, with $\log(M_{\kappa_{100}}/M_\odot) \simeq 0.57 \pm 0.08$ and 0.92 ± 0.12 for the graphitic and silicate models. These are an order of magnitude or more larger than the mass scales estimated in Table 2, and would require a radiated to kinetic energy ratio of $f \ll 1$ that is indicative of an explosively driven transient. Producing the absorption with a $\dot{M} \sim 10^{-3} M_\odot/\text{year}$ wind and the same velocity could produce these optical depths using far less mass, but it would produce an SED peaking in the short wavelength IRAC bands that is ruled out by the data.

Fig. 7 shows the expected visual and mid-IR light curves of this system normalized by the best fit silicate model to the SED. For each epoch we interpolated through our tabulated sequences of $R_{out}/R_{in} \equiv 2$ DUSTY models assuming fixed stellar properties, a 700 km/s expansion velocity, and the $\tau \propto 1/r^2$ geometric scaling of the optical depth. At the present time, only the $8\mu\text{m}$ band should show any variability in the mid-IR (2%/year), while the $24\mu\text{m}$ flux is nearly constant and the shorter wavelength IRAC bands are too faint compared to the level of contamination from other sources. Thus, it is not surprising that we found no mid-IR variability. Fig. 7 also shows the B band photometry of the early phases from Tammann & Sandage (1968). Even though these fluxes presumably represent sums over the unresolved stars, the star seems to take almost ten years to fade, which seems long compared to reasonable dust formation time scales of less than one year (Eqn. 3). While the data are too sketchy for a detailed model, the early light curve is only consistent with forming enough dust to produce the proposed obscuration in 2004 if the mass loss occurred over a very extended period of time (decades).

If the absorption is now due to an expanding shell, the optical fluxes should be rising by 5% (R-band) to 15% (U-band) per year as shown in Fig. 7. We have been monitoring NGC 2403 with the LBT, and Fig. 8 shows the reference, slope and rms images (see §3) of the region around SN 1954J. At the estimated position of SN 1954J, DAOPHOT estimates $R = 22.4$ mag, consistent with the earlier ground based observations by Smith et al. (2001). For an expanding shell, this is also roughly the expected magnitude of the star given the expected brightening from the epoch of the HST observations, so the LBT observations are probably inconsistent with such a brightening because the measured flux includes the contaminating emission from the nearby unresolved stars (see Fig. 5). There is little evidence for variability at this location in either the slope or the rms images. Formally, we estimate an R-band slope of $(180 \pm 30) L_\odot/\text{year}$ with an rms residual

of $740L_{\odot}$, but the detections are not overwhelmingly convincing in this or the other bands. As shown in Fig. 7, the rate of change is also flatter than expected for an expanding shell of material. Thus, the LBT data argues against an expanding shell. Note that this argument is independent of the actual expansion velocity as the optical depth evolution depends only on the elapsed time once the scale of the optical depth is set by the photometric model (see Eqn. 15).

The preponderance of the evidence for SN 1954J/V12 is inconsistent with the standard picture. Van Dyk et al. (2005) make a clear case for identifying star #4 as the counterpart to SN 1954J/V12 because it seems to be the only plausible source of the broad $H\alpha$ line emission. The mid-IR flux limits allow star #4 to be a surviving star obscured by an expanding, dusty shell, but the intrinsic stellar luminosity and temperature have to be quite low, $T_* \simeq 15000$ K and $L_* \simeq 10^{5.0}-10^{5.3}L_{\odot}$. The SED does not allow the present day obscuration to be due to a wind, but the lack of optical variability and the early-time light curve appear to be inconsistent with the presence of an expanding shell formed in a short transient. Moreover, the $\gtrsim M_{\odot}$ of ejecta needed to produce the present day optical depth is difficult to reconcile with a radiatively driven ejection mechanism given the low luminosity and short duration of the transient. Fully characterizing the spectral energy distribution of the candidate star and continued monitoring should clarify the nature of this source.

4.3. SN 1961V in NGC 1058: Dead and Loving It!

In Kochanek et al. (2011) we carried out a similar study of SN 1961V in NGC 1058, arguing that the lack of any mid-IR emission indicated that SN 1961V was a real, if peculiar, Type II_n supernova, a conclusion supported by Smith et al. (2011) on energetic grounds. Van Dyk & Matheson (2011) recently argued against this conclusion, so we include a brief discussion of it here. Up to minor differences, Van Dyk & Matheson (2011) obtain the same mid-IR limits as the analysis in Kochanek et al. (2011). They significantly revised the earlier HST data analyses, settling on a V band magnitude of $V \simeq 24.7 \pm 0.2$ mag for the surviving star. They then model the available data assuming low metallicity, hot (30000 K) stellar models with foreground Galactic extinction to derive $A_V \simeq 2$ mag (beyond the Galactic contribution) and a luminosity $L \simeq 10^{6.0}L_{\odot}$. Thus, one part of their argument is to make the surviving star roughly three times fainter than the typical estimates for the progenitor star used by Kochanek et al. (2011), arguing that the star was already in outburst in the decades before the transient. Their estimate of the absorption is completely consistent with our results since producing an absorption corresponding to $A_V = 2$ with the standard silicate DUSTY models requires exactly the value used by Kochanek et al. (2011), $\tau_V = 4.5$ (see the discussion in §2.4). Thus, the luminosity and optical depth estimates are basically mutually consistent, and in reality the only way Van Dyk & Matheson (2011) found to rescue the impostor hypothesis was to have essentially no dust in the ejecta.

They still, however, require dust, so they put it all in the foreground as an additional intervening $A_V \simeq 2$ dust screen,⁴ but they do not then consider the consequences of this model for the inferred properties of the

⁴They put it so close to the star (1 pc) that it contributes the long wavelength emission in their Figure 4, but this is unimportant

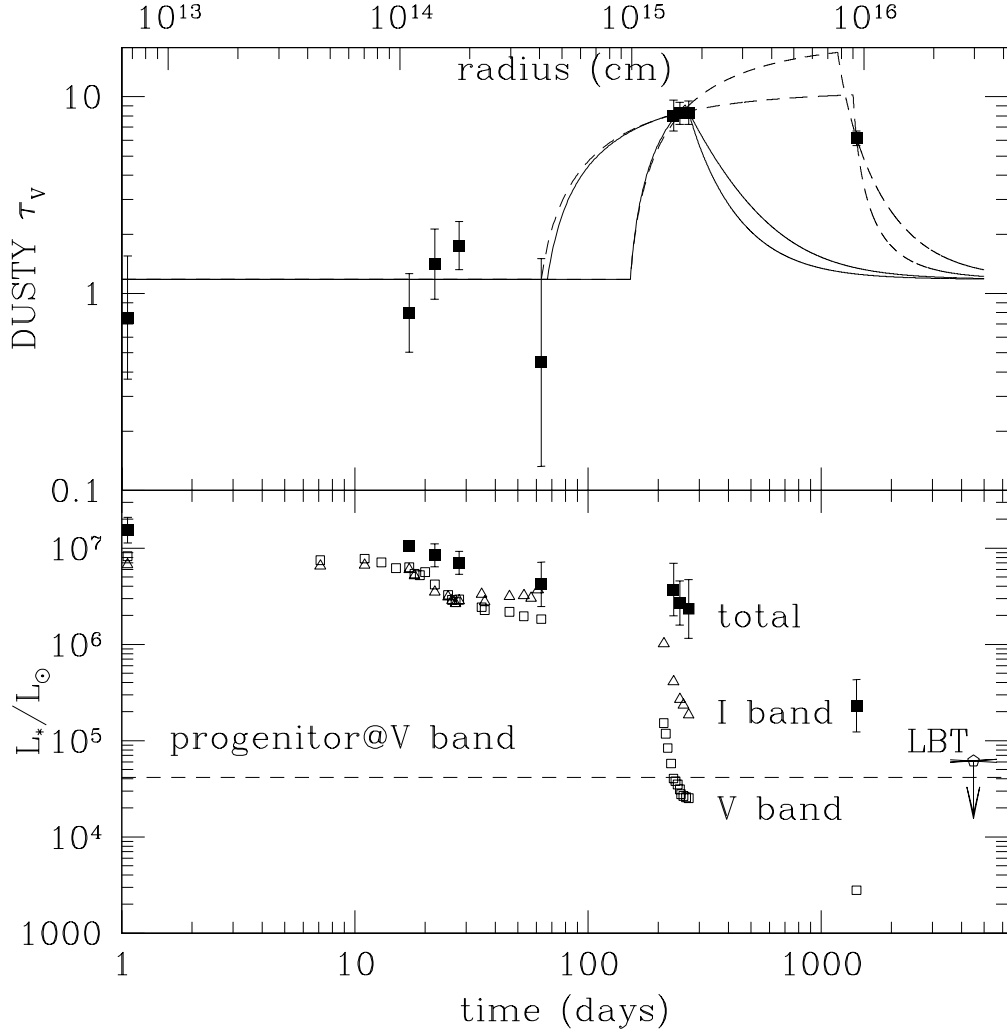


Fig. 9.— Evolution of SN 1997bs. The lower panel shows the evolution of the estimated total (filled squares), I band (open triangles) and V band (open squares) luminosities as compared to the V band luminosity of the progenitor (dashed line). The LBT point should be viewed as an upper limit. The lines through the point indicate the limits on the rate of change of the V-band luminosity from the LBT data. The upper panel also shows the evolution of the silicate optical depth τ_V . The points are the results of DUSTY fits to the SED which are then modeled as a constant plus a finite duration wind (Eqn. 14). The solid curve ignores the final HST epoch and terminates the mass ejection as soon as possible, while the dashed curve includes the final HST epoch. Two time scales for the onset of dust formation are shown, where the earlier time scale corresponds to a very high dust formation temperature and the later time scale corresponds to normal assumptions. Note the rapidity of the decline in the optical depth when the wind ends. The upper radius axis assumes an ejecta velocity of 765 km/s following Table 2.

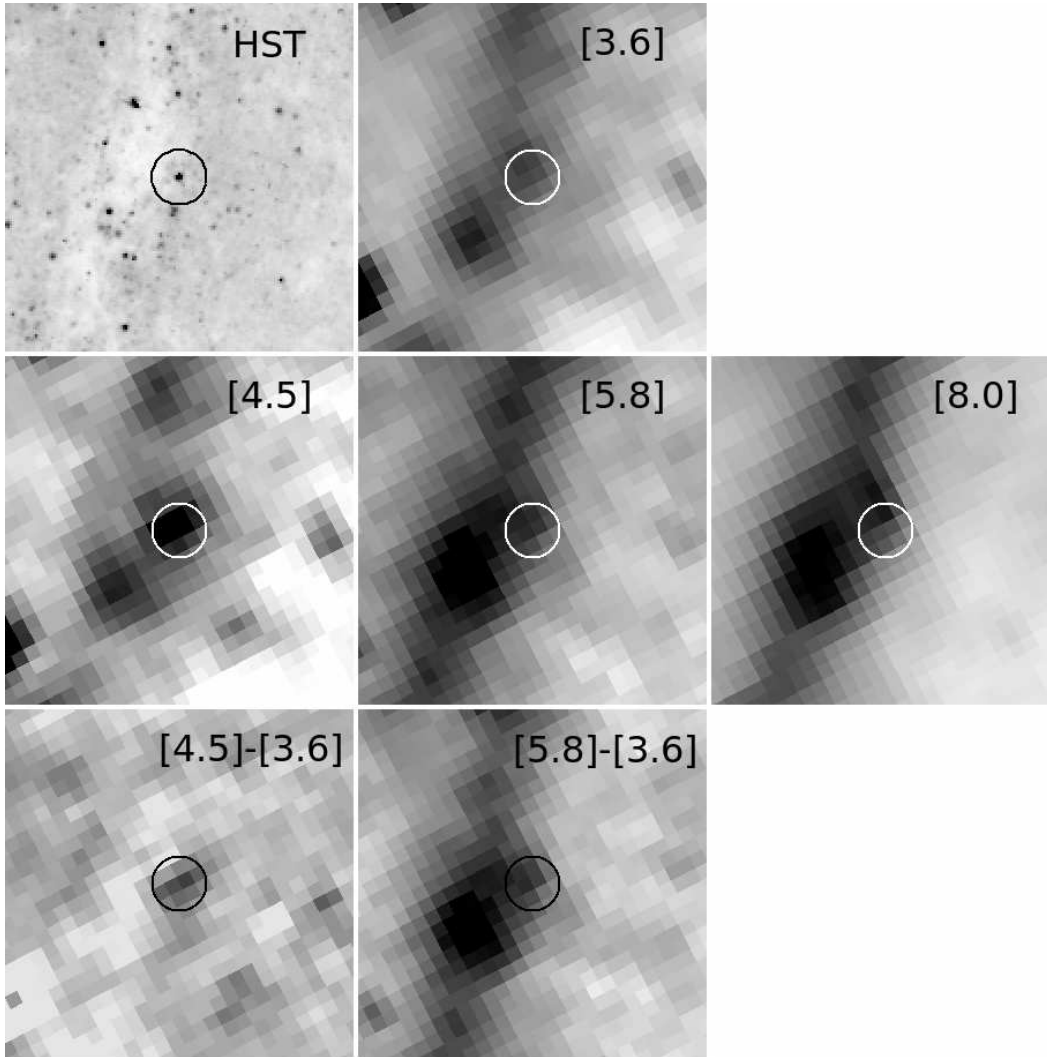


Fig. 10.— The environment of SN 1997bs. The top left and middle panels show the HST and $3.6\mu\text{m}$ images of the region. The HST image was taken during the transient. The center left, middle and right panels show the 4.5 , 5.8 and $8.0\mu\text{m}$ images. The bottom left, middle and right panels show the $[4.5]-[3.6]$ and $[5.8]-[3.6]$ wavelength-differenced images. There is no $24\mu\text{m}$ data and the wavelength-differencing procedure failed for the $[8.0]$ image. A $1''.2$ radius circle marks the position of the transient.

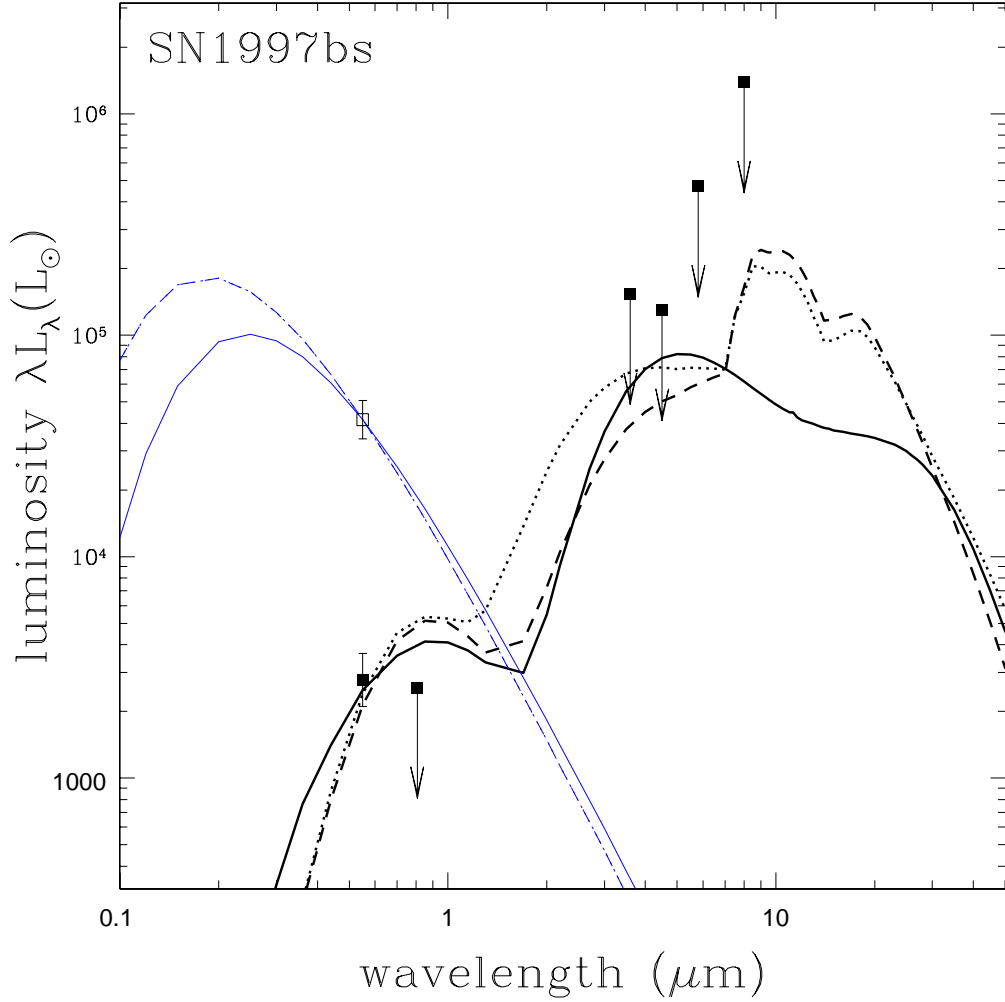


Fig. 11.— The spectral energy distribution of SN 1997bs. The open square shows the progenitor flux estimate from Van Dyk et al. (1999). The filled squares show the optical fluxes in 2001 from Li et al. (2002) and our limits on the mid-IR fluxes. The graphitic shell model (solid lines) has a $T_* = 15000$ K, $L_* = 10^{5.1} L_\odot$ progenitor (thin line) obscured by a $\tau_V = 3.5$ shell with the inner edge expanding at 740 km/s. The silicate shell model (dashed lines) has a $T_* = 20000$ K, $L_* = 10^{5.4} L_\odot$ progenitor (thin line) obscured by a $\tau_V = 6.5$ shell expanding at 680 km/s. The dotted curve shows a silicate wind model with an inner edge temperature of 1000 K. All the models have some conflict with the Li et al. (2002) I-band upper limit, and these are severe for wind models with hotter inner-edge dust temperatures.

progenitor and the transient. First, the progenitor moves from having $m_B \simeq 18$ and $B-V \simeq 0.6$ ($T \simeq 6000$ K) to $m_B^{corr} \simeq 15.4$ and $(B-V)_{corr} \simeq 0$ ($T > 10000$ K). This corresponds to a shift from $M_B \simeq -12$ and $M_{bol} \simeq -12$ to $M_B^{corr} \simeq -14.6$ and $M_{bol}^{corr} \simeq -15$ at a temperature that is no longer characteristic of a (great) LBV eruption ($T \sim 7000$ K, Humphreys & Davidson 1994). Moreover, if the progenitor properties were already extreme, they are now bizarre even if interpreted as a star in a multi-decade long outburst ($L_* \simeq 10^8 L_\odot$ emitting 10^{50} ergs/decade). Similarly, SN 1961V at peak was already as bright as a typical Type II SN, $M_B \simeq -17$, but with the additional foreground extinction it actually peaked at $M_B^{corr} \simeq -20$, making it unusually bright even for a Type II supernova (see Li et al. 2011). There is also a similar bluewards shift in the estimated temperature/color. The total radiated energy rises from $\simeq 10^{49.6}$ ergs to $10^{50.8}$ ergs, well over an order of magnitude larger than η Carinae (e.g. Humphreys & Davidson 1994). In short, forming no dust in the ejecta and instead placing it in the foreground certainly allows an impostor to evade the arguments of Kochanek et al. (2011), but at the price of enormously strengthening the energetic arguments of Smith et al. (2011) that it must have been a supernova. We discussed having no dust as an alternative (if unlikely) solution in Kochanek et al. (2011), but argued this then required a very hot ($T_* \sim 10^5$ K) surviving star so that it would be faint in the optical due to bolometric corrections rather than dust in order to avoid these problems. As a result, we see no reason to revisit our conclusions in Kochanek et al. (2011) in light of Van Dyk & Matheson (2011) – this is an ex-star.

4.4. SN 1997bs in NGC 3627

SN 1997bs was the first SN transient (1997 April 15, JD 2450693) discovered by the LOSS survey (Treffers et al. 1997) and was classified as a Type II_n (Van Dyk et al. 2000). It peaked at $V \simeq 17$ and then faded to $V \simeq 23.5$ over 9 months. Van Dyk et al. (1999) identified a candidate progenitor with $V \simeq 22.86 \pm 0.16$ mag, making the late time emission significantly fainter than that of the progenitor. The progenitor magnitude corresponds to a luminosity of $L_* = 10^{4.8}$ to $10^{5.4} L_\odot$ for the temperature range $T_* = 7500$ K to 20000 K. As discussed in Van Dyk et al. (2000), the color evolution of the transient is peculiar, with a rapid evolution to the red that is indicative of dust formation. In Fig. 9 we show DUSTY silicate dust estimates of the optical depth and luminosity evolution based on the optical fluxes and limits, where we have used a $\log T_* = 3.875 \pm 0.2$ (± 0.4) prior on the temperature during (after) the transient. At the peak, the models require a modest optical depth, $\tau_V \simeq 1$, but after a few months the optical depth starts to rise rapidly, almost reaching $\tau_V \simeq 10$ after 9 months before starting to fall. Also note that the duration and energetics of the transient are very different after correcting for the dust extinction – far from fading rapidly to below the flux of the progenitor in the first year, as suggested by the optical light curves, the total luminosity is roughly constant at $3 \times 10^6 L_\odot$. After almost 4 years, Li et al. (2002) found that the source had continued to fade while becoming bluer rather than redder, with $V \simeq 25.8 \pm 0.3$ and $I > 25$ in early 2001.

Fig. 10 shows the mid-IR images of the region from 2004. There are no clear mid-IR detections, although the proximity of the source to a dust lane and the extended PAH emission makes it difficult to

to our discussion.

search for faint dusty point sources even in the wavelength-differenced images. There may be a point source present in the $4.5\mu\text{m}$ images, but most of its flux vanishes in the wavelength differenced images. We do not feel there are any significant detections and we view our aperture photometry results as upper limits. This leads to the late time SED of SN 1997bs shown in Fig. 11. Here we combine the optical fluxes in 2001 from Li et al. (2002) with the limits from the 2004 Spitzer observations. This should be viewed as characteristic of the optical epoch. When the optical depth is large, the visual fluxes are exponentially sensitive to the optical depth while the mid-IR fluxes are relatively insensitive to the optical depth and primarily affected by the weaker and slower dependence of the dust temperature on radius. The optical fluxes in 2001 are both fainter than the progenitor at V band, and bluer than the transient in their V–I color.

We modeled this SED by normalizing the DUSTY models to the $V = 22.86 \pm 0.16$ magnitude of the progenitor, and then fitting the fainter Li et al. (2002) optical magnitudes. There is no difficulty finding models with expansion velocities of $v_w = 765$ km/s as illustrated in Fig. 11. The star is not very luminous, with $L_* = 10^{5.1 \pm 0.2}$ and $10^{5.3 \pm 0.2} L_\odot$ for the graphitic and silicate models, and preferred temperatures of $T_* = 15000$ and 20000 K, respectively. If we drop the flux of the progenitor from the fits, still lower luminosities are allowed. The DUSTY optical depths are $\tau_V = 3.5 \pm 0.3$ and 6.0 ± 0.5 where, as usual, the silicate models have higher total optical depths but the two models have comparable effective optical depths $\tau_{e,V}$. The results including the mid-IR limits are consistent with the earlier estimates using only the optical data. For our standard opacities, these correspond to ejected masses of $\log(M_{\kappa,100}/M_\odot) = -1.4 \pm 0.1$ and -1.2 ± 0.1 , respectively, that are somewhat larger than the estimates in Table 2. Unlike SN 1954J, the mid-IR limits are weak enough to allow reasonable fits with a steady wind rather than an ejected shell provided the dust temperature at the inner edge is rather cool ($T \lesssim 1000$ K), and we show an example in Fig. 11.

This latter point may be crucial because the optical depth history in Fig. 9 is not consistent with a short duration transient in 1997. In our discussion of η Carinae, the problem was that a shell of material with the present day optical depth would be too optically thick at earlier times. Here the problem is that a shell with the optical depth observed in the first year would be too optically thin to obscure the star in 2001. For a steady mass loss rate, the optical depth is dominated by the inner edge, $\tau \propto 1/R_{in}$ with $R_{in} \simeq R_f$ set by the dust formation radius (Eqn. 13). When dust formation stops, the time scale for the optical depth to drop is only $t_f \simeq R_f/v_w$ which is far too rapid. We can illustrate this by fitting the optical depth model from Eqn. 15 to the optical depth history, including an additional constant optical depth τ_c to model any additional foreground or distant circumstellar dust. Fig. 9 shows two examples producing reasonable fits. The first model has $\Delta t = 202$ days, $t_f = 67$ days, $\tau_0 = 9.8$ and $\tau_c = 1.2$, while the second has $\Delta t = 109$ days, $t_f = 152$ days, $\tau_0 = 18.9$ and $\tau_c = 1.2$. We do not include error estimates because we only seek to make a qualitative point. The key point point is the rapid collapse of the optical depth at time $\Delta t + t_f$ when the last of the ejecta reaches R_f . By the time of the later HST, LBT and/or Spitzer observations, the optical depth should be negligible. Sustaining the optical depth requires sustaining the mass loss. For example, the evolution including the optical depth estimate for 2001 can be fit using $\Delta t = 1309$ days, $t_f = 63$ days, $\tau_0 = 9.5$ and $\tau_c = 1.2$, or $\Delta t = 1026$ days, $t_f = 152$ days, $\tau_0 = 17.8$ and $\tau_c = 1.2$, as also shown in Fig. 9. Once again, the optical depth goes into a steep decline on time scale t_f after time $\Delta t + t_f$.

We illustrated this for two different values of t_f in order to discuss whether the possible rise in optical

depth after one month can also be due to dust formation in the ejecta. The models with $t_f = 152$ days were chosen to have $R_f = t_f v_w \simeq 10^{15}$ cm for an expansion velocity of $v_w = 765$ km/s (Table 1) and a dust formation temperature near $T_d \simeq 1500(L/10^6 L_\odot)^{1/4}$ K. The problem for the models with early dust formation at $t_f = 67$ days is that they must form dust at unphysically high temperatures $T_d \simeq 2200(L/10^6 L_\odot)^{1/4}$ K. Dust formation in the ejecta after only a few weeks implies still higher temperatures and must be impossible. Since only progenitors heavily obscured by dust have high enough wind densities to reform dust in a pre-existing wind (see Kochanek 2011a), this strongly suggests that the very early-time color changes are due to changes in temperature or the presence of emission lines. The larger color changes of the later phases are too large to be explained by anything other than dust.

We have also been monitoring NGC 3627 with the LBT. As with SN 1954J, we lack a clear detection of the individual star and report the DAOPHOT photometry for the estimated position of SN 1997bs in Table 5 and the difference imaging light curves in Table 6. With $V = 22.44$ mag, the DAOPHOT magnitude is consistent with the progenitor flux but really represents an upper bound since the measured flux cannot represent that of a single isolated star (compare Fig. 10 and Fig. 8). If we treat the estimates as measurements, the best fits are for relatively low luminosities $L_* \simeq 10^{4.8} L_\odot$ and temperatures $T_* \simeq 8000$ K with no dust (except Galactic), but none of the models are statistically consistent with the data. All we can be certain of is that if the star is not obscured, it is not very luminous. With five R-band epochs spread over 3.7 years, we see no evidence for variability, as shown in Fig. 8. The estimated slope of the R-band light curve is $(0 \pm 260)L_\odot/\text{year}$ with an rms residual of $1100L_\odot$ – if the star is there, its variability is remarkably low ($\lesssim 2\%$). The two models shown in Fig. 9 predict changes at V-band of 1-4% over the period of the LBT observations, so the lack of variability is marginally consistent with the model.

In short, the standard picture of SN 1997bs as a brief eruption leading to a surviving star obscured by the ejecta from the transient cannot be correct in its details. First, while the optical peak of the transient was short, 45 days (Table 1), the luminosity remained high for at least 9 months, as did the period of high mass loss. Second, keeping the progenitor obscured either at the time of the HST observations in 2001 or during our later LBT observations requires the high mass loss rate ($\dot{M} \sim 10^{-3} M_\odot/\text{year}$) to have continued for a still longer period of time, possibly even to the present day. In this scenario, the star identified with SN 1997bs by Li et al. (2002) probably has to be an unassociated star because matching it to the progenitor from Van Dyk et al. (1999) requires the SED of a hot star ($T_* > 10^4$ K) and dust cannot form in the presence of the soft UV radiation produced by such hot stars (see Kochanek 2011a). A cooler $T_* \simeq 7500$ K star that would facilitate dust production is strongly inconsistent with the limit on the V–I color from Li et al. (2002). The true optical depth would be higher, and the true surviving star is faint and hidden by the Li et al. (2002) source.

If the star found by Li et al. (2002) genuinely is the surviving star, then the most likely scenario is that the eruption did end sometime between 1998 and 2001, the optical depth did collapse as seen in Fig. 9, and the star is actually unobscured in 2001. It is fainter and bluer than the progenitor because of a change in photospheric temperature rather like the scenario proposed by Goodrich et al. (1989) for SN 1961V where an LBV switches from a cooler S Doradus phase to its normal hot state. We should note, however, that the progenitor of SN 1997bs appears to be significantly fainter than the typical LBV. One can generate

additional scenarios, but resolving the nature of SN 1997bs depends on obtaining better data to tightly measure or constrain the present day SED in the optical, near and mid-IR.

4.5. SN 1999bw in NGC 3198

There are few details on SN 1999bw. It was discovered by LOSS (Li 1999, 15 April 1999, JD 2451284) and classified as a Type II_n SN similar to SN 1997bs based on the narrow Balmer line widths (Garnavich et al. 1999, Filippenko et al. 1999). The transient peaked at $V \simeq 18.4$ mag and then faded to $V \simeq 24$ after roughly 600 days (Li et al. 2002). Smith et al. (2011) appear to reject the Li et al. (2002) detection due to an un-discussed change in the estimated position, and instead assign a limit of $F555W > 26.7$ mag (3σ) with further non-detections in October 2006 ($F606W > 27.7$ mag) and April 2008 ($F606W > 27.8$ and $F814W > 26.8$ mag). Very few observations were obtained near the peak, although Smith et al. (2011) note that the $B-V \simeq 0.8$ color was suggestive of foreground or circumstellar extinction. Sugerman et al. (2004) reported detecting it in all 4 IRAC bands in May 2004, at flux densities of 0.02 ± 0.01 , 0.04 ± 0.01 , 0.11 ± 0.02 and 0.19 ± 0.04 mJy in the [3.6], [4.5], [5.8] and [8.0] bands, corresponding to a 450 K black body with luminosity of $10^{6.2} L_{\odot}$ (their reported flux at our adopted distance from Table 1) and a black body radius of 1.6×10^{16} cm that corresponds to an expansion velocity $v_{ej} \simeq 1000$ km/s. If we fit their estimates with a DUSTY model of a hot star completely obscured by silicate dust, so there is no escaping flux from the star, the best fit is for a dust radius of 2×10^{16} cm with a luminosity of $10^{6.0} L_{\odot}$ and inner/outer edge dust temperatures of 800/200 K. Our fits to the Spitzer data are broadly consistent with Sugerman et al. (2004). There are no constraints on the progenitor of SN 1999bw. As shown in Fig. 12, the source is easily seen in the mid-IR (2004-2008) but with no signs of an optical counterpart (2001-2008).

In agreement with Smith et al. (2011), if we fit the optical SED obtained at the transient peak, the models require moderate extinction independent of the assumed temperature. For silicate DUSTY models we find $\tau_V \simeq 2.5$ for $T_* = 10^4$ K and $L_* \simeq 10^{7.3} L_{\odot}$. The temperature is not well-constrained by the data, so cooler temperatures allow lower optical depths and luminosities with the reverse for higher temperatures. Without near/mid-IR data to constrain the dust temperature, this can be either foreground or circumstellar extinction. If this dust was circumstellar, then SN 1999bw peaked in the mid-IR rather than the optical, similar to the 2008 NGC 300 transient (Kochanek 2011a).

Fig. 13 shows the evolution of the SED from 2004 to 2008. Here we combine the optical limits from Smith et al. (2011) with our infrared estimates from Tables 3 and 4. We use the 2001 optical limit as a bound in 2004 and 2005 and the 2005 $24\mu\text{m}$ limit as a bound in 2001, as the most likely evolution given the available data is to fade in the optical and brighten in the far-IR. Clearly at some point between the transient peak and 2001 the system formed large quantities of dust and became a mid-IR dominated transient even if it was not one at peak. The graphitic models provide modestly better fits, but the parameters for the two dust types are generally similar. Fig. 13 also shows the probability-weighted mean graphitic SED models and the dispersion around them.

Without any optical detections or a progenitor flux, the models simply demand that the optical depth is

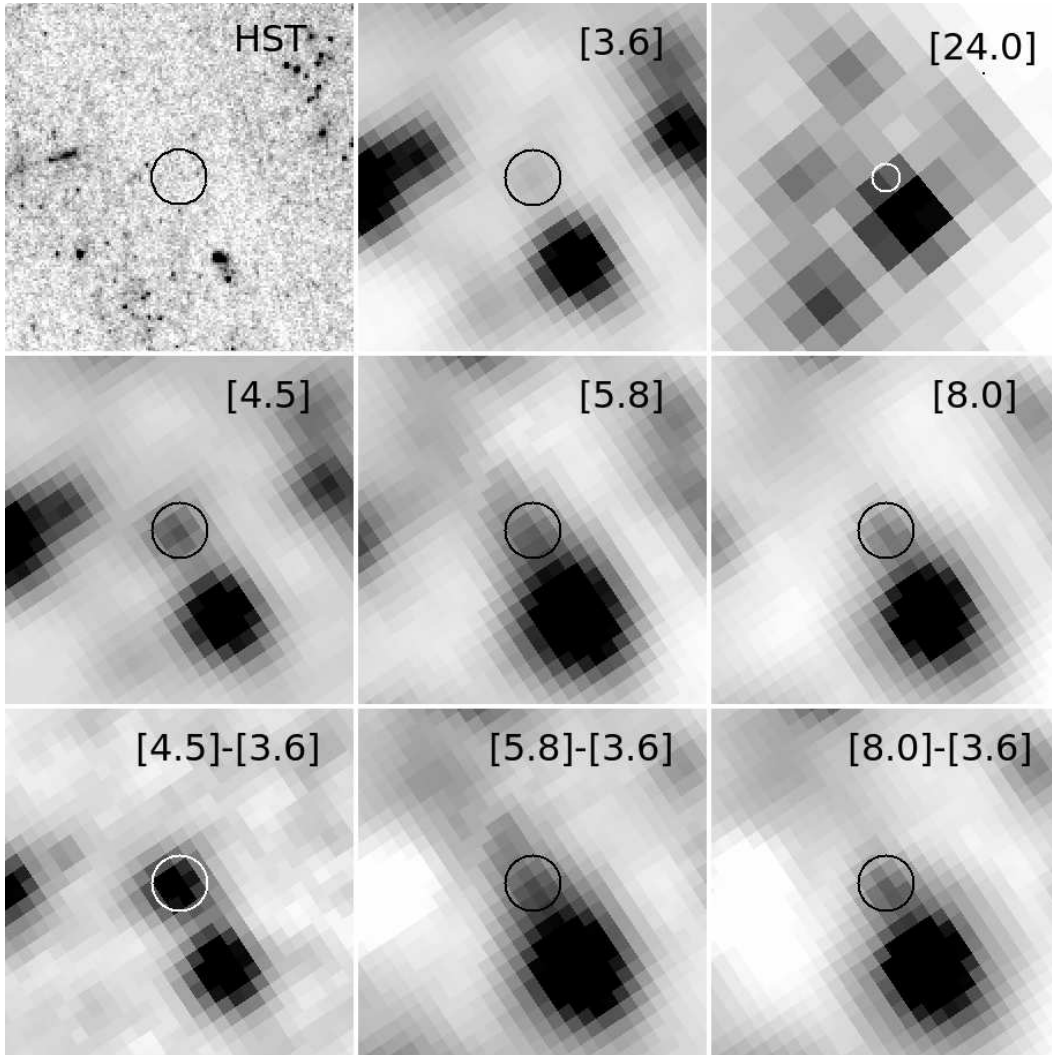


Fig. 12.— The environment of SN 1999bw. The top left, middle and right panels show the HST, 3.6 and $24\mu\text{m}$ images of the region, where the angular scale of the $24\mu\text{m}$ image is twice that of the other panels. The center left, middle and right panels show the 4.5, 5.8 and $8.0\mu\text{m}$ images. The bottom left, middle and right panels show the $[4.5]-[3.6]$, $[5.8]-[3.6]$ and $[8.0]-[3.6]$ wavelength-differenced images. A $1''.2$ radius circle marks the position of the transient. The HST image is from January 2001 while the mid-IR images are the averages of the available epochs.

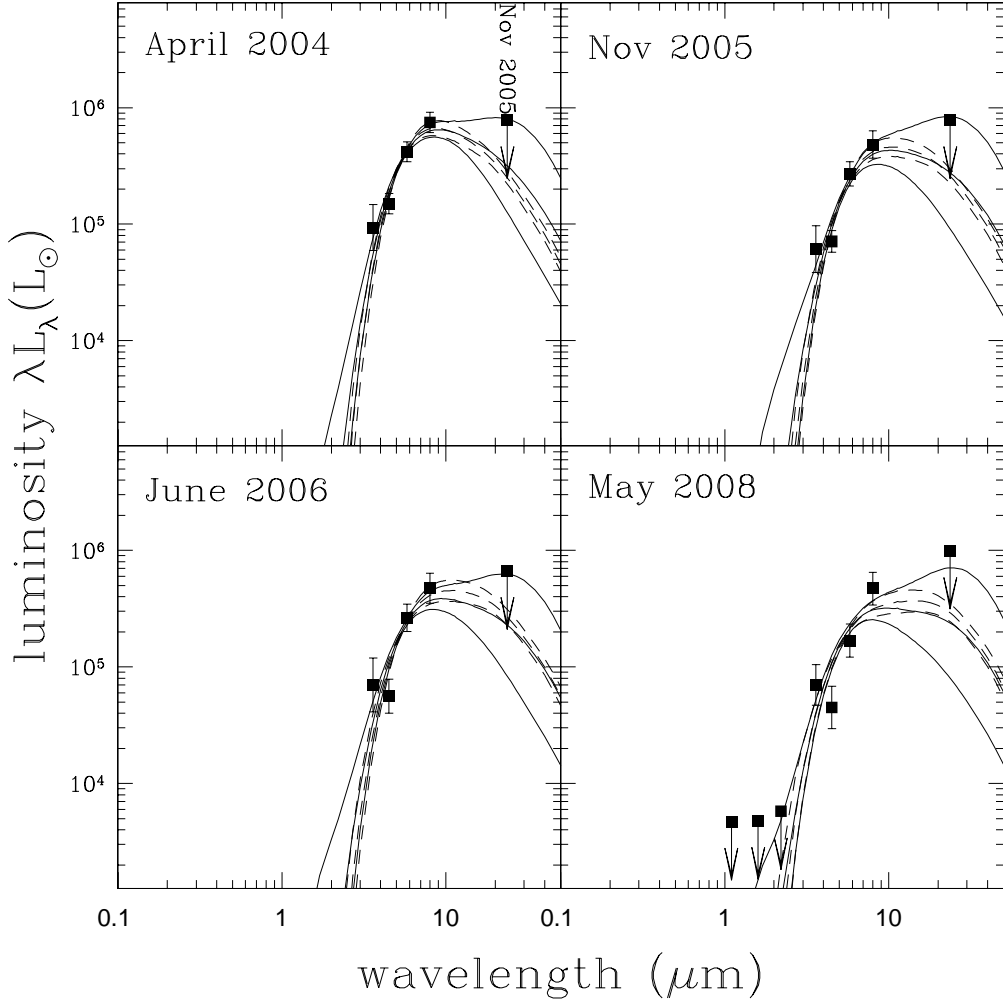


Fig. 13.— The spectral energy distributions of SN 199bw in 2004, 2005, 2006 and 2008. The 2001 optical detection from Li et al. (2002) is used as an upper limit in 2004 and 2005, and the 2005 $24\mu\text{m}$ upper limit is used as an upper limit in 2004. The solid curves show the probability-weighted average graphitic SED models and their dispersions with no constraint on the shell radius, while the dashed curves constrain the inner radius by a 630 ± 30 km/s expansion velocity prior. The near-IR limits are shown at 1σ , as appropriate for constraining models. The optical flux limits in 2008 are fainter than $10^3 L_{\odot}$ and are not shown.

high at all epochs with the limit determined by the stellar temperature – for $T_* = 10000$ K we find $\tau_V \gtrsim 50$ in 2008, while a hotter $T_* = 30000$ K star only requires $\tau_V \gtrsim 20$. The limits largely hold for all epochs, so we have no strong constraints on the evolution of the optical depth. Either dust model fits the data well. The luminosity was roughly constant from 2004 to 2008 at $L_* \simeq 10^{6.0 \pm 0.2} L_\odot$ depending on the specific model, possibly with a modest fading of 0.2 dex. There is no strong evolution in the dust temperature. This means that the energy radiated in the later phases, $E \simeq 10^{48}$ ergs, significantly exceeds that from the peak, $E \simeq 2 \times 10^{45} (\Delta t_{1.5}/10 \text{ days})$ ergs (Table 1), unless the un-observed duration of the peak was quite long, $\Delta t_{1.5} \gtrsim 1$ year. The best models prefer dust radii somewhat larger than expected for an inner radius expanding at 630 km/s and are certainly inconsistent with the outer radius expanding at this velocity for our standard $R_{out}/R_{in} = 2$ models. The ejected mass of $M_E \simeq 0.4(\tau_V/10)(100 \text{ cm}^2/\text{g}/\kappa_V)(v_w/630 \text{ km/s})^2 M_\odot$ required to have a high optical depth in 2008, 9 years after the peak, is far more than expected from the observed short duration transient (Table 2). Either SN 1999bw was an explosive transient with $f \ll 1$ or the true duration was far longer, with $\Delta t_{1.5} \simeq 0.3$ years for $f \simeq 1$. The SEDs are also well-fit by a dusty graphitic wind.

Since the SEDs are marginally consistent with an expanding shell, it is possible that SN 1999bw was a simple eruption ejecting $M \sim 1 M_\odot$ of material at 630 km/s from a luminous $L_* \simeq 10^6 L_\odot$ star. The amount of mass loss needed to explain the SED and its evolution seems to imply transient energies that are incompatible with a radiatively driven ejection, although this is not certain given the incomplete early-time light curve. It seems far more likely that SN 1999bw is similar to SN 2008S and the 2008 NGC 300 transient as originally suggested by Thompson et al. (2009). The dust probably present at peak, the complete, long-lived shrouding with a dust radius that is somewhat large for the velocity estimate, and the mid-IR luminosity are all very similar to these two transients (see Kochanek 2011a).

4.6. SN 2000ch in NGC 3432

Papenkova & Li (2000) identified a new variable star in NGC 3432 in May 2000 and Filippenko (2000) argued that it was a sub-luminous Type IIn analogous to SN 1997bs or SN 1999bw and likely to be an LBV outburst rather than a SN. The initial outburst was studied in detail by Wagner et al. (2004), and Pastorello et al. (2010) report on three subsequent transients in 2008 and 2009. The first peak, on 3 May 2000 (JD 2451668) is the only one prior to the Spitzer observations. This is clearly a variable star. In quiescence, the star is very luminous, $R \simeq 19.5$ ($M_R \simeq -10.7$) with peaks in the transients at $R \simeq 18$ ($M_R \simeq -12$) and post-transient minima near $R \simeq 21$ ($M_R \simeq -9$) that are interpreted as obscuration by newly formed dust. In outburst, the SEDs are relatively well fit by $T_* \sim 8000$ to 10000 K with excesses in the U-band and due to H α emission in the R-band. In quiescence it seems to have a cooler temperature, $T_* \simeq 5000$ K. SN 2000ch is easily detected both in the optical and in the mid-IR, as shown in Fig. 14.

SN 2000ch was observed with Spitzer only twice, with IRAC in December 2007 and MIPS in May 2008, where Pastorello et al. (2010) measured B, V and R magnitudes of 20.10 ± 0.21 , 19.75 ± 0.12 and 18.67 ± 0.20 mag on 2008 Mar 12, roughly between the observations. We picked an epoch from Wagner et al.

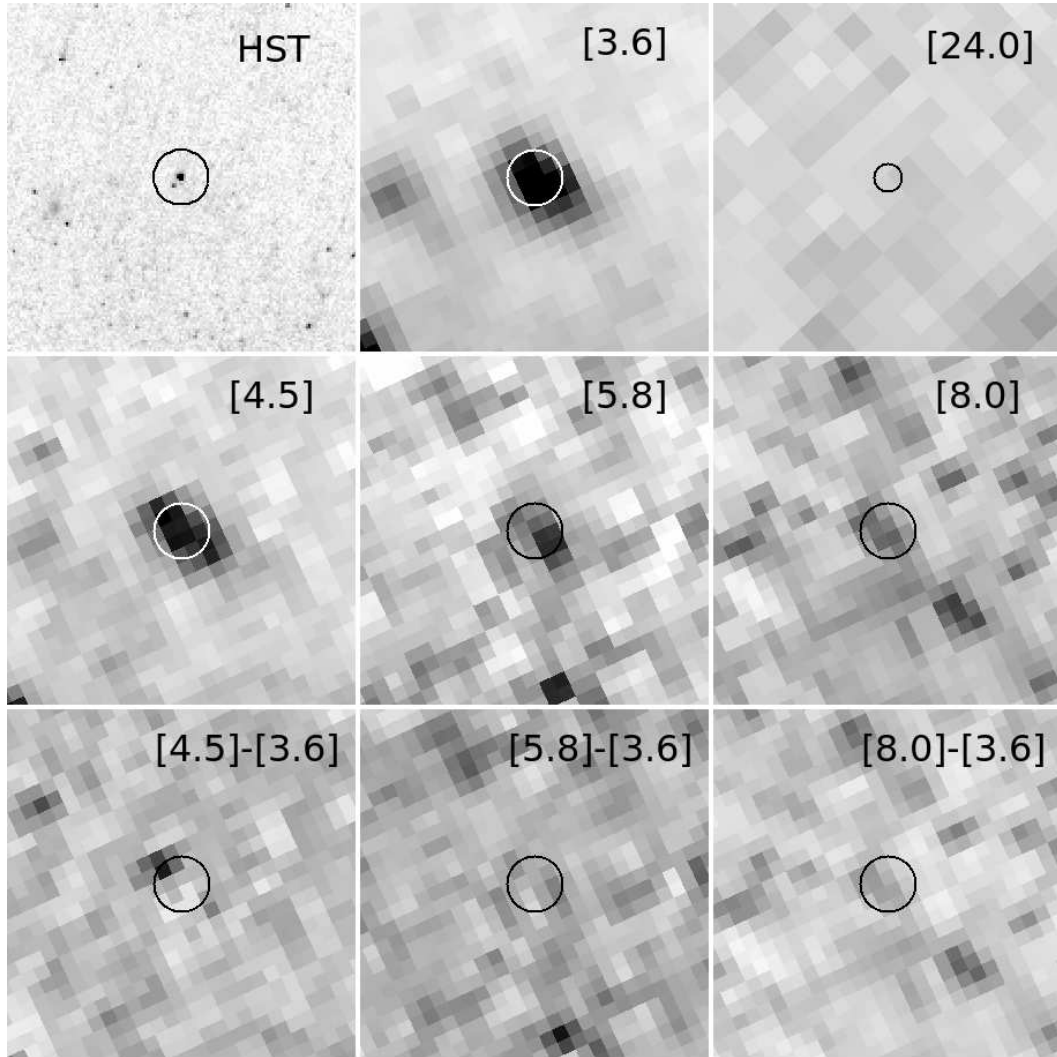


Fig. 14.— The environment of SN 2000ch. The top left, middle and right panels show the HST, 3.6 and $24\mu\text{m}$ images of the region, where the angular scale of the $24\mu\text{m}$ image is twice that of the other panels. The center left, middle and right panels show the 4.5, 5.8 and $8.0\mu\text{m}$ images. The bottom left, middle and right panels show the $[4.5]-[3.6]$, $[5.8]-[3.6]$ and $[8.0]-[3.6]$ wavelength-differenced images. A $1''.2$ radius circle marks the position of the transient.

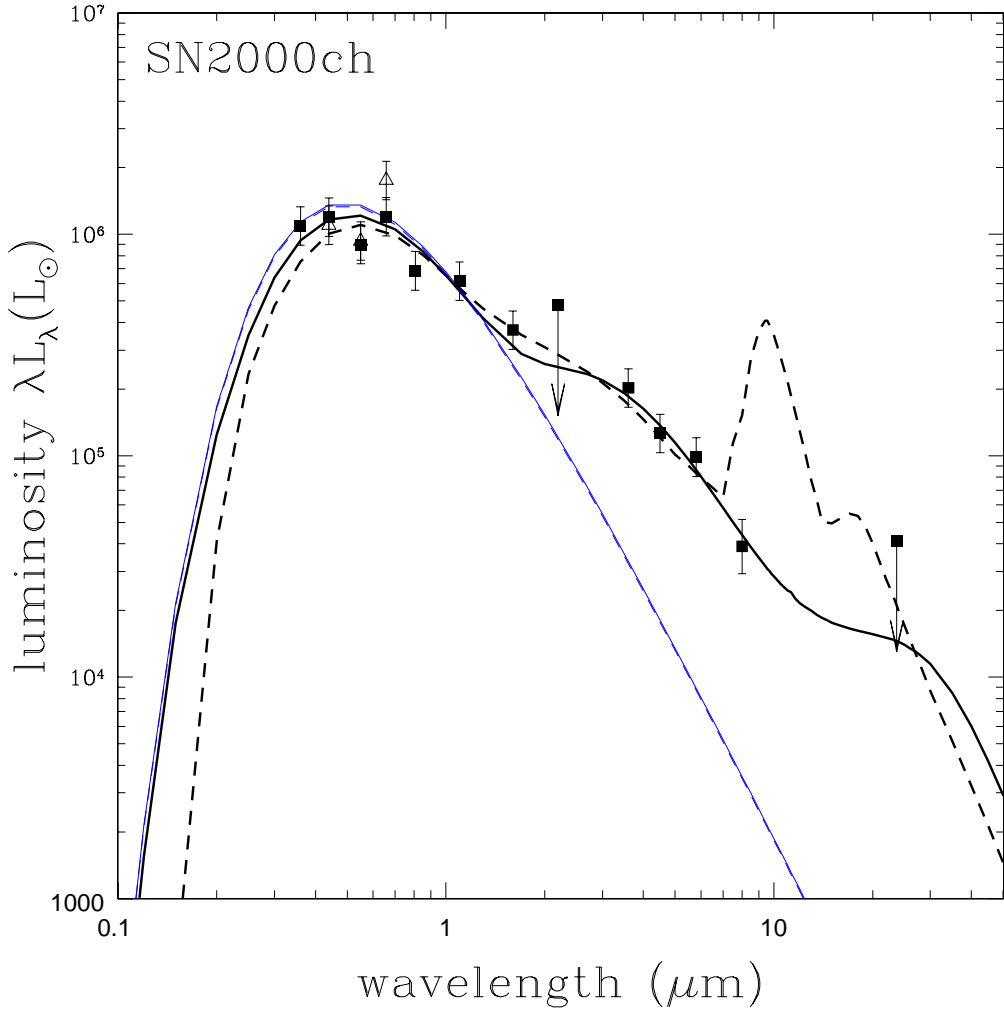


Fig. 15.— The spectral energy distribution of SN 2000ch. The mid-IR SED combines the IRAC data from December 2007 with the MIPS data from May 2008, although the star seemed to be in quiescence during this period based on Pastorello et al. (2010). The open triangles show the B, V and R data from near the midpoint of this period (March 2008) from Pastorello et al. (2010), and they are largely hidden by the filled squares showing a very similar SED measured in May 2000 by Wagner et al. (2004) that also included near-IR measurements. The solid (dashed) curves are DUSTY wind fits for $\tau_V = 0.2$ of graphitic ($\tau_V = 1$ of silicate) dust around a $T_* = 7500$ K, $L_* \simeq 10^{6.3} L_\odot$ star. The thick curves show the model of the observed SED and the thin curves show the model SED of the unobscured star.

(2004) (2000 May 21) with similar B, V, R magnitudes that also had U, I, J, H and a K limit as an extended model of the SED. As we see in Fig. 15, the star probably has a modest mid-IR excess. Shell models expanding at 1400 km/s fail to fit the SED well. More slowly expanding (460 km/s) graphitic shells can fit the SED well, but silicate shells always have problems because of the strong $8\mu\text{m}$ feature. The models generically have a $T_* = 7500\text{ K}$, $L_* \simeq 10^{6.3}L_\odot$ star, small optical depths and relatively hot dust. All the shell models have the further problem that an optical depth of $\tau_V \simeq 0.1$ in 2008 would be $\tau_V \simeq 1$ in 2003. For comparison, one of the faintest epochs in Pastorello et al. (2010) (24 November 2008) is well fit with no circumstellar dust, $T_* = 7500\text{ K}$ and $L_* \simeq 10^{5.3}L_\odot$. Formally, the ejecta masses in the best fit shell models are $\log(M_{E\kappa_{100}}/M_\odot) = -1.8 \pm 0.2$ and -3.2 ± 0.1 for the graphitic and silicate models. While Wagner et al. (2004) propose that the post-eruption flux minima are due to dust formation, they are too close to the transient and too short lived to be consistent with the optical depth evolution of a geometrically expanding shell.

The simplest way to have a slowly varying optical depth and an effective dust radius different from that predicted by the apparent velocities is to produce the dust in a relatively steady wind rather than an impulsive ejection. Fig. 15 shows the silicate and graphitic DUSTY wind models fit to the SED rather than the usual shell models. The graphitic model fits well, with $\tau_V = 0.2$. The silicate model, with $\tau_V = 1$, fits less well because of the $8\mu\text{m}$ peak. Correlations between the variability of the star and dust formation in the wind can then help to explain some of the correlations. For example, the dust formation radius $R_f \propto L_*^{1/2}$ (Eqn. 1) while the optical depth of a wind is $\tau \propto R_f^{-1}$ (Eqns. 13 and 14), so increasing the luminosity drives the dust formation radius outwards and the optical depth down to make the star bluer independent of any change in the stellar temperature. There may also be correlated changes in the mass loss rate, and the dust opacity will change due to both changes in the gas density at the dust formation radius and changes in the stellar spectrum (see, Kochanek 2011b). In short, we propose that the dust-related behaviors of SN 2000ch are due to modulated dust formation in a quasi-steady wind rather than strongly transient mass ejections associated with the luminosity peaks. Near-IR (particularly K-band) and mid-IR light curves would test this scenario in detail.

4.7. SN 2001ac in NGC 3504

SN 2001ac was discovered by Beckmann & Li (2001) on 12 March 2001 (JD 2451981) at about 18.2 mag and Matheson & Calkins (2001) reported that it had a Type IIn spectrum similar to SN 1997bs and SN 1999bw. Observations prior to the transient in 1995 show no source, but the limits are of limited use because the position is near the chip edge in V band (F606W) and the other filter is in the UV (F218W). There is no source apparent in the post-transient HST images from 2008 November 18/22, with optical (3σ) limits of 26.5, 26.3, 25.8 and 26.1 mag (3σ , Smith et al. 2011) The epoch of the HST band is close to those of the Spitzer data (2008 June 20 for IRAC and 2008 January 5 for MIPS).

Fig. 16 shows the HST I band and Spitzer images of the region. There appears to be a relatively bright, red mid-IR source at the transient position in the IRAC images, and no obvious source at $24\mu\text{m}$. We have

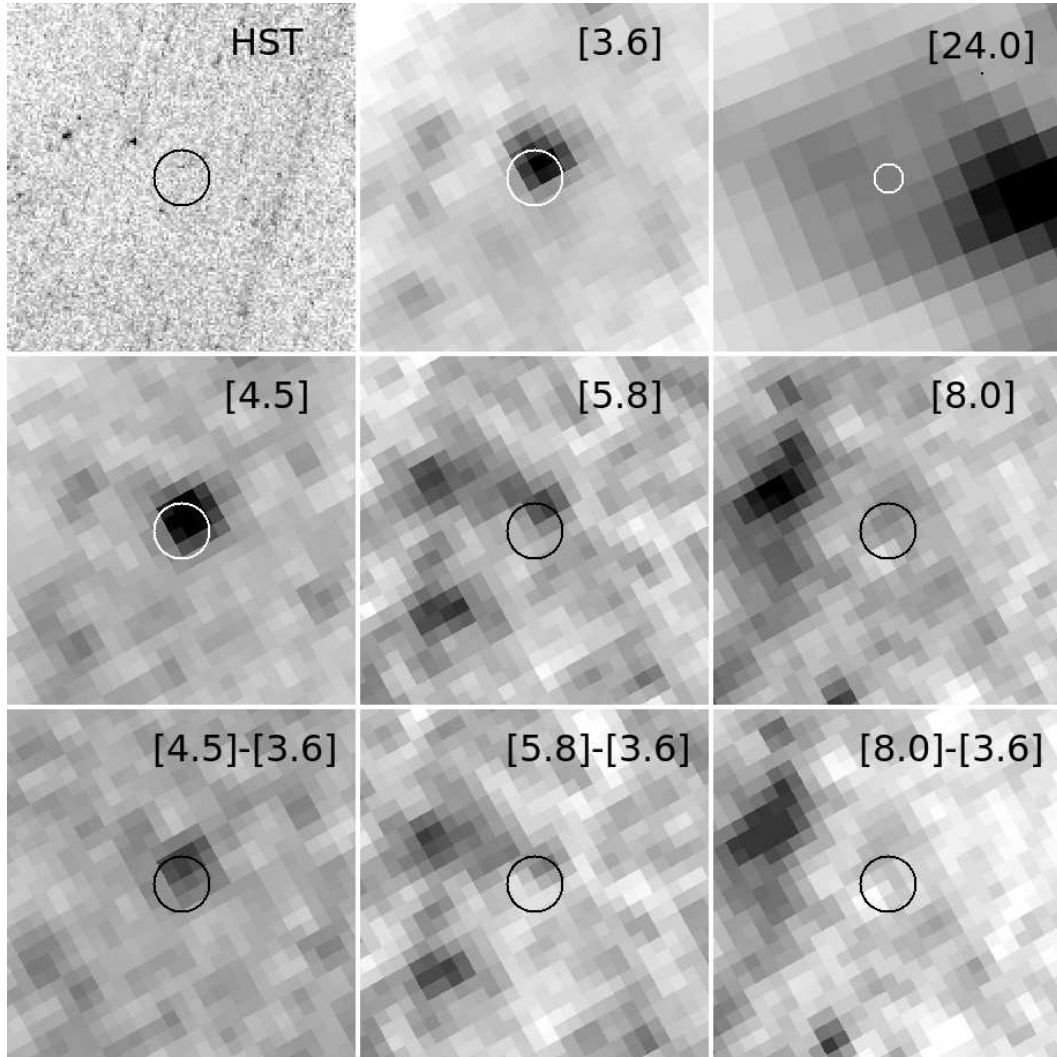


Fig. 16.— The environment of SN 2001ac. The top left, middle and right panels show the HST, 3.6 and $24\mu\text{m}$ images of the region, where the angular scale of the $24\mu\text{m}$ image is twice that of the other panels. The center left, middle and right panels show the 4.5, 5.8 and $8.0\mu\text{m}$ images. The bottom left, middle and right panels show the $[4.5]-[3.6]$, $[5.8]-[3.6]$ and $[8.0]-[3.6]$ wavelength-differenced images. A $1''.2$ radius circle marks the position of the transient.

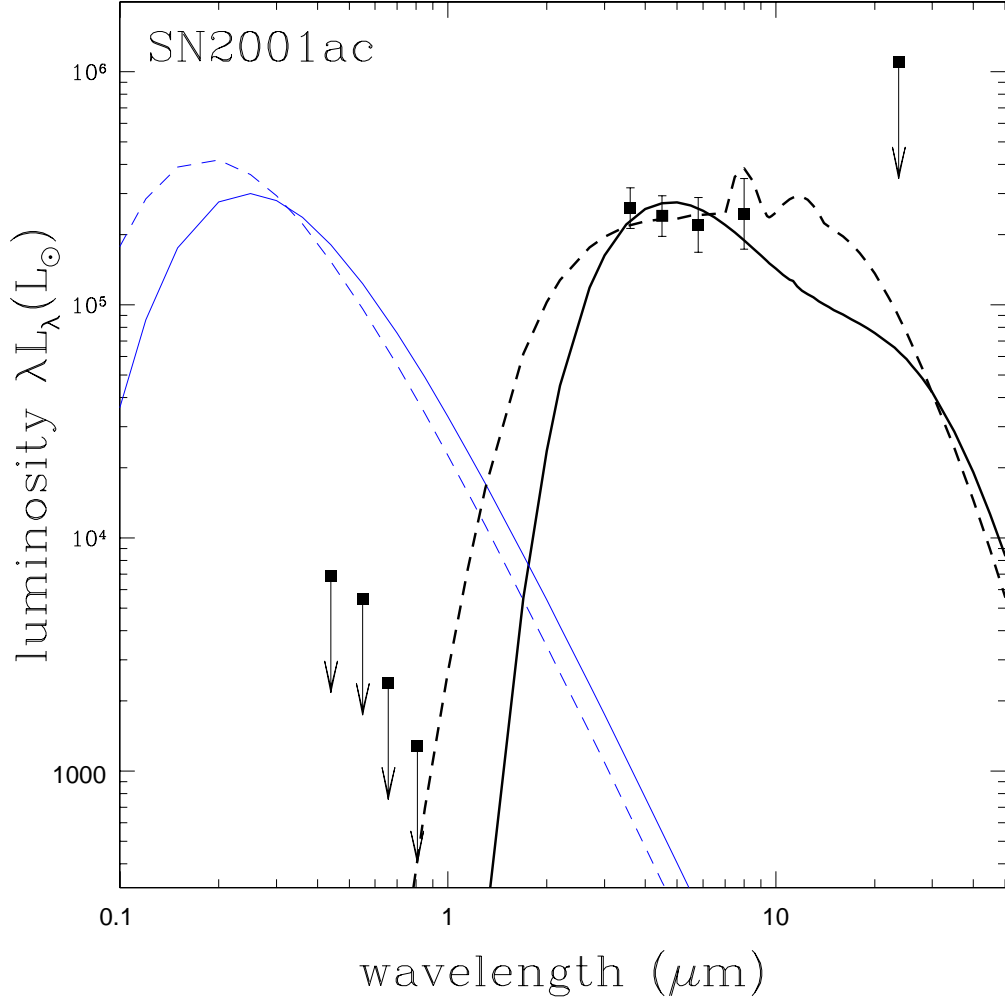


Fig. 17.— The spectral energy distribution of SN 2001ac. The November 2008 optical limits are from Smith et al. (2011). The Spitzer observations are from June 2008 (IRAC) and January 2008 (MIPS). The optical limits have been converted to 1σ so that model offsets can be properly interpreted. These models show relatively high optical depth ($\tau_V = 25$ for graphitic and 18.5 for silicate dust), slowly expanding shells around a $T_* = 20000$ K star. The stellar luminosities are $L_* = 10^{5.6} L_\odot$ (solid, graphitic dust) and $L_* = 10^{5.8} L_\odot$ (dashed, silicate dust). There are acceptable fits for moderately lower optical depths, particularly if we increase the (unconstrained) stellar temperature. The thin curves show the model for the unobscured source.

no trouble modeling the SED with a 290 km/s expansion velocity, and in Fig. 17 we show models with $T_* = 20000$ K and $L_* = 10^{5.6}L_\odot$ for graphitic dust and $L_* = 10^{5.8}$ for silicate dusts. High stellar temperatures are not required, but the stellar luminosity does not depend strongly on the temperature. The nominal optical depths are high, $\tau_V = 25$ and 18.5 for the graphitic and silicate models shown in Fig. 17, with hotter models allowing modestly lower optical depths. Averaging over the models we find $\log \tau_V \simeq 1.3 \pm 0.1$. The ejected masses for these optical depths are of order $\log(M_E \kappa_{100}/M_\odot) = -1.0 \pm 0.2$ for either model, consistent with $f \gg 1$ and a radiatively driven mechanism. This is the only example where the silicate optical depths are similar to the graphitic, but this is driven by the lack of optical measurements for either the progenitor or the post-transient source. Both types of dust fit the SED reasonably well, but the dust temperature at the inner edge has to be high, with $T_d = 1000$ K and 1300 K for the models in the figure. If the Spitzer source is not related to SN 2001ac, a surviving, un-obscured star can be luminous only if very hot, with $L_* \simeq 10^{3.9}L_\odot$ for $T_* = 10000$ and $L_* = 10^{5.3}L_\odot$ for $T_* = 40000$ K.

Complete understanding of this system requires either detecting an optical counterpart or observing the time evolution of the mid-IR properties. If there is an ejected shell of dusty material, the warm Spitzer mid-IR fluxes should be falling relatively rapidly because of the expansion of the shell, and the optical depth will be constrained by the reappearance of the star in the optical. For example, the V band luminosity will reach the present limit circa 2015 for the silicate model and 2037 for the graphitic model for the models in Fig. 17.

4.8. SN 2002bu in NGC 4242

SN 2002bu was discovered by Puckett & Gauthier (2002) on 2002 March 28 (JD 2452362) and was classified as a Type II_n (FWHM ~ 1100 km/s) by Ayani et al. (2002). Foley et al. (2007) show a light curve covering the first 70 days, noting that it declines much more slowly than a typical Type II and is relatively red ($B-R \simeq 1.5$) at the end of this period. The early light curve from Smith et al. (2011) is consistent with no extra extinction if the transient is initially cool (7500 K at peak) and then cools further (5000 K after 3 months). If we fix the temperature at 10000 K, then the best fit models have modest optical depths at peak ($\tau_V \simeq 1$), which then increases to $\tau_V \simeq 3$ after three months. There is not, however, enough spectral coverage to choose between changes in temperature and extinction. At the last optical epoch, the ejecta should still be close enough to the star ($R \sim 7 \times 10^{14}$ cm) to avoid dust formation (Eqn. 1), so any new dust would have to be reformed in a preexisting dense wind.

By 2004/2005 this has clearly changed, as illustrated by the HST I band image and the Spitzer images of the region shown in Fig. 18. No optical counterpart is apparent, but, as noted by Thompson et al. (2009), there is a bright, red mid-IR source. The lack of any bright sources in the HST images means we could make no independent check of the header astrometry, but no source is apparent at the nominal position with limits of roughly $\gtrsim 25$ mag in all four bands (Table 4). Fig. 19 shows the SED, combining the HST upper bounds from March/April 2005 with the Spitzer observations from April/May 2004. We have little difficulty matching the SED with expansion values similar to the estimate by Smith et al. (2011) in Table 2.

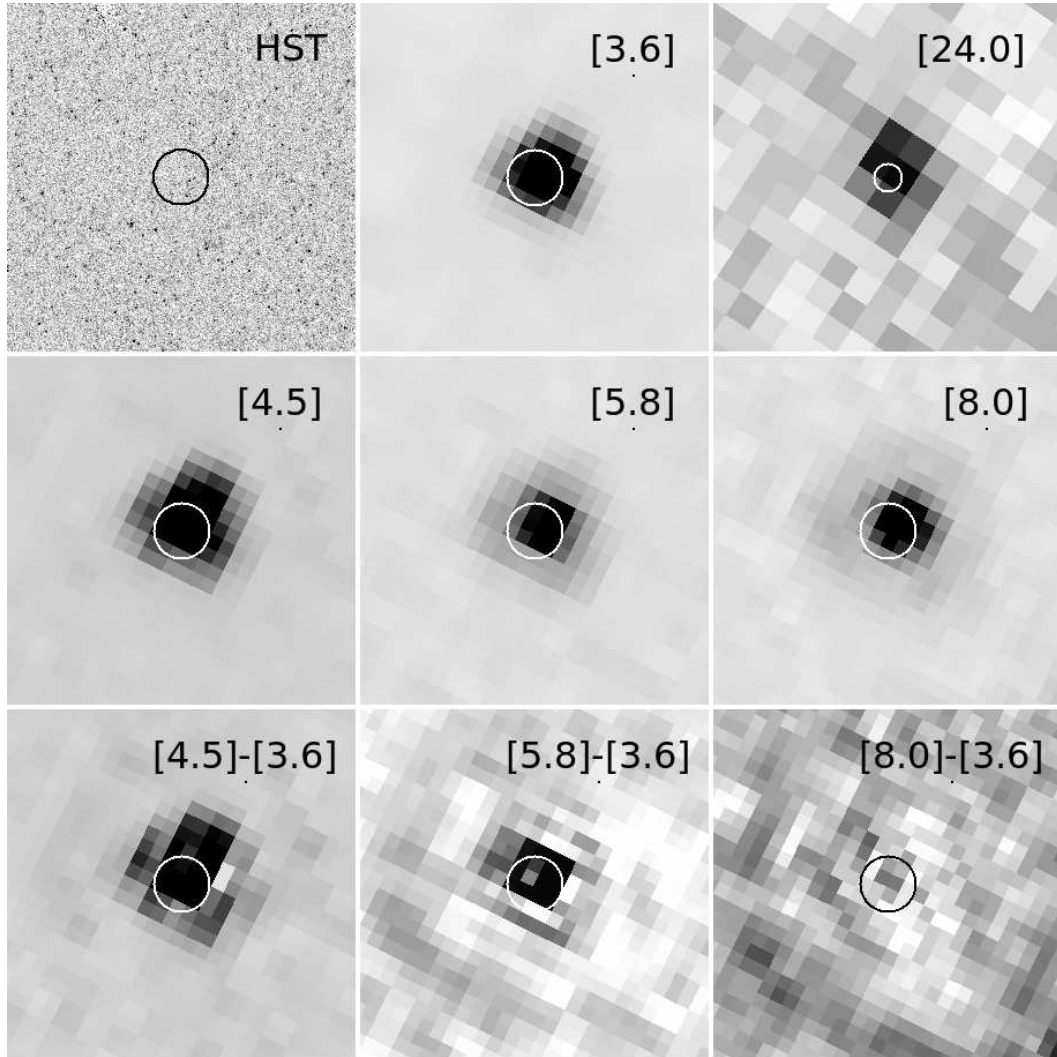


Fig. 18.— The environment of SN 2002bu. The top left, middle and right panels show the HST, 3.6 and $24\mu\text{m}$ images of the region, where the angular scale of the $24\mu\text{m}$ image is twice that of the other panels. The center left, middle and right panels show the 4.5, 5.8 and $8.0\mu\text{m}$ images. The bottom left, middle and right panels show the $[4.5]-[3.6]$, $[5.8]-[3.6]$ and $[8.0]-[3.6]$ wavelength-differenced images. A $1''.2$ radius circle marks the position of the transient.

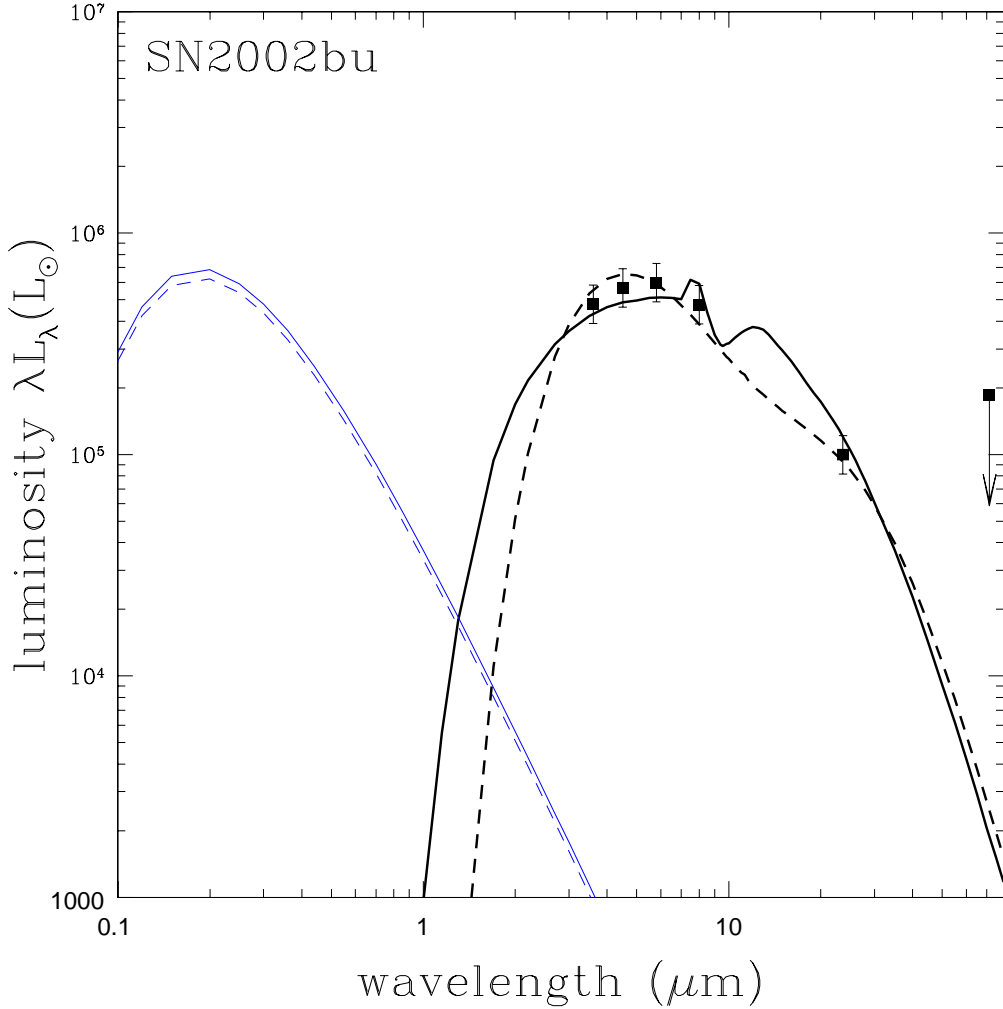


Fig. 19.— The spectral energy distribution of SN 2002bu. The mid-IR SED combines the Spitzer data from April/May 2004 with the HST upper bounds from March/April 2005. These models have optically thick $\tau_V = 30$ shells expanding at roughly 800 km/s around a $T_* = 20000$ K, $L_* \simeq 10^{5.9} L_\odot$ star with graphitic (solid) or silicate (dashed) dust. The thick black curves show the observed SED and the thin curves show the SED of the unobscured star. Note that the wavelength range has been expanded to include the limit at $70 \mu\text{m}$. The 1σ optical limits are fainter than $10^3 L_\odot$ and are not shown.

Fig. 19 uses expansion speeds of 825 and 790 km/s for the graphitic and silicate models, respectively, and a $T_* = 20000$ K, $L_* = 10^{5.9}$ and $10^{6.0}L_\odot$ star. The particular models have optical depths of $\tau_V = 30$, but the optical depth is not well constrained without an optical detection. Producing this optical depth requires $\log(M_{E\kappa_{100}}/M_\odot) \simeq -0.9 \pm 0.2$ of ejected material depending on the parameters and the dust type, which is consistent with our estimates for a radiatively driven process (Table 2).

The available data are consistent with a transient ejecting a shell, although they are also consistent with the different phenomenology of SN 2008S, the 2008 NGC 300 transient and SN 1999bw. If the mid-IR emission is due to an illuminated, expanding shell, the 3.6 and 4.5 μm fluxes should be very different today because the shell radius will quintuple and the dust temperature will be halved between 2004 and 2012. At 3.6 μm the source should be roughly ten times fainter than in 2004. Similarly, if the optical depth in 2004 was $\tau_V \sim 30$, then the source should be reappearing in the optical as well because the optical depth will have dropped to $\tau_V \sim 1$. These issues can be easily addressed by new observations.

4.9. SN 2002kg/V37 in NGC 2403

SN 2002kg was discovered on 26 October 2003 (JD 2452827) and initially classified as a Type II_n SN based on its narrow emission lines (Schwartz et al. 2003a). Weis & Bomans (2005) identified it with the LBV V37 in Tammann & Sandage (1968), reconstructed its historical light curve, showed it was a strong H α source and also found it in post-transient HST observations. Maund et al. (2006) found that V37 had B, V and I magnitudes of 20.9 ± 0.3 , 20.65 ± 0.15 and 20.9 ± 0.6 roughly two years before the transient (the correct SN 2002kg magnitudes for Maund et al. (2006) are found in Maund et al. (2008)), similar to its typical historical fluxes. This corresponds to a luminosity of $10^{5.0}L_\odot$ for $T_* = 10^4$ K (cooler black bodies fit poorly) or $10^{5.5}L_\odot$ for 20000 K. The transient only brightened by $\Delta V \simeq -2.2 \pm 0.2$ magnitudes, from $M_V \simeq -8.2$ to $M_V \simeq -10.4$, a level which it seems to have achieved several times since its discovery (Weis & Bomans 2005). Maund et al. (2006) estimate that the local extinction is of order $E(B-V) \simeq 0.17 \pm 0.02$.

Fig. 20 shows the region around SN 2002kg. The HST V band (F606W) image is from August 2004. The mid-IR images combine the available epochs and there is no evidence for mid-IR variability. There appears to be a counterpart to SN 2002kg in the IRAC bands, which subtracts well in the wavelength differenced images, indicating that the source is not dominated by dust. There is a 24 μm peak slightly East of our estimate of the position which does not seem to be associated with the source. In fact, it is likely an artifact of some kind since it only appears in one of the SST epochs.

While there is no good evidence for mid-IR variability, the source is clearly varying in the optical, as illustrated in Fig 8. The source is fading, since there is a strong Slope detection, but relatively steadily, since there is little signal in the RMS image. Such tricks are hardly needed for SN 2002kg/V37, and it is included in Fig. 8 as a contrast to the behaviors of SN 1954J and SN 1997bs. Fig. 21 shows the combined light curves from Maund et al. (2006) and our LBT observations (Table 5). The source is clearly fading, and at relatively constant colors except for the R-band flux, which seems to drop faster than the other bands. The SED, shown in Fig. 22, suggests that the R band flux in Maund et al. (2006) is significantly enhanced by H α emission.

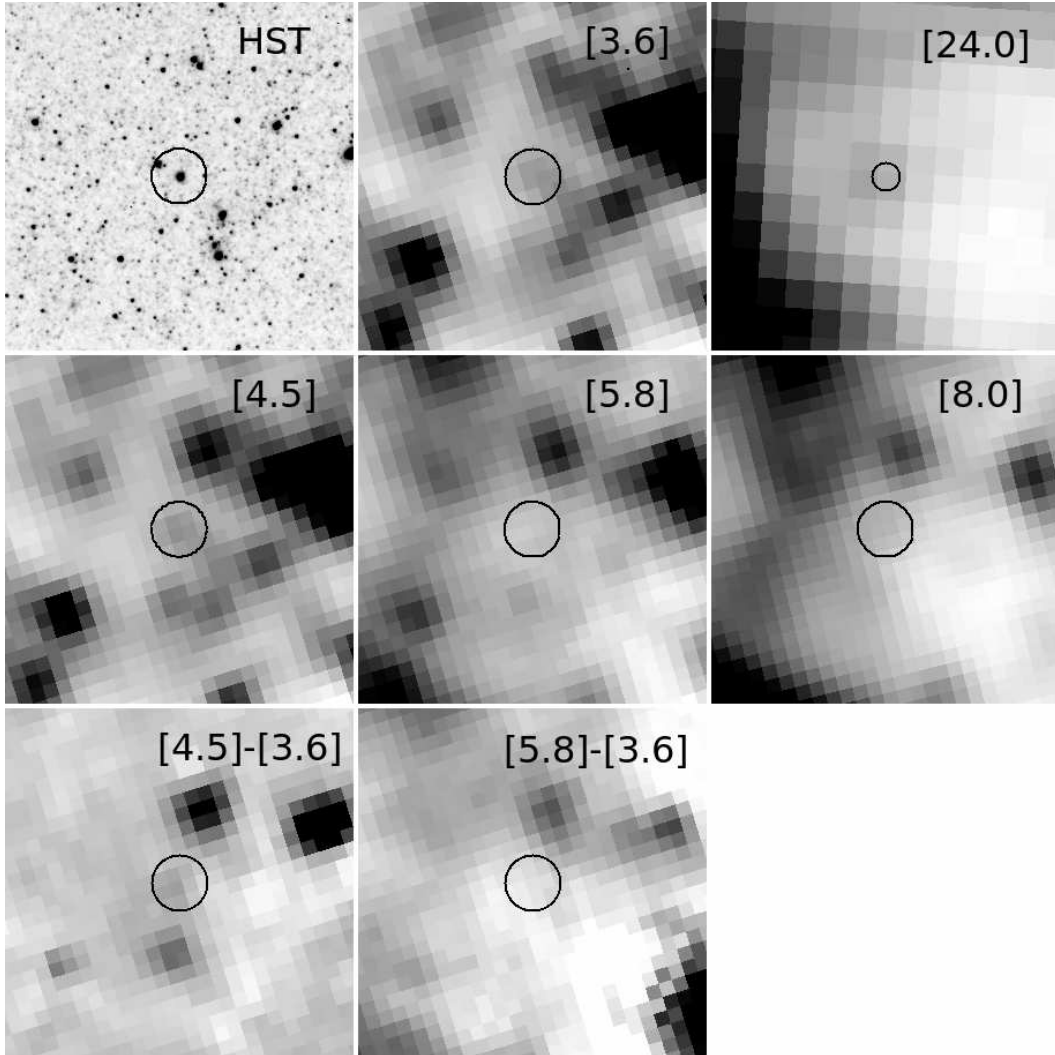


Fig. 20.— The environment of SN 2002kg/V37 in NGC 2403. The top left, middle and right panels show the HST, 3.6 and $24\mu\text{m}$ images of the region, where the angular scale of the $24\mu\text{m}$ image is twice that of the other panels. The center left, middle and right panels show the 4.5, 5.8 and $8.0\mu\text{m}$ images. The bottom left, middle and right panels show the $[4.5]-[3.6]$ and $[5.8]-[3.6]$ wavelength-differenced images. The subtraction procedure failed for the $[8.0]$ micron image. A $1''.2$ radius circle marks the position of the transient.

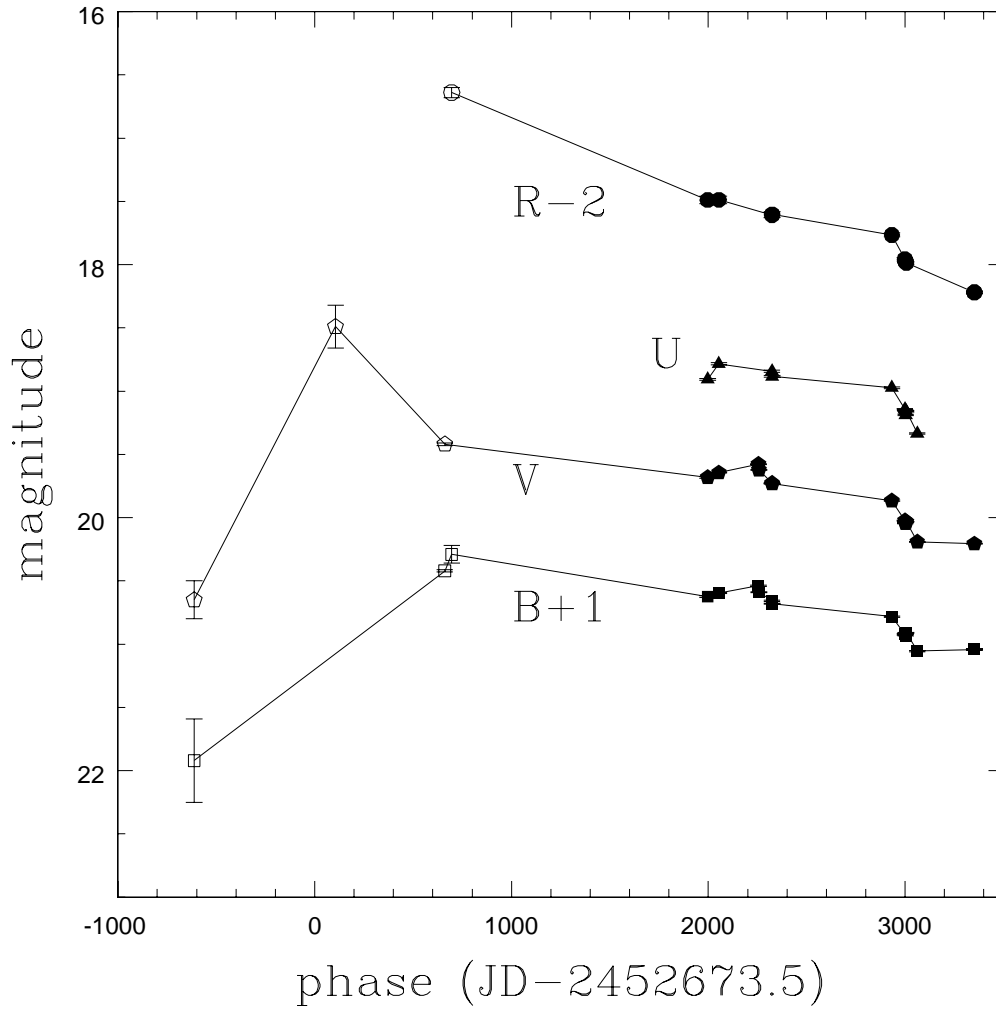


Fig. 21.— Optical light curves of SN 2002kg. The data prior to 1000 days after the transient is from Maund et al. (2006) (open points) and the data afterward is from the LBT (filled points). The source is slowly fading with roughly constant optical colors.

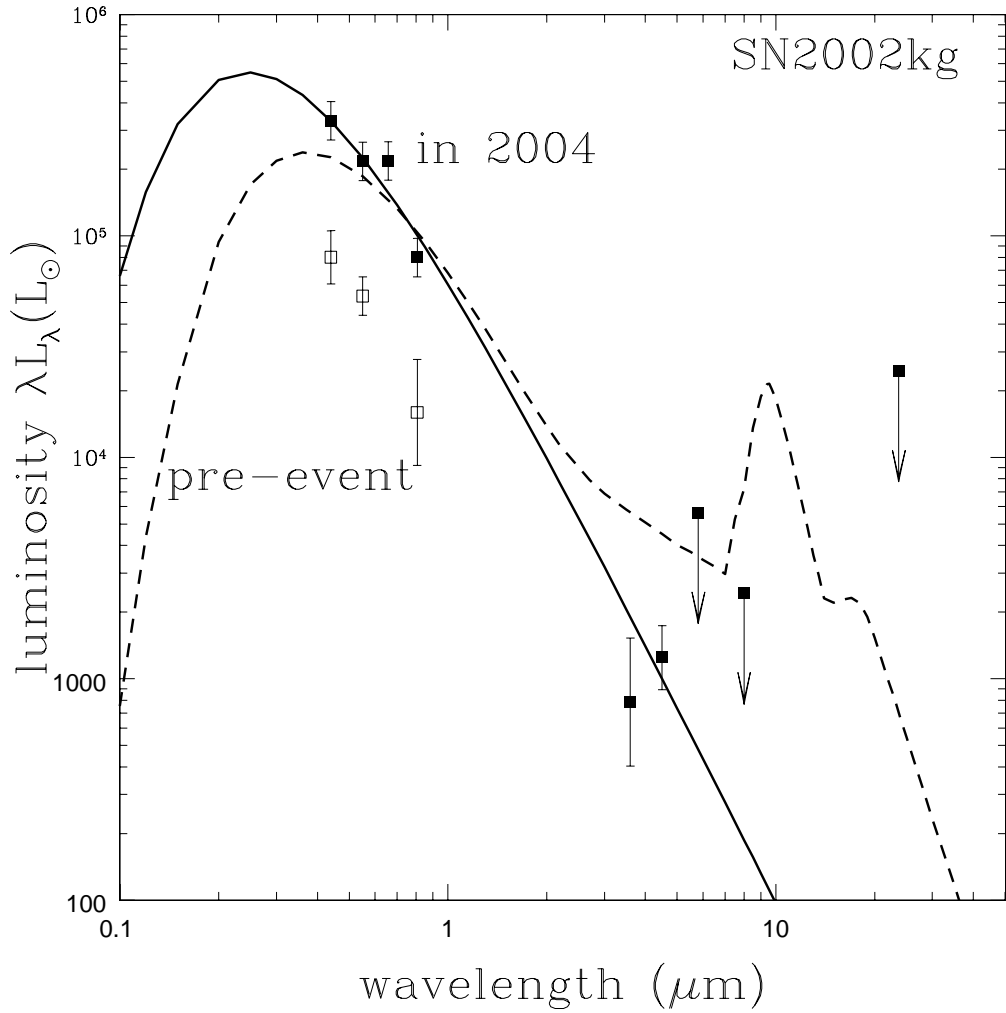


Fig. 22.— The spectral energy distribution of SN 2002kg in 2004, two years post-peak. The solid line is a model with $T_* = 15000$ K, $L_* = 10^{5.9} L_\odot$ and no dust, while the dashed line shows a silicate model with $T_* = 10000$ K, $L_* = 10^{5.6} L_\odot$ with $\tau_V = 0.1$ of dust at $R_{in} = 2 \times 10^{15}$ cm (350 km/s for 2 years). The filled squares show the SED in late 2004 where the optical points are from Maund et al. (2008). The open squares show the pre-transient SED.

At the present mean rate of decline, $\simeq 0.14$ mag/year at V band, it will return to its quiescent magnitude in another ~ 3 years. In units of luminosity, the R-band decline seen in Fig. 8 is about $13000L_{\odot}$ /year with rms residuals of $2300L_{\odot}$.

Fig. 22 shows our models of the SED, where we match the last Maund et al. (2006) epoch, two years post peak, to the mid-IR fluxes measured in the same year. The best fit models have no dust, and $\tau_V = 0.1$ models grossly over-predict the mid-IR fluxes. These limits imply a negligible amount of ejected mass ($M \lesssim 10^{-4}M_{\odot}$). The SED is reasonably well fit with $T_* = 15000$ K, no dust, and $L_* \simeq 10^{5.9}L_{\odot}$, as shown in Fig. 22. In our limited sampling of temperatures, it can be as cool as $T_* = 10000$ K with $L_* \simeq 10^{5.8}L_{\odot}$, and hotter models are somewhat preferred, although the luminosities become unreasonable, with $L_* \simeq 10^{6.9}L_{\odot}$ by the time $T_* = 40000$ K. The LBT data is also consistent with a hot ($T_* > 10000$ K) star and no dust.

4.10. SN 2003gm in NGC 5334

SN 2003gm was discovered by Schwartz et al. (2003b) on 6 July 2002 (JD 2452884) at 17 mag, and Patat et al. (2003) reported that it had a Type IIn spectrum similar to SN 1997bs. Maund et al. (2006) identified the progenitor as a yellow supergiant with $M_V \simeq -7.5 \pm 0.2$ and $V - I \simeq 0.8 \pm 0.3$ ($V = 24.2 \pm 0.1$ and $I = 23.4 \pm 0.2$) assuming a (kinematic) distance of 20.05 Mpc. The measured, but poorly sampled, transient peak had $B \simeq 18.5$, $R \simeq 17.8$ and $I \simeq 18.0$, so the peak brightness of $M_I \simeq -13.6$ was faint compared to a normal SN. HST observations roughly a year later identified the source with $B \simeq 26.07 \pm 0.09$, $V \simeq 25.12 \pm 0.07$ and $I \simeq 24.90 \pm 0.08$ (Maund et al. 2006), significantly fainter than before the transient. Smith et al. (2011) find fluxes of with $F_{450W} > 26.0$ (3σ), $F_{555W} = 25.28 \pm 0.25$, $F_{675W} = 24.73 \pm 0.31$ and $F_{814W} = 23.81 \pm 0.13$ mag in December 2008, which seems to imply a significant fading at B, little change at V and a significant brightening at I over the intervening four years. If we assume no additional circumstellar dust, the progenitor is consistent with a yellow ($T_* \simeq 7500$ K) star with a luminosity of $L_* \simeq 10^5L_{\odot}$, as found by Maund et al. (2006).

Fig. 23 shows the F814W HST image from a year after the outburst (2004 May 24, JD 2453150), the IRAC 3.6 and $4.5\mu\text{m}$ images and the $[3.6] - [4.5]$ wavelength differenced image. There is a source in the IRAC images whose position is consistent with the location of SN 2003gm, but there are multiple HST sources, so the match is uncertain. Since the optical source is far fainter than the progenitor and the mid-IR source is consistent with dust emission, we proceed on the assumption that they are the same source. Fig. 24 shows the SED in 2008/2009, combining the Smith et al. (2011) HST fluxes from December 2008 with the Spitzer fluxes from August 2009. Fits simultaneously constrained by the progenitor fluxes from Maund et al. (2006) are poor, so we fit only these transient fluxes. There are solutions that match the slow expansion rate in Table 1 with a $T_* = 10000$ to 20000 K temperature, luminosity $L_* \simeq 10^{5.9 \pm 0.1}L_{\odot}$, and very hot $T_d \simeq 1500$ K dust at the inner edge. Because the dust is so close to the formation radius at $R_{in} \simeq 10^{15.4}$ cm, little mass is needed, with $M_E \simeq 0.01M_{\odot}$. Models that simultaneously try to match the progenitor work poorly because for reasonable temperatures and little extinction of the progenitor, it is significantly less luminous than the transient, with $L_* \simeq 10^{5.1}$ for $T_* = 10000$ K and $L_* \simeq 10^{5.7}$ for $T_* = 20000$ K. The luminosity seen in 2008 can

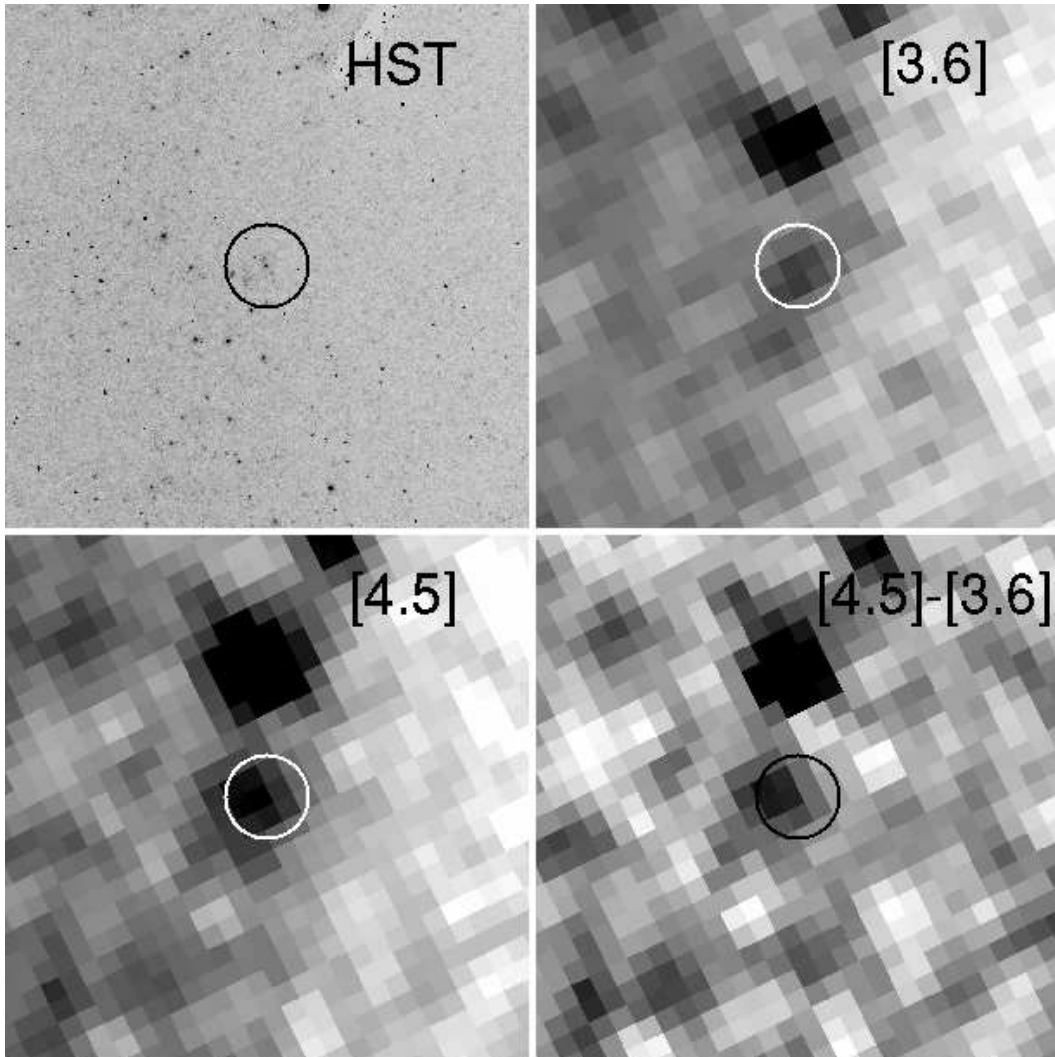


Fig. 23.— The environment of SN 2003gm. The top left and right panels show the HST and $3.6\mu\text{m}$ images of the region, while the lower left and right panels show the [4.5] and [4.5]–[3.6] wavelength-differenced images. A $1''.2$ radius circle marks the position of the transient.

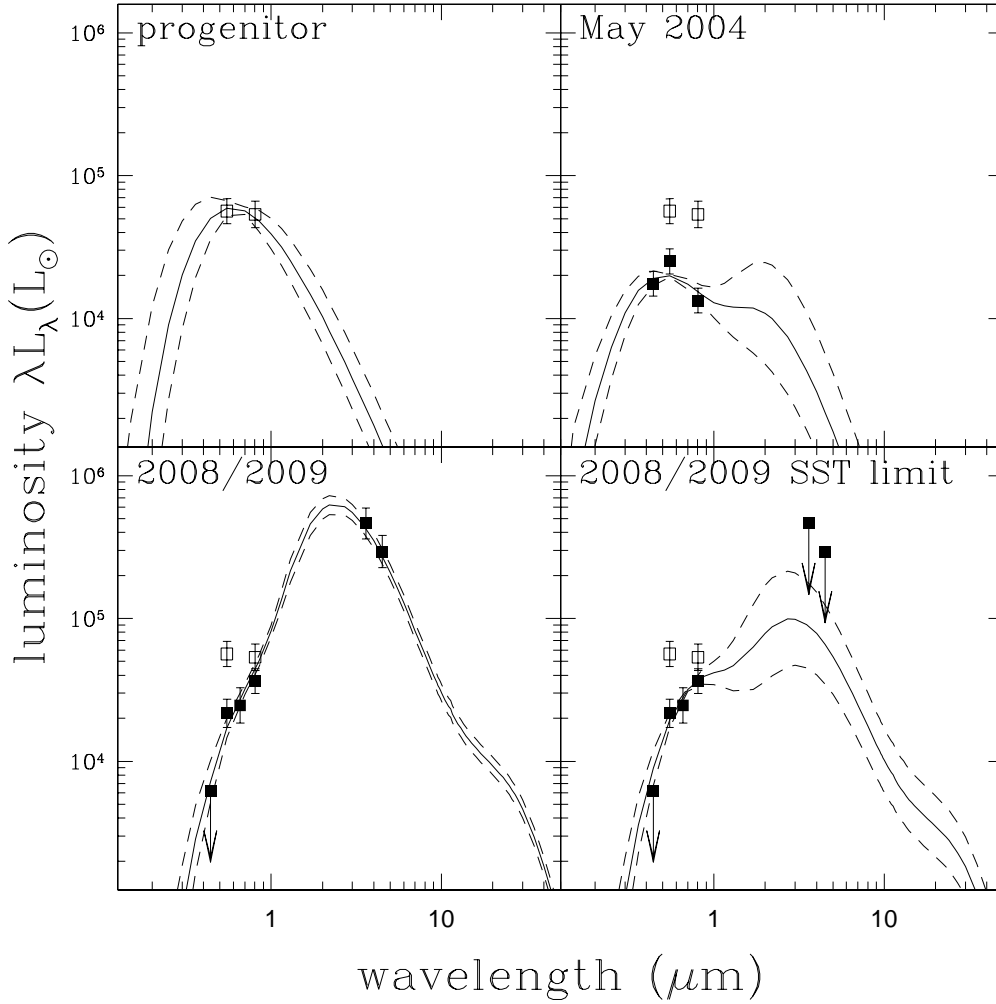


Fig. 24.— Spectral energy distributions for SN 2003gm. The progenitor (open squares) properties from Maund et al. (2006) are shown in each panel. The solid lines are the probability weighted mean SED fits and the dashed lines are the rms dispersion about the mean SED for the graphitic dust models. The upper left panel shows fits to the progenitor fluxes from Maund et al. (2006) with no additional circumstellar dust. The upper right panel shows the SED in May 2004 (solid points), also from Maund et al. (2006). The lower panels show the SED combining the optical data from December 2008 (Smith et al. 2011) with the mid-IR data from August 2009. The models in the lower panels treat the mid-IR fluxes as either a measurement (left) or an upper bound (right). In May 2004 the source seems to be fainter than the progenitor but it is difficult to be certain without any near/mid-IR data.

only be reached for a very hot star, but the SED in 2008 is inconsistent with such high temperatures. In 2004, the transient seems to have been considerably bluer and lower luminosity. The preferred models are probably cooler, less luminous and little obscured compared to 2008, with T_* in the range from 7500 to 20000 K, luminosity $L_* \simeq 10^{4.8 \pm 0.3} L_\odot$. The optical depths are $\tau_V \simeq 2.0 \pm 0.1$ and 4.6 ± 0.3 for the graphitic and silicate models, and the two models fit equally well. The ejected mass need only be $\log(M_{E\kappa_{100}}/M_\odot) \simeq -2.5 \pm 0.1$ for the graphitic models and -2.3 ± 0.1 for the silicate, consistent with a low efficiency radiatively driven transient. The inner radius of the dust, $R_{in} \simeq 10^{15.3}$ cm, roughly corresponds to the dust formation radius (Eqn. 1) for its luminosity, consistent with the high inner edge dust temperatures, (1500 and 2000 K) of the best models. Neither fit is perfect, but with the observations separated by a year this may not be surprising.

There are two problems with this model arising from the fact that the optical fluxes changed little between May 2004, one year post peak, and December 2008, over 5 years post-peak. The first is simply that at the earlier epoch the inner edge of the ejecta would lie over 5 times closer to the star and would have over twice the temperature, but dust simply cannot form/survive at temperatures of 3000-4000 K. This suggests that the velocities must be higher than 130 km/s. Making it circumstellar dust that was not associated with the transient is ruled out by the luminosity and color of the progenitor. The SED does allow higher dust radii and ejecta velocities, although the fits are poorer. The second problem is the familiar one that the optical depth should have been over 25 times higher in May 2004, which is inconsistent with the modest changes in the optical fluxes. If the dust is associated with the transient, then the dust must be forming in a relatively steady, low optical depth wind, which is consistent with $R_{in} \simeq R_f$ and dust temperatures close to the destruction temperature. The wind velocity may have to be somewhat higher than 130 km/s in order for dust to form and grow since $R_f/130 \text{ km/s} \simeq 5$ years is significantly larger than the elapsed time from the peak to May 2004.

5. Discussion

The standard picture of these transients is that the stars undergo a relatively short duration eruption with high mass loss rates, forming a shell of material that forms dust and then obscures the star at later times. The most striking result of our survey is that we find no source (with adequate data to draw a conclusion) that is consistent with this standard picture. The problem for the standard picture is that expanding shells of material impose a tyranny of geometry on the evolution of the system because the optical depth drops as $\tau \propto 1/r^2 \propto 1/t^2$. Optical fluxes depend exponentially on the optical depth and it generally requires physically unreasonable changes in luminosity and temperature to balance the effects of the evolution in the optical depth on the optical fluxes. The problem is generic to transient radial outflows, not just to spherical shells. It may be a failure of imagination, but we have found no plausible, generic means of avoiding this basic scaling and some, such as the growth of inhomogeneities in the ejecta, that will make the problem worse.

To make these events stellar transients, in many cases the simplest solution is to make them long lived. The optical transient is simply a sign post that the star is transitioning from a low mass loss rate to a high

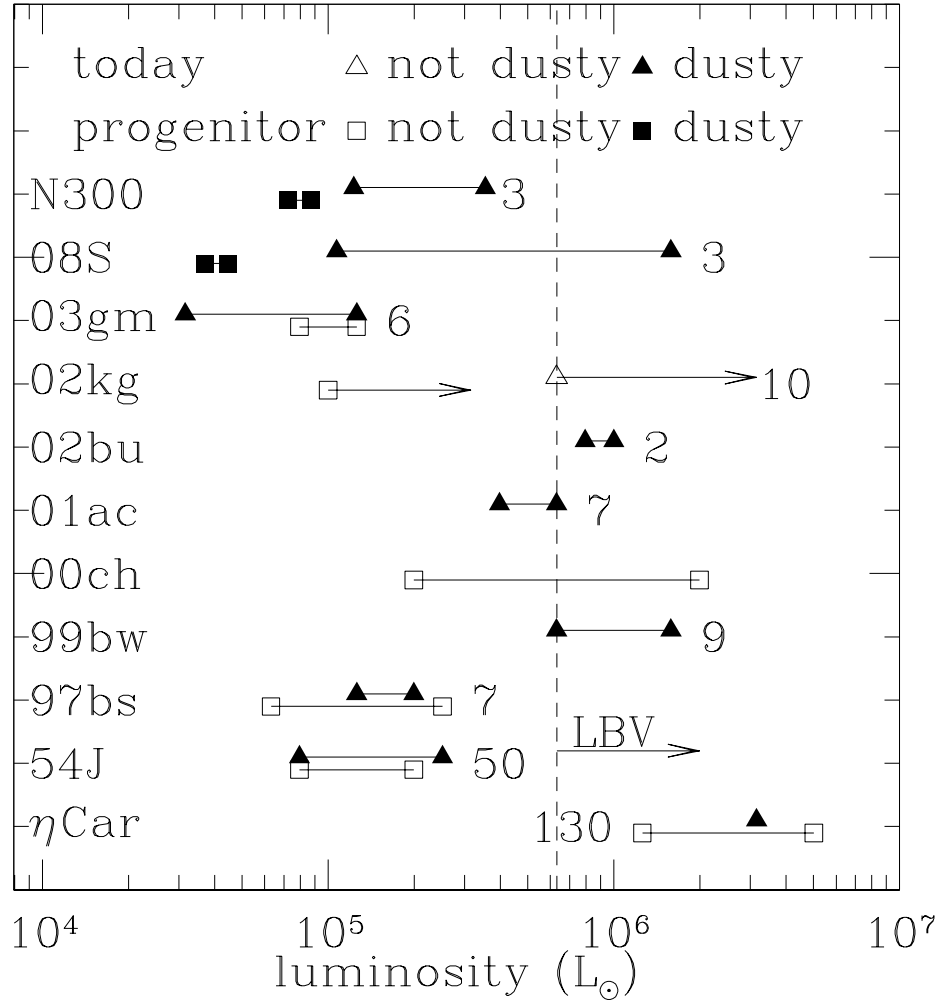


Fig. 25.— Progenitor and present day luminosities of the transients. For each object, the lower bar with squares shows the allowed range of luminosities for the progenitor stars while the upper bar with triangles shows the allowed range of luminosities at the time of the most recent mid-IR observations. The number gives the number of years between the transient peak and the mid-IR observations. The symbols are filled if most of the energy is radiated in the mid-IR by dust, and open if most is direct emission from the photosphere. Except for the two variable stars, SN 2000ch and SN 2001kg/V37, the present day emissions of all the other systems are dominated by circumstellar dust. For SN 1954J and SN 1997bs, the dust emission is not directly observed. The vertical dotted line shows the minimum luminosity for a LBV (e.g. Smith & Owocki 2006). See the discussions of the individual objects for any caveats.

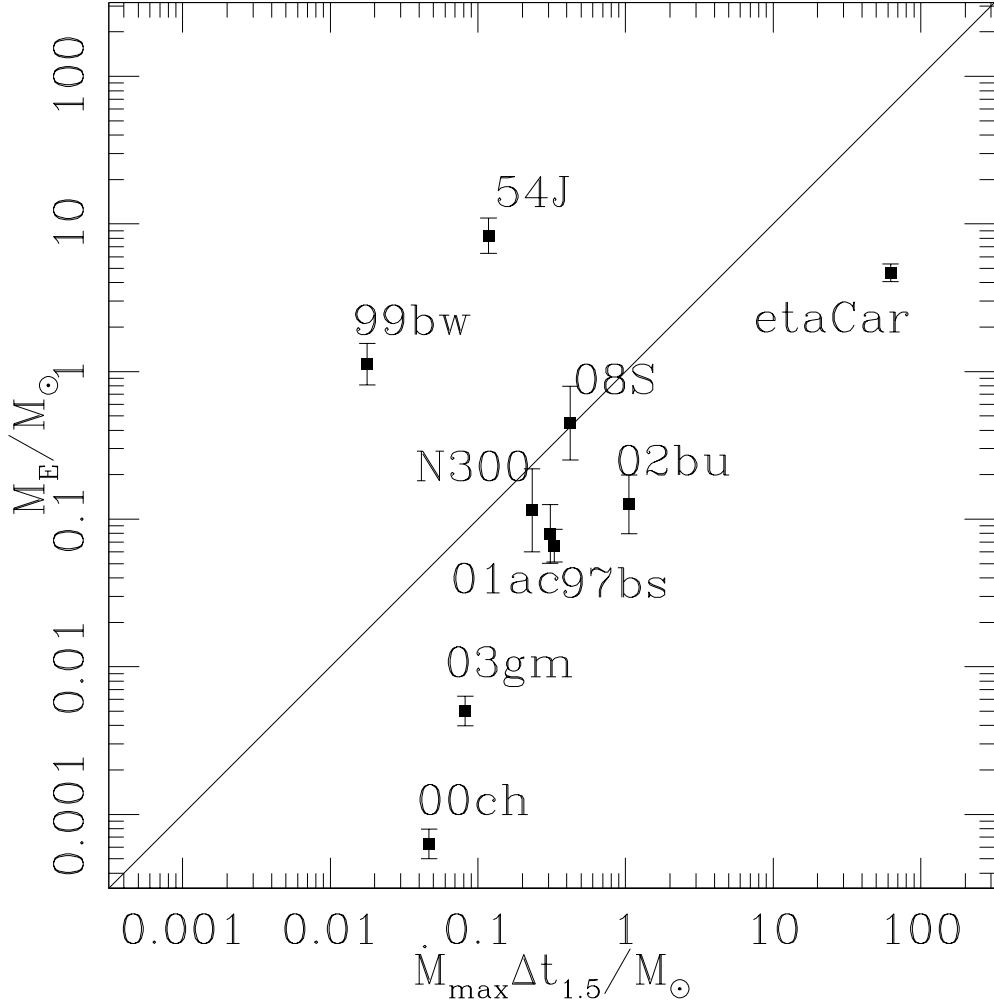


Fig. 26.— The maximum ejected mass for radiative processes, $\dot{M}_{max}\Delta t_{1.5}$ (Eqn. 6, Table 2), as compared to the mass estimated from the DUSTY model optical depths, M_E , for silicate dusts. The estimates of M_E are proportional to $M_E \propto \kappa_{100}^{-1} R_{in}^2$ where R_{in} is constrained by a combination of the SED and the velocities from Table 1. Radiatively driven transients obscured by the ejected material should lie below the diagonal line. Because there is only a lower bound on $\Delta t_{1.5}$ for SN 1999bw, it can be shifted to the right as $\log(\Delta t_{1.5}/10\text{days})$ by extending the transient to be longer than the lower limit of $\Delta t_{1.5} > 10$ days (see Table 1).

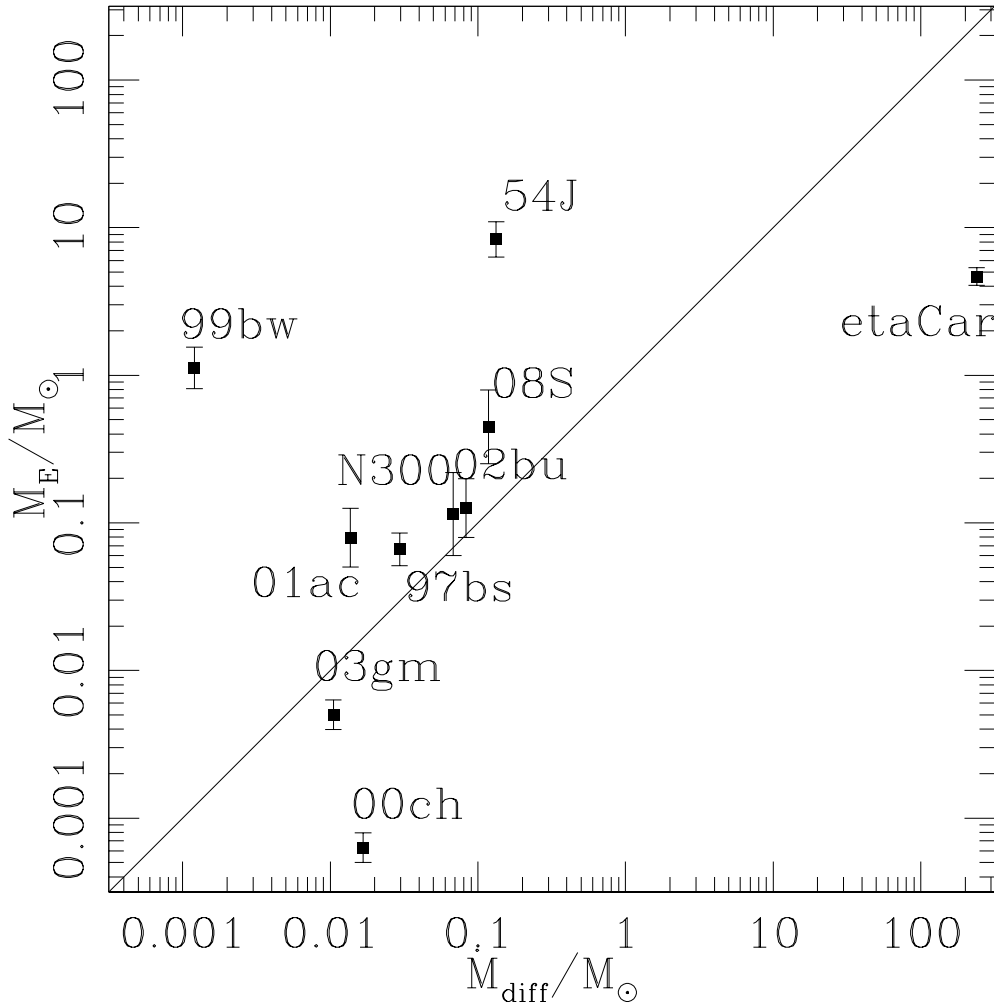


Fig. 27.— Estimates of the ejected masses for explosive processes, M_{diff} (Eqn. 9, Table 2), as compared to the mass estimated from the DUSTY model optical depths, M_E , for silicate dusts. The estimates of M_E are again proportional to $M_E \propto \kappa_{100}^{-1} R_{in}^2$. Explosive transients obscured by the ejected material should lie close to the diagonal line. Because there is only a lower bound on $\Delta t_{1.5}$ for SN 1999bw, it can be shifted to the right as $\log(\Delta t_{1.5}/10\text{days})$ by extending the transient duration.

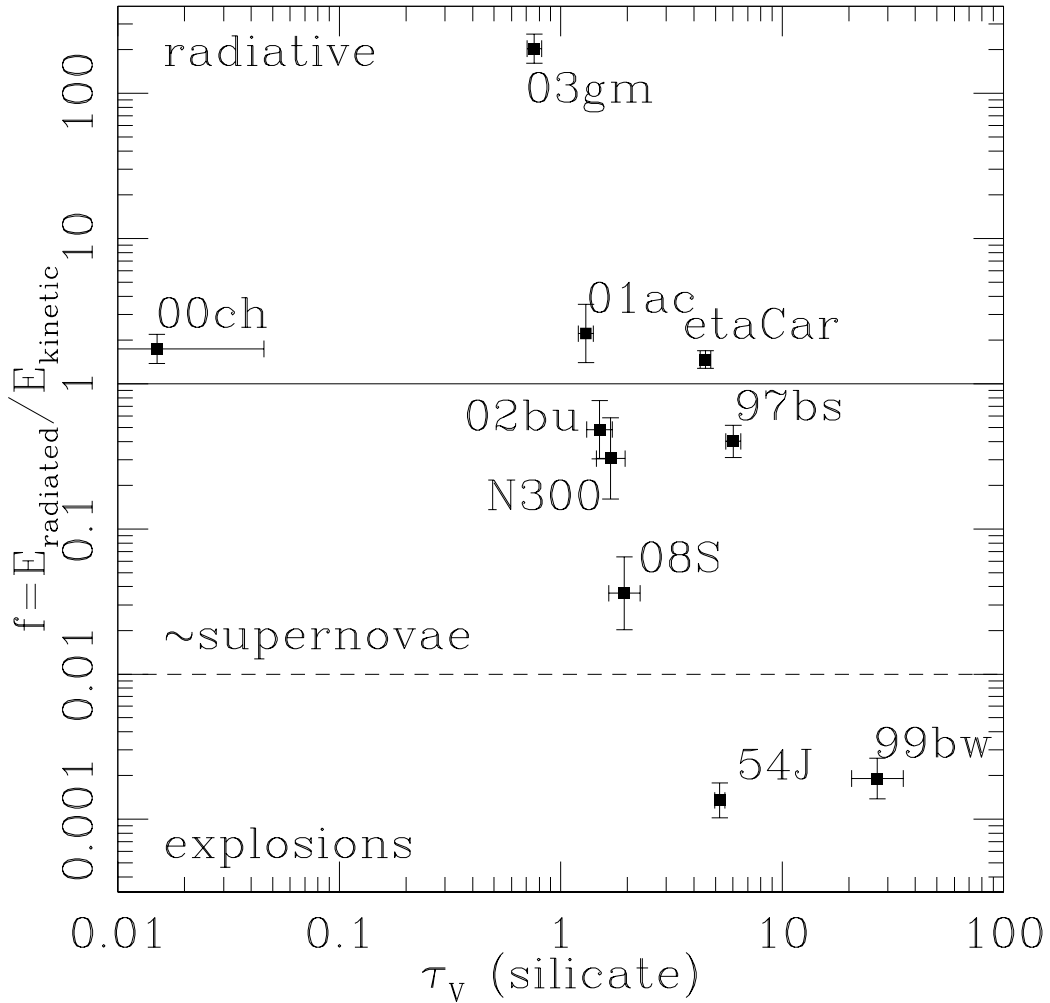


Fig. 28.— The mechanism diagnostic $f = E_{\text{radiated}}/E_{\text{kinetic}}$ as a function of the DUSTY silicate optical depth τ_V for the most recent mid-IR epoch. Radiatively driven models should generally have $f \gg 1$ and explosions should have $f \ll 1$, where $f = 1$ is indicated by the solid line. Typical supernovae have $f \simeq 0.01$, which is shown by the dashed line. SN 2002kg is not shown since it shows no evidence of dust. SN 1999bw can be shifted upwards by $\log(\Delta t_{1.5}/10 \text{ days})$ because the true event duration is unknown.

mass loss rate. For these typically hot stars, a mass loss rate of order $\dot{M} \gtrsim 10^{-2.5} M_{\odot}/\text{year}$ leads to dust formation because the wind shields the dust formation region from the UV emissions of the generally hot stars and the high densities allow particle growth (see Kochanek 2011a). Due to a combination of the fading of the initial transient and the formation of dust, the star fades in the optical to be fainter than the progenitor *but the star remains in the high mass loss state!* The advantage of a steady wind is that it has a roughly constant optical depth once the dust starts to form, which is far more consistent with the available data. When the star leaves the high mass loss state and drops below the threshold for dust formation, the optical depth initially drops on the time scale to cross the dust formation radius and then settles onto the $\tau \propto 1/t^2$ scaling of a shell.

In particular, this is the only solution we found to explain the historical visual light curve of η Carinae – η Carinae went into a high mass loss state circa 1850 and came out of it circa 1950. As it exited the high mass loss phase, it dropped in luminosity and reverted to a hotter temperature. This is by far the simplest explanation for the long period of roughly constant visual luminosity and color. If all the dust was produced in a short lived period circa 1850, there is no physically reasonable evolution in the stellar luminosity and temperature that can reproduce the observed light curve – the luminosity must change by an order of magnitude just to compensate for a change in optical depth of $\Delta\tau_{e,V} = \ln 10 = 2.3$, while the optical depth of the ejecta should have changed by almost two orders of magnitude over that period! The only effective counter to the effects of expansion on the optical depth is to steadily raise the opacity as the shell expands, but we have been unable to identify any realistic mechanism for doing so. It is more likely that the effective opacity is diminishing as the shell becomes less homogeneous with paths through the ejecta of lower optical depth than the mean.

For the extragalactic sources, the existing data suggest this solution for SN 1997bs, SN 1954J and SN 2003gm if they are to be explained as stellar transients. Of these three sources, only SN 2003gm is clearly a bright mid-IR source, while we only obtained upper limits for SN 1997bs and SN 1954J. The optical light curves of SN 1997bs require dust formation with an optical depth of order $\tau_V \simeq 10$ after 9 months strongly indicating that the mass loss rate was high for an extended period after the transient faded in the optical. SN 1999bw, SN 2001ac, and SN 2002bu (and possibly SN 2003gm) seem more likely to have the physics of SN 2008S (see Kochanek 2011a) as previously noted for most of these cases in Thompson et al. (2009). They generally show signs of extinction at peak, become completely obscured post-transient, have long lived luminosities of $10^{5.5}$ to $10^{6.0} L_{\odot}$, and show some signs that the dust initially appears at radii larger than allowed by the expansion speed. Like SN 2008S, these systems were probably obscured by dust forming in a dense pre-existing wind. The dust is then largely destroyed by the transient but then starts to reform as the transient fades because of the very high wind densities. The reformed dust again cloaks the system and the late time luminosity is powered by the continued expansion of the shock wave through the wind. The case is strongest for SN 1999bw, whose mid-IR SED changed little between April 2004 and May 2008.

Two of the sources we consider, SN 2000ch and SN 2002kg/V37, are optically variable sources without strong mass loss or significant dust creation. Both sources have also had repeated episodes of optical variability (Weis & Bomans 2005, Pastorello et al. 2010). SN 2002kg shows no signs of dust, while SN 2000ch appears to have a low optical depth dusty wind. While they have been referred to as LBV's, the very lumi-

nous star associated with SN 2000ch has luminosity/temperature variations opposite (Pastorello et al. 2010) from those normally associated with LBVs (Humphreys & Davidson 1994), while SN 2002kg/V37 is of fairly low luminosity for an LBV. The inverted color evolution of SN 2000ch could be created by the stellar variability modulating the dust properties of a wind though variations in the formation radius or grain size with stellar luminosity and mass loss rate.

Fig. 25 provides a summary of the luminosities of the progenitors and for the most recent mid-IR epoch for each object. We also include the estimates for SN 2008S and the 2008 NGC 300 transient from Kochanek (2011a). There are many caveats to these estimates (as discussed in the previous sections), but there are some general patterns. First, of the systems where we can estimate the progenitor luminosity, only the two sources known to simply be variable stars, SN 2002kg/V37 and SN 2000ch, can be above the frequently used luminosity limit of $10^{5.8}L_{\odot}$ for LBVs (e.g. Smith & Owocki 2006). In general, these transients do not seem to be associated with very massive, very luminous stars, so the entire analogy with the (great) eruptions of LBVs seems weak since they are generally lower luminosity stars far from their Eddington limits. These are largely transients from stars with $L_* < 10^{5.3}L_{\odot}$, which corresponds to $M_* \lesssim 25M_{\odot}$ in the Marigo et al. (2008) models. As noted in Kochanek (2011b), they also have far higher expansion velocities than is typically observed for the shells around Galactic LBVs. This could be related to the observation by Dessart et al. (2010) that the envelopes of lower mass ($M_* \lesssim 15M_{\odot}$) stars are far less tightly bound, which makes it far easier for them to produce lower luminosity and energy (explosive) transients. Broadly speaking, there is no convincing evidence that there is any relationship between the progenitors of the supernova impostors and LBVs.

Second, in all cases where we have information on both the progenitor luminosity and the late time luminosity of a (potentially) surviving star, there is no evidence that the stars ever become significantly sub-luminous compared to their progenitors. Physically, this is expected because stars are self-gravitating systems and essentially cannot be significantly sub-luminous at the surface without also being out of hydrostatic equilibrium. If significantly sub-luminous, a star must start to dynamically contract, and the potential energy release returns the star to hydrostatic equilibrium. The recovery time discussed by Smith et al. (2011), $t_R = \Delta E/L_*$, is not really relevant for the stellar luminosity because the dominant means of reheating an envelope with too little thermal energy is Kelvin-Helmholtz contraction rather than the energy radiated from the interior. Moreover, the sources observed at late times are frequently brighter rather than fainter than their progenitors.

Figures 26 and 27 compare the mass loss estimates from the SED models to the predictions given in Table 2 for radiatively ($\dot{M}_{max}\Delta t_{1.5}$ from Eqn. 6) and explosively (M_{diff} from Eqn. 9) driven transients. In most cases, either scenario is arguably consistent with the mass required to support the observed optical depths given all the other uncertainties. If the transients are driven radiatively and all the mass has to be ejected in $\Delta t_{1.5}$, then a large fraction of the available energy/luminosity has to be used to accelerate the ejected material. If, however, much of the mass loss occurs over a period significantly longer than the optical transient, as seems to be the case for many of the systems (e.g. η Carinae and SN 1997bs in particular), there should be little difficulty radiatively driving the necessary mass loss. The two problematic systems in either scenario are SN 1954J and SN 1999bw, where far more mass is needed to produce the late-time optical

depths than can be accounted for in either model. Extending the transient in SN 1999bw can help, but seems unlikely to solve the problem. SN 1954J is still more problematic because the 50 year time scale makes the dust radius very large and hence requires a great deal of ejected mass to retain a finite optical depth. These are the clearest cases where the mass estimates appear to require different physics, where the simplest solution is to use a longer lived wind for SN 1954J and to make SN 1999bw an object like SN 2008S and the 2008 NGC 300 transient. It is not a coincidence that the oldest systems other than η Carinae show the greatest problems, because systems with different physics that are then modeled as an ejected shell will have estimates of M_E that will tend to increase with the elapsed time (as t^2). Observing such a trends for the younger systems (e.g. SN 2002bu, SN 2008S, and the NGC 300 transient) would provide additional evidence that they are a separate class of transients.

Finally, Figure 28 shows estimates of the ratio of radiated to kinetic energy $f = E_{rad}/E_{kinetic}$ (Eqn. 11) as another diagnostic of the transient mechanism. We show it as a function of the silicate DUSTY model optical depths τ_V , which can be used as a proxy for changes in the ejecta mass since $\tau_V \propto M_E$ and $f \propto M_E^{-1}$. The picture is broadly similar for the graphitic models. Most of these transients are more consistent with an explosive origin for the transient, with $f < 1$. While a radiatively driven transient can have $f < 1$ when the observed luminosity is significantly less than the true luminosity because most of it is absorbed into accelerating the ejecta (Eqn. 6, Owocki et al. 2004), it is difficult to then understand why these systems show no significant differences in their external appearance. A number of systems, particularly SN 1954J, SN 1999bw, SN 2008S have $f \ll 1$ and probably cannot be reconciled with a short duration radiatively driven process. We argued in Kochanek (2011a) that SN 2008S and the NGC 300 transient had to be explosive in nature in order to explain the destruction of the dust that obscured the progenitors, so perhaps all these transients are driven by an initial (weak?) explosion, as discussed in Dessart et al. (2010). After ejecting some mass in the initial optical transient, many of the systems then move into a high mass loss state as the envelope re-equilibrates following the explosion in order to explain the wind-like features needed to explain many of the systems.

For the present study we have simply assumed that there is a surviving star powering the present day emissions. Aside from the variable stars SN 2000ch and SN 2002kg, there is no solid evidence this is correct. Most of the observed luminosities are also consistent with being powered by a shock expanding through a dense circumstellar medium as Kochanek (2011a) posited for SN 2008S and the NGC 300 transient. Optical spectra or X-ray observations can test this hypothesis, but for heavily obscured sources behind a veil of dust and gas it is difficult to make these tests. The most powerful argument against these sources being SNe remains the overall energetics, but it is awkward that no compelling case can be made for any other mechanism (see, for example, the discussions in Thompson et al. (2009) or Smith et al. (2011)).

The biggest problem for characterizing these sources is the fragmentary nature of the data. In particular, it is almost certain that some of our particular conclusions are incorrect because we are interpreting such fragmentary data. For example, many of the sources show signs of absorption at the transient peak, but there are no near/mid-IR observations to detect the emissions that result if the dust is circumstellar – SN 1999bw and SN 2002bu may well have had their peak emissions in the mid-IR rather than the optical. Since we now know that dust and dust formation in the ejecta are a key part of the physics, it is essential

to characterize these transients beyond the time scales on which dust can form, typically 6 months to a year, both in the optical to observe the increasing optical depth, and in the near/mid-IR to determine the dust temperature/formation radius. The evolution in the following year rapidly determines whether the mass loss was associated with the short optical transient or if the star has entered a high mass loss state and is generating a relatively steady wind. At later times, we should both see the dust temperature dropping and the reappearance of the stars as the optical depth drops. For the objects we discuss, most of the questions can be answered by coarsely monitoring their optical through mid-IR SEDs over a period of years. In the optical and near-IR this is relatively straight forward given the capabilities of HST but will require greater wavelength coverage and moderately deeper exposures than have generally been obtained. Warm Spitzer can effectively monitor the mid-IR emission in the short term, but JWST may be required to address some final puzzles because it will largely eliminate the problem of confusion and will again allow measurements at the longer wavelengths (principally 8-24 μ m) needed to fully characterize the dust emission. Whatever the failings of our analysis, these transients are creatures of the near/mid-IR and simply cannot be understood without data at these wavelengths.

We thank R.M. Wagner for supplying images of SN 2000ch, and J.F. Beacom, J.-L. Prieto, and T.A. Thompson for discussions and comments. CSK, DMS and KZS are supported by NSF grant AST-0908816. KZS is also supported by NSF grant AST-1108687. Based in part on observations made with the Large Binocular Telescope. The LBT is an international collaboration among institutions in the United States, Italy and Germany. The LBT Corporation partners are: the University of Arizona on behalf of the Arizona university system; the Istituto Nazionale di Astrofisica, Italy; the LBT Beteiligungsgesellschaft, Germany, representing the Max Planck Society, the Astrophysical Institute Potsdam, and Heidelberg University; the Ohio State University; and the Research Corporation, on behalf of the University of Notre Dame, University of Minnesota and University of Virginia. This work is based in part on observations made with the Spitzer Space Telescope, which is operated by the Jet Propulsion Laboratory, California Institute of Technology under a contract with NASA and on observations made with the NASA/ESA Hubble Space Telescope, and obtained from the Hubble Legacy Archive, which is a collaboration between the Space Telescope Science Institute (STScI/NASA), the Space Telescope European Coordinating Facility (ST-ECF/ESA) and the Canadian Astronomy Data Centre (CADC/NRC/CSA). This research has made use of the NASA/IPAC Extragalactic Database (NED) which is operated by the Jet Propulsion Laboratory, California Institute of Technology, under contract with the National Aeronautics and Space Administration.

LBT, Spitzer, HST

A. A Non-Parametric Model For The Light Curve of η Carinae

Consider a model with mass loss rate $\dot{M}(t)$, constant velocity v_w , luminosity $L(t)$, and temperature $T(t)$ defined annually from 1850 to 2010. By an appropriate choice of numerical variables we can restrict the luminosity to the range $6 < \log L(t)/L_\odot < 8$, and the temperature to the range $7000 \text{ K} < T_* < 40000 \text{ K}$. The primary assumption of the model is that the material ejected at time t_e can be treated as an expanding shell

with optical depth

$$\tau(t|t_e) \simeq 2000 \left(\frac{\dot{M}}{M_\odot/\text{year}} \right) \left(\frac{500 \text{ km/s}}{v_w} \right)^2 \left(\frac{\kappa_V}{31 \text{ cm}^2/\text{g}} \right) \left(\frac{\text{year}}{t_-} - \frac{\text{year}}{t_+} \right) \quad (\text{A1})$$

at some later time t where

$$t_\pm = \max(t_f, t_o - t \pm \Delta t/2) \quad (\text{A2})$$

determine the inner and outer radii of the material and the dust formation radius is $R_f = v_w t_f$. Essentially, each year of the transient is treated as a shell of material evolving as in Eqn. 15. We set $t_f = 5$ years and $v_w = 500$ km/s, which is roughly correct. The optical depth is scaled to the effective absorption opacity for silicates ($\kappa_{e,V} = 32 \text{ cm}^2/\text{g}$). In these models the only effect of changing the velocity or the opacity is to rescale the \dot{M} so as to keep the optical depth fixed, $\tau \propto \dot{M}\kappa/v_w$. The model also only allowed dust formation when $T < 10000$ K and $\dot{M} > 10^{-3}M_\odot/\text{year}$, loosely following the criteria from Kochanek (2011a), although models without these criteria have the same qualitative properties. The V-band light curve was then fit using Eqn. 18. Priors were used to keep the luminosity, temperature and mass loss rates smooth and to favor declining luminosities and mass loss rates and increasing temperatures. The optical depth in 1974 was constrained to roughly match the SED models. Finally, a prior was used to try to maximize the mass loss. By experimenting with the priors we attempted to drive the solutions towards various scenarios, but only one class of solutions worked.

REFERENCES

- Alard, C., & Lupton, R. H. 1998, ApJ, 503, 325
- Alard, C. 2000, A&AS, 144, 363
- Ayani, K., Kawabata, T., & Yamaoka, H. 2002, IAU Circ., 7864, 4
- Beckmann, S., & Li, W. D. 2001, IAU Circ., 7596, 1
- Berger, E., et al. 2009, ApJ, 699, 1850
- Bond, H. E., Bedin, L. R., Bonanos, A. Z., Humphreys, R. M., Monard, L. A. G. B., Prieto, J. L., & Walter, F. M. 2009, ApJ, 695, L154
- Botticella, M. T., et al. 2009, MNRAS, 398, 1041
- Botticella, M. T., Smartt, S. J., Kennicutt, R. C., Jr., et al. 2011, arXiv:1111.1692
- Clark, J. S., Crowther, P. A., Larionov, V. M., Steele, I. A., Ritchie, B. W., & Arkharov, A. A. 2009, A&A, 507, 1555
- Chu, Y.-H., Gruendl, R. A., Stockdale, C. J., Rupen, M. P., Cowan, J. J., & Teare, S. W. 2004, AJ, 127, 2850
- Davidson, K., & Ruiz, M. T. 1975, ApJ, 202, 421

- Davidson, K. 1987, *ApJ*, 317, 760
- Dessart, L., Livne, E., & Waldman, R. 2010, *MNRAS*, 405, 2113
- Draine, B. T., & Lee, H. M. 1984, *ApJ*, 285, 89
- Draine, B. T. 2011, *Physics of the Interstellar and Intergalactic Medium* by Bruce T. Draine. Princeton University Press, 2011. ISBN: 978-0-691-12214-4,
- Elitzur, M., & Ivezić, Z. 2001, *MNRAS*, 327, 403
- Falk, S. W., & Arnett, W. D. 1977, *ApJS*, 33, 515
- Fernández-Lajús, E., et al. 2009, *A&A*, 493, 1093
- Filippenko, A. V., Barth, A. J., Bower, G. C., Ho, L. C., Stringfellow, G. S., Goodrich, R. W., & Porter, A. C. 1995, *AJ*, 110, 2261
- Filippenko, A. V. 1997, *ARA&A*, 35, 309
- Filippenko, A. V., Li, W. D., & Modjaz, M. 1999, *IAU Circ.*, 7152, 2
- Filippenko, A. V. 2000, *IAU Circ.*, 7421, 3
- Foley, R. J., Smith, N., Ganeshalingam, M., Li, W., Chornock, R., & Filippenko, A. V. 2007, *ApJ*, 657, L105
- Freedman, W. L., et al. 2001, *ApJ*, 553, 47
- Garcia-Segura, G., Mac Low, M.-M., & Langer, N. 1996, *A&A*, 305, 229
- Garnavich, P., Jha, S., Kirshner, R., Calkins, M., & Brown, W. 1999, *IAU Circ.*, 7150, 1
- Gieren, W., Pietrzyński, G., Soszyński, I., Bresolin, F., Kudritzki, R.-P., Minniti, D., & Storm, J. 2005, *ApJ*, 628, 695
- Goobar, A. 2008, *ApJ*, 686, L103
- Goodrich, R. W., Stringfellow, G. S., Penrod, G. D., & Filippenko, A. V. 1989, *ApJ*, 342, 908
- Horiuchi, S., Beacom, J. F., Kochanek, C. S., et al. 2011, *ApJ*, 738, 154
- Humphreys, R. M., & Davidson, K. 1994, *PASP*, 106, 1025
- Humphreys, R. M., Davidson, K., & Smith, N. 1999, *PASP*, 111, 1124
- Humphreys, R. M., Bond, H. E., Bonanos, A. Z., et al. 2011, *arXiv:1109.5131*
- Ivezic, Z., & Elitzur, M. 1997, *MNRAS*, 287, 799

- Ivezic, Z., Nenkova, M., & Elitzur, M. 1999, User Manual for DUSTY, University of Kentucky Internal Report <http://www.pa.uky.edu/~moshe/dusty/>
- Kashi, A., Frankowski, A., & Soker, N. 2010, *ApJ*, 709, L11
- Khan, R., Stanek, K. Z., Prieto, J. L., Kochanek, C. S., Thompson, T. A., & Beacom, J. F. 2010, *ApJ*, 715, 1094
- Kochanek, C. S., Beacom, J. F., Kistler, M. D., Prieto, J. L., Stanek, K. Z., Thompson, T. A., Yuksel, H. 2008, *ApJ*, 684, 1336
- Kochanek, C. S. 2009, *ApJ*, 707, 1578
- Kochanek, C. S., Szczygieł, D. M., & Stanek, K. Z. 2011, *ApJ*, 737, 76
- Kochanek, C. S. 2011a, *ApJ*, 741, 37
- Kochanek, C. S. 2011b, *ApJ*, 743, 73
- Kudritzki, R.-P., & Puls, J. 2000, *ARA&A*, 38, 613
- Leaman, J., Li, W., Chornock, R., & Filippenko, A. V. 2010, arXiv:1006.4611
- Li, W. D. 1999, *IAU Circ.*, 7149, 1
- Li, W., Filippenko, A. V., Van Dyk, S. D., Hu, J., Qiu, Y., Modjaz, M., & Leonard, D. C. 2002, *PASP*, 114, 403
- Li, W., Leaman, J., Chornock, R., et al. 2011, *MNRAS*, 412, 1441
- Lien, A., Fields, B. D., & Beacom, J. F. 2010, *Phys. Rev. D*, 81, 083001
- Marigo, P., Girardi, L., Bressan, A., Groenewegen, M. A. T., Silva, L., & Granato, G. L. 2008, *A&A*, 482, 883
- Martin, J. C., Davidson, K., & Koppelman, M. D. 2006, *AJ*, 132, 2717
- Matheson, T., & Calkins, M. 2001, *IAU Circ.*, 7597, 3
- Mathis, J. S., Rumpl, W., & Nordsieck, K. H. 1977, *ApJ*, 217, 425 S. J., Kudritzki, R. P., Podsiadlowski, P., & Gilmore, G. F. 2004, *Nature*, 427, 129
- Maund, J. R., et al. 2006, *MNRAS*, 369, 390
- Maund, J. R., et al. 2008, *MNRAS*, 387, 1344
- Ohsawa, R., et al. 2010, *ApJ*, 718, 1456
- Ostriker, E. C., Stone, J. M., & Gammie, C. F. 2001, *ApJ*, 546, 980

- Owocki, S. P., Gayley, K. G., & Shaviv, N. J. 2004, *ApJ*, 616, 525
- Papenkova, M., & Li, W. D. 2000, *IAU Circ.*, 7415, 1
- Pastorello, A., et al. 2010, arXiv:1006.0504
- Patat, F., Pastorello, A., & Aceituno, J. 2003, *IAU Circ.*, 8167, 3
- Prieto, J. L. 2008, *The Astronomer's Telegram*, 1550, 1
- Prieto, J. L., et al. 2008b, *ApJ*, 681, L9
- Prieto, J. L., Sellgren, K., Thompson, T. A., & Kochanek, C. S. 2009, *ApJ*, 705, 1425
- Prieto, J. L., et al. 2010, *The Astronomer's Telegram*, 2406, 1
- Puckett, T., & Gauthier, S. 2002, *IAU Circ.*, 7863, 1
- Puls, J., Vink, J. S., & Najarro, F. 2008, *A&A Rev.*, 16, 209
- Pumo, M. L., et al. 2009, *ApJ*, 705, L138
- Rest, A., Prieto, J. L., Walborn, N. R., et al. 2011, arXiv:1112.2210
- Robinson, G., Hyland, A. R., & Thomas, J. A. 1973, *MNRAS*, 161, 281
- Robinson, G., Mitchell, R. M., Aitken, D. K., Briggs, G. P., & Roche, P. F. 1987, *MNRAS*, 227, 535
- Sahu, D. K., Anupama, G. C., Srividya, S., & Muneer, S. 2006, *MNRAS*, 372, 1315
- Schlegel, D. J., Finkbeiner, D. P., & Davis, M. 1998, *ApJ*, 500, 525
- Schlegel, E. M. 1990, *MNRAS*, 244, 269
- Schwartz, M., Li, W., Filippenko, A. V., & Chornock, R. 2003, *IAU Circ.*, 8051, 1
- Schwartz, M., Holvorcem, P., & Li, W. 2003, *IAU Circ.*, 8164, 1
- Sirianni, M., Jee, M. J., Benitez, N. et al. 2005, *PASP*, 117, 1049
- Smith, N., Humphreys, R. M., & Gehrz, R. D. 2001, *PASP*, 113, 692
- Smith, N., Gehrz, R. D., Hinz, P. M., et al. 2003, *AJ*, 125, 1458
- Smith, N., Vink, J. S., & de Koter, A. 2004, *ApJ*, 615, 475
- Smith, N., & Owocki, S. P. 2006, *ApJ*, 645, L45
- Smith, N., et al. 2009, *ApJ*, 697, L49
- Smith, N. 2009, arXiv:0906.2204

- Smith, N., Li, W., Silverman, J. M., Ganeshalingam, M., & Filippenko, A. V. 2011, *MNRAS*, 415, 773
- Stetson, P. B. 1987, *PASP*, 99, 191
- Sugerman, B., Meixner, M., Fabbri, J., & Barlow, M. 2004, *IAU Circ.*, 8442, 2
- Szczygieł, D. M., Prieto, J. L., Kochanek, C. S., Stanek, K. Z., Thompson, T. A., Beacom, J. F., Garnavich, P. M., & Woodward, C. E. 2011, *ApJ*, submitted
- Tammann, G. A., & Sandage, A. 1968, *ApJ*, 151, 825
- Thompson, T. A., Prieto, J. L., Stanek, K. Z., Kistler, M. D., Beacom, J. F., & Kochanek, C. S. 2009, *ApJ*, 705, 1364
- Toalá, J. A., & Arthur, S. J. 2011, *ApJ*, 737, 100
- Treffers, R. R., Peng, C. Y., Filippenko, A. V., Richmond, M. W., Barth, A. J., & Gilbert, A. M. 1997, *IAU Circ.*, 6627, 1 2006, *AJ*, 132, 729
- Tully, R. B., Shaya, E. J., Karachentsev, I. D., Courtois, H. M., Kocevski, D. D., Rizzi, L., & Peel, A. 2008, *ApJ*, 676, 184
- Van Dyk, S. D., Peng, C. Y., Barth, A. J., & Filippenko, A. V. 1999, *AJ*, 118, 2331
- Van Dyk, S. D., Peng, C. Y., King, J. Y., Filippenko, A. V., Treffers, R. R., Li, W., & Richmond, M. W. 2000, *PASP*, 112, 1532
- Van Dyk, S. D., Filippenko, A. V., & Li, W. 2002, *PASP*, 114, 700
- Van Dyk, S. D., Filippenko, A. V., Chornock, R., Li, W., & Challis, P. M. 2005, *PASP*, 117, 553
- Van Dyk, S. D., & Matheson, T. 2011, *arXiv:1112.0299*
- van Genderen, A. M., & The, P. S. 1984, *Space Sci. Rev.*, 39, 317
- Vink, J. S. 2009, in *Eta Carinae and the Supernova Impostors*, R. Humphreys & K. Davidson, eds. (Springer) [arXiv:0905.3338]
- Wagner, R. M., et al. 2004, *PASP*, 116, 326
- Walmswell, J. J., & Eldridge, J. J. 2011, *MNRAS*, 1859
- Weis, K., & Bomans, D. J. 2005, *A&A*, 429, L13 G. C., Campbell, A., Barlow, M. J., Sugerman, B. E. K., Meixner, M., & Bank, S. H. R. 2007, *ApJ*, 669, 525
- Wesson, R., et al. 2010, *MNRAS*, 403, 474
- Whitelock, P. A., Feast, M. W., Koen, C., Roberts, G., & Carter, B. S. 1994, *MNRAS*, 270, 364

Table 1. General Properties

Object	dist (Mpc)	$E(B-V)$	M (mag)		$\Delta t_{1.5}$ (days)	v_w (km/s)	$E = \nu L_\nu(1+f^{-1})$ (10^{48} ergs/s)	Δt (years)
η Carina	0.0023	0.51	-13.9 (B)		4400	650	58	129.3
SN 1954J	3.1	0.04	-11.2 (B)		100	700	0.11	50.0
SN 1961V	9.4	0.07	-17.8 (B)		200	3700	86	42.7
SN 1997bs	9.4	0.04	-13.8 (V)		45	765	0.31	3.9
SN 1999bw	13.5	0.02	-12.6 (R)		> 10	630	> 0.017	9.1
SN 2000ch	10.9	0.02	-12.6 (R)		25	1400	0.043	7.7
SN 2001ac	22.9	0.03	-13.9 (R)		50	287	0.29	6.8
SN 2002bu	5.8	0.01	-14.9 (R)		70	893	0.97	2.1
SN 2002kg	3.1	0.18	-10.3 (R)		365	350	0.075	5.6
SN 2003gm	20.2	0.05	-14.3 (I)		65	131	0.35	6.0
SN 2008S	5.6	0.35	-13.8 (R)		75	1100	0.39	2.6
NGC 300-OT	1.9	0.02	-13.1 (R)		80	560	0.22	1.6

Note. — We use the Cepheid distances from Freedman et al. (2001) for SN 1954J/V12 and SN 2002kg/V37 in NGC 2403, SN 1961V in NGC 1058 (assumed to be in a group with NGC 925), SN 1997bs in NGC 3627 and SN 1999bw in NGC 3198, the Cepheid distance of Gieren et al. (2005) for NGC 300, the distance adopted by Pastorello et al. (2010) for SN 2000ch, the distance adopted by Leaman et al. (2010) for SN 2001ac in NGC 3504, the distance adopted by Maund et al. (2006) for SN 2003gm in NGC 5334, and the distance used by Sahu et al. (2006) for SN 2004et in NGC 6946 for SN 2008S. Tully et al. (2008) report a Tully-Fisher distance estimate for SN 2002bu in NGC 4242. Galactic extinctions $E(B-V)$ are from Schlegel et al. (1998) except for η Carinae where we use the foreground extinction estimate of van Genderen & The (1984) and SN 2002kg where we used the estimate based on nearby stars from Maund et al. (2006). The transient magnitude M , duration $\Delta t_{1.5}$ and velocity v_w are taken from Smith et al. (2011). The elapsed time from the transient to the epoch of the mid-IR data used in the SED fits is Δt .

Table 2. Mass and Optical Depth Estimates

Object	$\dot{M}_{max}\Delta t_{1.5}$ (M_{\odot})	M_{diff} (M_{\odot})	M_E ($f^{-1}v^{-2}M_{\odot}$)	τ_V ($f^{-1}v^{-4}$)	λ_{peak} ($L_6^{-1/4}v^{1/2}\mu\text{m}$)
η Carina	63	240	14	3.1	22.5
SN 1954J	0.12	0.14	0.03	0.03	16.2
SN 1961V	95	2.9	0.64	0.05	28.2
SN 1997bs	0.34	0.03	0.06	9.4	5.0
SN 1999bw	> 0.02	> 0.01	> 0.01	> 0.21	7.3
SN 2000ch	0.05	0.02	0.01	0.04	9.8
SN 2001ac	0.31	0.02	0.35	140	3.8
SN 2002bu	1.06	0.09	0.13	57	3.6
SN 2002kg	0.09	0.89	0.07	26	3.8
SN 2003gm	0.38	0.02	2.1	5300	2.2
SN 2008S	0.43	0.12	0.04	6.7	4.8
NGC 300-OT	0.24	0.07	0.07	140	2.4

Note. — The three mass estimates are the upper limit for radiatively driven mass loss, $\dot{M}_{max}\Delta t_{1.5}$ (Eqn. 6) the estimate from the photon diffusion time scale, M_{diff} (Eqn. 9) and the estimate M_E based on the radiative efficiency f (Eqn. 11) where SN have $f \simeq 0.01$, near maximal radiatively driven winds have $f \simeq 1$ and normal radiatively driven winds have $f \gg 1$. The optical depth τ_V is estimated at the epoch of the measured SED based on M_E and assuming $\kappa_V = 100\kappa_{100} \text{ cm}^2/\text{g}$. The scaling of τ_V with f and velocity v_w is indicated. The expected peak wavelength of the SED is estimated for a luminosity of $L_* = 10^6 L_6 L_{\odot}$. The mass and optical depth limits for SN 1999bw are lower limits because there is only a lower bound on $\Delta t_{1.5}$ (see Table. 1).

Table 3. Spitzer Observations

SN	Date	MJD	PI/Program	$F_{3.6}$ (μJy)	$F_{4.5}$ (μJy)	$F_{5.8}$ (μJy)	$F_{8.0}$ (μJy)	F_{24} (μJy)	Comment/ F_{70} (μJy)
SN 1954J		merged data (1)		< 70	< 45	< 281	< 855	< 1570	
SN 1954J		merged data (1)		70 ± 21	45 ± 13	281 ± 65	855 ± 198	< 1570	
SN 1997bs	2004-05-22	53148	Kennicutt/159	< 68	< 72	336	1372		
SN 1997bs	2004-05-22	53148	Kennicutt/159	68 ± 20	72 ± 16	336 ± 68	1372 ± 286		
SN 1999bw	2004-04-30	53126	Kennicutt/159	20 ± 9	40 ± 4	144 ± 19	354 ± 68		
				20 ± 10	40 ± 20	110 ± 20	190 ± 40		S04
	2005-11-29	53704	Sugerman/20320	13 ± 6	19 ± 4	93 ± 22	230 ± 62	< 1100	
	2006-05-03	53859	Sugerman/20320	15 ± 8	15 ± 4	91 ± 25	226 ± 67	< 940	
	2008-05-13	54602	Meixner/40010	15 ± 6	12 ± 5	58 ± 19	224 ± 72	< 1400	
SN 2000ch	2007-12-27	54461	Kennicutt/40204	68 ± 6	50 ± 4	51 ± 4	40 ± 10		
	2008-05-20	54607	Fazio/40301					< 89	
SN 2001ac	2008-01-05	54471	Fazio/40349					< 530	
	2008-06-20	54638	Fazio/40349	19 ± 3	22 ± 2	26 ± 7	40 ± 14		
SN 2002bu	2004-04-25	53120	Fazio/69					750 ± 26	< 4200
	2004-05-02	53128	Fazio/69	544 ± 7	806 ± 9	1098 ± 12	1204 ± 20		
SN 2002kg		merged data (2)		3 ± 2	6 ± 2	< 35	< 21	< 630	
SN 2003gm	2009-08-08	55051	Sheth/60007	44 ± 11	35 ± 9				

Note. — Many of the observations assigned dates were observed over a few days to a week. In these cases, the Date is the date of the first observation and the MJD is the mean MJD of the sequences. The Comment/ F_{70} column contains either the $70\mu\text{m}$ flux or the reference of the alternate source of photometry for the epoch, where S04 is Sugerman et al. (2004). (1) The merged data for SN 1954J combined IRAC programs 159 (Kennicutt, 2004-10-08, 2004-10-12), 226 (Van Dyk, 2004-10-07, 2004-11-01, 2005-03-24), 20256 (Meikle, 2005-10-20, 2006-03-23), 30292 (Meikle, 2006-10-28, 2007-04-02), 30494 (Sugerman, 2006-10-31, 2007-04-2, 2007-11-19), 40010 (Meixner, 2007-11-23, 2008-04-12) and 40619 (Kotak, 2007-11-24, 2008-04-07) and MIPS programs 226 (Van Dyk, 2004-10-14) 30494 (Sugerman, 2006-12-01, 2007-04-13, 2007-11-29), 40010 (Meixner, 2007-10-24, 2008-04-14) and 40619 (Kotak, 2007-10-24, 2008-04-15). (2) The merged data for SN 2002kg removes program 226 and adds IRAC program 61002 (Freedman, 2009-11-14, 2009-12-03, 2009-12-20) from the list for SN 1954J.

Table 4. Hubble Observations

SN	Date	MJD	PI/Program	Filters and Limits (mag)			
SN 1999bw	2008-04-03	54559	Meixner/11229	F110W	F160W	F205W	
				< 23.11	< 22.20	< 21.18	
SN 2002bu	2005-03-20	53456	Filippenko/10272	F435W	F555W	F625W	F814W
				< 25.67	< 25.25	< 24.83	< 24.40

Note. — SN 1999W was observed with NICMOS/NIC2 and SN 2002bu was observed with ACS/HRC. These are 3σ upper limits derived from aperture photometry with standard aperture corrections.

Table 5. LBT Observations

SN	Date	MJD	U [mag]	B [mag]	V [mag]	R [mag]
SN 1954J	reference image		22.69 ± 0.06	23.35 ± 0.06	22.77 ± 0.12	22.36 ± 0.12
SN 1997bs	reference image		23.14 ± 0.06	22.54 ± 0.06	22.44 ± 0.06	22.42 ± 0.09
SN 2002kg	2008-03-09	54534	18.91 ± 0.01	19.62 ± 0.02	19.68 ± 0.01	19.49 ± 0.03
	2008-05-05	54591	18.78 ± 0.01	19.60 ± 0.02	19.64 ± 0.01	19.49 ± 0.03
	2008-11-22	54792	...	19.54 ± 0.02	19.58 ± 0.01	...
	2008-11-24	54794	...	19.59 ± 0.02	19.62 ± 0.01	...
	2009-01-30	54861	18.84 ± 0.01	19.66 ± 0.02	19.73 ± 0.01	19.61 ± 0.02
	2009-01-31	54862	18.88 ± 0.01	19.68 ± 0.02	19.73 ± 0.01	19.60 ± 0.02
	2010-10-01	55470	18.97 ± 0.01	19.78 ± 0.01	19.87 ± 0.01	19.77 ± 0.02
	2010-12-06	55536	19.14 ± 0.01	19.92 ± 0.01	20.02 ± 0.01	19.96 ± 0.01
	2010-12-08	55538	19.15 ± 0.01	19.92 ± 0.01	20.05 ± 0.01	19.97 ± 0.01
	2010-12-10	55540	19.19 ± 0.01	19.93 ± 0.01	20.03 ± 0.01	19.98 ± 0.01
	2010-12-13	55543	19.16 ± 0.01	19.91 ± 0.01	20.03 ± 0.01	19.99 ± 0.01
	2011-02-07	55599	19.33 ± 0.00	20.05 ± 0.01	20.19 ± 0.01	...
	2011-11-24	55889	...	20.04 ± 0.01	20.21 ± 0.01	20.22 ± 0.01

Note. — The light curve uncertainties include both the ISIS errors and the DAOPHOT uncertainties in the reference images. The magnitude calibration errors for SN 1954J and SN 2002kg are 0.04, 0.02, 0.01 and 0.03 mag in U, B, V and R respectively, while those for SN 1997bs are 0.04, 0.04, 0.02 and 0.01 mag.

Table 6. ISIS LBT Light Curves

SN	Date	MJD	F_U [μJy]	F_B [μJy]	F_V [μJy]	F_R [μJy]
SN 1954J	2008-03-09	54534	0.45 ± 0.12	0.53 ± 0.11	0.16 ± 0.09	0.67 ± 0.10
	2008-05-05	54591	0.21 ± 0.07	0.19 ± 0.05	0.58 ± 0.05	1.17 ± 0.06
	2008-11-22	54792	...	0.28 ± 0.06	0.16 ± 0.05	...
	2008-11-24	54794	...	0.11 ± 0.04	0.07 ± 0.03	...
	2009-01-30	54861	-0.02 ± 0.09	0.24 ± 0.08	0.58 ± 0.05	0.86 ± 0.08
	2009-01-31	54862	0.14 ± 0.07	0.08 ± 0.05	0.22 ± 0.04	0.52 ± 0.05
	2010-10-01	55470	0.02 ± 0.11	0.23 ± 0.09	1.03 ± 0.07	1.07 ± 0.07
	2010-12-06	55536	-0.18 ± 0.07	0.37 ± 0.06	-0.04 ± 0.05	0.18 ± 0.06
	2010-12-08	55538	0.09 ± 0.06	-0.08 ± 0.04	-0.30 ± 0.04	0.06 ± 0.05
	2010-12-10	55540	-0.02 ± 0.10	-0.08 ± 0.09	-0.36 ± 0.07	0.02 ± 0.08
	2010-12-13	55543	-0.10 ± 0.06	-0.00 ± 0.04	-0.20 ± 0.04	0.04 ± 0.04
	2011-02-07	55599	-0.37 ± 0.09	0.21 ± 0.09	-0.15 ± 0.07	1.04 ± 0.07
	2011-11-24	55889	...	0.04 ± 0.09	0.54 ± 0.07	1.24 ± 0.08
SN 1997bs	2008-05-04	54590	0.11 ± 0.04	0.14 ± 0.03	0.29 ± 0.04	-0.03 ± 0.05
	2009-01-30	54861	0.10 ± 0.04	-0.02 ± 0.04	0.49 ± 0.06	0.05 ± 0.06
	2009-03-22	54912	-0.02 ± 0.05	0.10 ± 0.05	-0.22 ± 0.08	-0.10 ± 0.06
	2010-01-12	55208	-0.04 ± 0.06	-0.27 ± 0.06	0.05 ± 0.07	...
	2010-12-13	55543	0.14 ± 0.04	-0.09 ± 0.04	0.22 ± 0.04	0.06 ± 0.06
	2011-02-11	55603	0.03 ± 0.05	-0.14 ± 0.05	0.31 ± 0.05	...
	2012-01-01	55927	0.02 ± 0.03	0.03 ± 0.03	...	-0.18 ± 0.04

Note. — These light curves are changes in flux relative to the reference image. Since we lack a clear measurement of the source fluxes in the reference images, there is some freedom in selecting the constant flux that needs to be added to these values.